

OPEN

Linearity, Bias, Intrascanner Repeatability, and Interscanner Reproducibility of Quantitative Multidynamic Multiecho Sequence for Rapid Simultaneous Relaxometry at 3 T

A Validation Study With a Standardized Phantom and Healthy Controls

Akifumi Hagiwara, MD,*† Masaaki Hori, MD, PhD,* Julien Cohen-Adad, PhD,*‡§ Misaki Nakazawa, MS,* Yuichi Suzuki, PhD,† Akihiro Kasahara, PhD,† Moeko Horita, BS,*|| Takuya Haruyama, BS,*|| Christina Andica, MD,* Tomoko Maekawa, MD,*† Koji Kamagata, MD, PhD,* Kanako Kunishima Kumamaru, MD, PhD,* Osamu Abe, MD, PhD,† and Shigeki Aoki, MD, PhD*

Objectives: The aim of this study was to evaluate the linearity, bias, intrascanner repeatability, and interscanner reproducibility of quantitative values derived from a multidynamic multiecho (MDME) sequence for rapid simultaneous relaxometry.

Materials and Methods: The NIST/ISMRM (National Institute of Standards and Technology/International Society for Magnetic Resonance in Medicine) phantom, containing spheres with standardized T1 and T2 relaxation times and proton density (PD), and 10 healthy volunteers, were scanned 10 times on different days and 2 times during the same session, using the MDME sequence, on three 3 T scanners from different vendors. For healthy volunteers, brain volumetry and myelin estimation were performed based on the measured T1, T2, and PD. The measured phantom values were compared with reference values; volunteer values were compared with their averages across 3 scanners.

Results: The linearity of both phantom and volunteer measurements in T1, T2, and PD values was very strong ($R^2 = 0.973-1.000, 0.979-1.000, \text{ and } 0.982-0.999$, respectively). The highest intrascanner coefficients of variation (CVs) for T1, T2, and PD were 2.07%, 7.60%, and 12.86% for phantom data, and 1.33%, 0.89%, and 0.77% for volunteer data, respectively. The highest interscanner CVs of T1, T2, and PD were 10.86%, 15.27%, and 9.95% for phantom data, and 3.15%, 5.76%, and 3.21% for volunteer data, respectively. Variation of T1 and T2 tended to be larger at higher values outside the range of those typically observed in brain tissue.

The highest intrascanner and interscanner CVs for brain tissue volumetry were 2.50% and 5.74%, respectively, for cerebrospinal fluid.

Conclusions: Quantitative values derived from the MDME sequence are overall robust for brain relaxometry and volumetry on 3 T scanners from different vendors. Caution is warranted when applying MDME sequence on anatomies with relaxometry values outside the range of those typically observed in brain tissue.

Key Words: SyMRI, synthetic MRI, quantitative MRI, brain, relaxometry, automatic brain segmentation, myelin estimation

(*Invest Radiol* 2018;54: 39–47)

In clinical practice, T1-, T2-, and fluid-attenuated inversion recovery, and other contrast-weighted magnetic resonance imaging (MRI) scans are assessed on the basis of relative signal differences. The signal intensity depends on sequence parameters and scanner settings, but also on B0 and B1 inhomogeneity, coil sensitivity profiles, and RF amplification settings, making quantitative comparisons difficult. Tissue relaxometry is a more direct approach to obtaining scanner-independent values. Absolute quantification of tissue properties by relaxometry has been reported in research settings for characterization of disease,¹ assessment of disease activity,² and monitoring of treatment effect.³ A number of methods have been proposed for simultaneous relaxometry of T1 and T2,⁴⁻⁷ but due to the additional scanning time required, these methods had not been widely introduced into clinical practice.

Recently, a multidynamic multiecho (MDME) sequence for rapid simultaneous measurement of T1 and T2 relaxation times and proton density (PD), with correction of B1 field inhomogeneity, was proposed for full head coverage within approximately 6 minutes,⁸ and has shown promising results on 1.5 T and 3 T scanners in healthy subjects⁹ and patients with multiple sclerosis (MS),¹⁰ brain metastases,¹¹ Sturge-Weber syndrome,¹² and bacterial meningitis.¹³ These quantitative values allow postacquisition generation of any contrast-weighted image via synthetic MRI, obviating the need for additional conventional T1-weighted and T2-weighted imaging required in routine clinical settings.¹⁴ The acquired maps are inherently aligned, thus avoiding potential errors due to image coregistration for multiparametric quantification of a certain area. In addition, brain tissue volumes,¹⁵ including myelin,¹⁶ can be automatically calculated and potentially used to assess brain tissue loss associated with normal aging, neuroinflammatory, or neurodegenerative diseases.^{17,18} Myelin estimation based on the MDME sequence has shown high repeatability¹⁹ and good correlation with histological measures in postmortem human brain²⁰ and with other myelin estimation methods.²¹

According to the Quantitative Imaging Biomarkers Alliance of the Radiological Society of North America, 3 metrology criteria are critical to the performance of a quantitative imaging biomarker: accuracy (linearity and bias), repeatability, and reproducibility.²² Previous studies evaluated T1, T2, and PD values acquired with the MDME sequence on a 1.5 T

Received for publication May 24, 2018; and accepted for publication, after revision, July 27, 2018.

From the *Department of Radiology, Juntendo University School of Medicine; †Department of Radiology, Graduate School of Medicine, The University of Tokyo, Tokyo, Japan; ‡NeuroPoly Lab, Institute of Biomedical Engineering, Polytechnique Montreal; §Functional Neuroimaging Unit, CRIUGM, Université de Montréal, Montreal, Quebec, Canada; and ||Department of Radiological Sciences, Graduate School of Human Health Sciences, Tokyo Metropolitan University, Tokyo, Japan.

Conflicts of interest and sources of funding: This work was supported by AMED under grant number JP181k1010025; ImPACT Program of Council for Science, Technology, and Innovation (Cabinet Office, Government of Japan); JSPS KAKENHI grant number 16K19852; JSPS KAKENHI grant number JP16H06280, Grant-in-Aid for Scientific Research on Innovative Areas—Resource and Technical Support Platforms for Promoting Research “Advanced Bioimaging Support”; and the Japanese Society for Magnetic Resonance in Medicine. The authors declare no conflict of interest.

Supplemental digital contents are available for this article. Direct URL citations appear in the printed text and are provided in the HTML and PDF versions of this article on the journal’s Web site (www.investigativeradiology.com).

Correspondence to: Akifumi Hagiwara, MD, Department of Radiology, Juntendo University School of Medicine, 1-2-1, Hongo, Bunkyo-ku, Tokyo, Japan, 113-8421. E-mail: a-hagiwara@juntendo.ac.jp

Copyright © 2018 The Author(s). Published by Wolters Kluwer Health, Inc. This is an open-access article distributed under the terms of the Creative Commons Attribution-Non Commercial-No Derivatives License 4.0 (CCBY-NC-ND), where it is permissible to download and share the work provided it is properly cited. The work cannot be changed in any way or used commercially without permission from the journal.

ISSN: 0020-9996/19/5401-0039

DOI: 10.1097/RLI.0000000000000510

scanner, by assessing accuracy,^{23,24} repeatability,²⁴ and reproducibility using different head coils.²⁴ However, to our knowledge, no study has compared quantitative values acquired with the MDME sequence on different scanners.

The aim of this study was to evaluate linearity, bias, intrascanner repeatability, and interscanner reproducibility of quantitative values derived from the MDME sequence using three 3 T scanners all from different vendors. In addition, we investigated the robustness of brain tissue volume measurements made using the MDME sequence.

MATERIALS AND METHODS

MR Acquisition and Postprocessing

The MDME sequence was performed on GE Healthcare (Discovery 750w, Milwaukee, WI), Siemens Healthcare (MAGNETOM Prisma, Erlangen, Germany), and Philips (Ingenia, Best, the Netherlands) 3 T scanners (scanner α , β , and γ , respectively). This sequence is a multislice, multisaturation delay, multiecho, fast spin-echo sequence, using combinations of 2 echo times and 4 delay times to produce 8 complex images per slice. To retrieve T1, T2, and PD maps while accounting for B1 inhomogeneity, a least square fit was performed on the signal intensity (I) of these images by minimizing the following equation:

$$I = A \cdot PD \cdot \exp(-TE/T2) \frac{1 - \{1 - \cos(B_1\theta)\} \exp(-TI/T1) - \cos(B_1\theta) \exp(-TR/T1)}{1 - \cos(B_1\alpha) \cos(B_1\theta) \exp(-TR/T1)}$$

where α is the applied excitation flip angle 90 degrees and θ is the saturation flip angle of 120 degrees. A is an overall intensity scaling factor that takes into account several elements, including sensitivity of the coil, amplification of the radiofrequency chain, and voxel volume. The details of the sequence composition and postprocessing are described elsewhere.²³ The postprocessing was performed using SyMRI software (version 8.0; SyntheticMR AB, Linköping, Sweden), resulting in T1, T2, and PD maps. The characteristics of the 3 scanners and the detailed acquisition parameters of the MDME sequence are shown in Supplementary Table 1 and Supplementary Table 2 (both in Supplemental Digital Content 1, <http://links.lww.com/RLI/A400>) for phantom and volunteer studies, respectively. We used the predetermined parameters provided by each vendor without any change. For volunteers, 3-dimensional (3D) T1-weighted images were also acquired on scanner α . The acquisition parameters of the 3D T1-weighted inversion-recovery spoiled gradient echo images were as follows: repetition time, 7.6 milliseconds; echo time, 3.09 milliseconds; inversion time, 400 milliseconds; bandwidth, 244 Hz/pixel; thickness, 1 mm; field of view, 256 × 256 mm; matrix size, 256 × 256; acquisition time, 5 minutes 45 seconds.

Phantom Study

The NIST/ISMRM (National Institute of Standards and Technology/International Society for Magnetic Resonance in Medicine) MRI system phantom (High Precision Devices, Inc, Boulder, CO), consisting of multiple layers of sphere arrays with known T1, T2, and PD values, was used. Reference values, confirmed by magnetic resonance spectroscopy, were provided by NIST.^{25,26} The T1 and T2 spheres were filled with NiCl₂ and MnCl₂ solutions, respectively. We selected 6 T1 spheres and 10 T2 spheres with T1 and T2 values within the clinically relevant dynamic range (300–4300 milliseconds and 20–2000 milliseconds, respectively). All 14 PD spheres from the phantom were used in the study. The PD spheres consisted of different concentrations of water (H₂O) and heavy water (D₂O). The container of the phantom was filled with distilled water. The reference values for T1, T2, and PD at 20°C are shown in Supplementary Table 3 (Supplemental Digital Content 1, <http://links.lww.com/RLI/A400>).

The phantom was scanned 10 times each on scanners α , β , and γ over a 2-month period, with an interval of at least 1 day between consecutive scans. The phantom was placed for 30 minutes before each scan. The temperature of the phantom was 20°C ± 1°C, measured after each scan.

A circular region of interest of 1.150 cm² was placed in the center of each sphere on T1, T2, and PD maps using OsiriX Imaging Software, Version 7.5 (<http://www.osirix-viewer.com>), to include as much of the sphere as possible while avoiding partial volume with the edge. Regions of interest on all the spheres were simultaneously copied and pasted on the data acquired at different times, and the mean values were recorded.

Volunteer Study

This study was approved by the institutional review boards, and written informed consent was acquired from all participants. Ten healthy volunteers (3 men; mean age, 24.7 years; age range, 21–32 years) were included. None of the participants had a history of a major medical condition, neurological or psychiatric disorder, and all had normal structural MRIs.

Each participant was scanned twice during each session on scanners α , β , and γ (in that order) over a 1-week period, with sessions at least 1 day apart. The subjects were removed from the scanner after the first scan and repositioned for the second scan.

T1, T2, and PD maps were acquired for all participants and processed using SyMRI software⁸ to obtain gray matter (GM), white matter (WM), and cerebrospinal fluid (CSF) segmentation, volumetry of brain tissues, and myelin estimation. Tissue volume fractions were calculated for each voxel. Voxels not categorized as GM, WM, or CSF were classified as other brain material (NoN). Myelin volume fraction (MVF) in

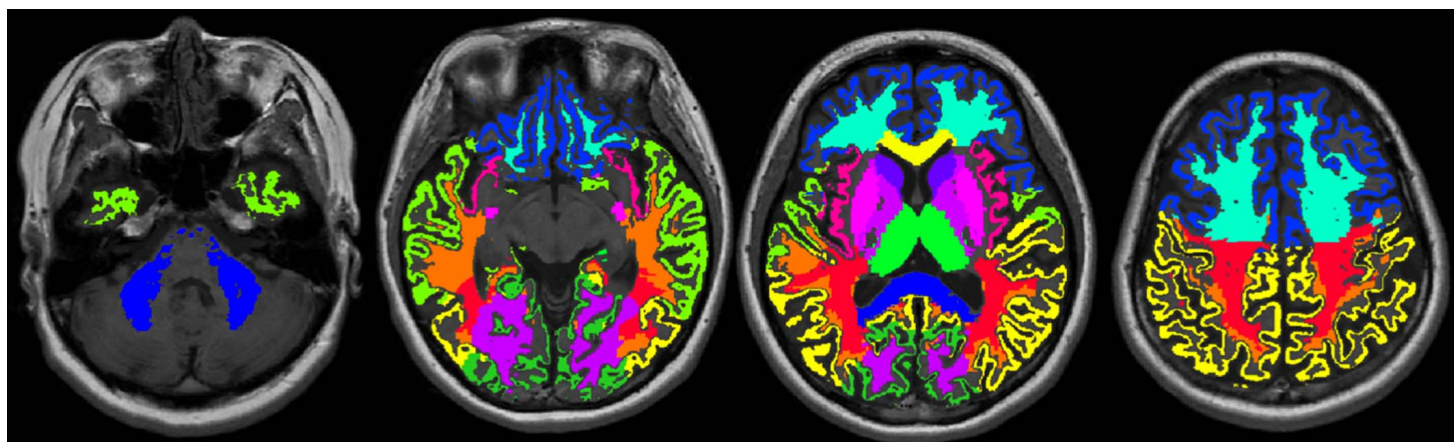


FIGURE 1. Example of volume of interest measurement. Volumes of interest are overlaid on T1-weighted images.

each voxel was estimated based on a 4-compartment model,¹⁶ using T1, T2, and PD values of myelin, excess parenchymal water, cellular water, and free water partial volumes. The 4-compartment model assumes that the relaxation behavior of each compartment contributes to the effective relaxation behavior of each voxel, while considering the magnetization exchange rates between partial volume compartments. The details of brain segmentation and myelin estimation are described elsewhere.^{15,16} The total volumes of GM, WM, CSF, NoN, and myelin (MYV) were calculated by multiplying the aggregated volume fraction of each tissue type and the voxel volume.^{15,16} The brain parenchymal volume (BPV) was calculated as the sum of GM, WM, and NoN. The borderline of intracranial volume (ICV) was defined at points where PD = 50%.²⁷

T1, T2, PD, and MVF maps were used for the volume of interest (VOI) analysis. We created 16 VOIs: 8 GM (frontal, parietal, temporal and occipital GM, insula, caudate, putamen, and thalamus) and 8 WM (frontal, parietal, temporal and occipital WM, genu and splenium of corpus callosum, internal capsules, and middle cerebellar peduncles) VOIs in the Montreal Neurological Institute space. Other than those of splenium, VOIs from the left and right were combined for analysis. Aggregate GM and WM VOIs were also created by combining these regional VOIs. Volume of interest analysis was performed using FMRIB Software Library (FSL, <http://fsl.fmrib.ox.ac.uk/fsl/fslwiki/FSL>). We transformed VOIs created in the Montreal Neurological Institute space to the space of each subject using the FSL linear and nonlinear image registration tool (FLIRT and FNIRT), based on the synthetic T1-weighted (TR, 500; TE, 10) and 3D T1-weighted images. The GM and WM masks were generated from the synthetic T1-weighted images using FMRIB's Automated Segmentation Tool (FAST). These masks were then thresholded at 0.9 and used on the T1, T2, PD, and MVF maps to compute average values within the GM and WM. Figure 1 shows an example of VOI measurements.

Statistical Analysis

Ten measurements of the spheres in the phantom were averaged for each of the 3 scanners. Linear regression was performed for these values versus the reference values. Bland-Altman analysis was performed to assess agreement between the reference values and those acquired on each scanner. Linear regression was also performed for the values from the first scans of volunteers on scanners α , β , and γ versus the average values obtained from these scanners.

Coefficients of variation (CVs) were calculated within each scanner (intra-scanner CV) and across scanners (inter-scanner CV). For the phantom study, the intra-scanner CV was calculated based on the

10 scans. The inter-scanner CV was calculated using the average values from each of the 3 scanners. For the volunteer study, the intra-scanner CVs were calculated per subject (based on the scan and rescan) and then averaged across subjects. Inter-scanner CVs were calculated for each subject using the data of the first scan, then averaged into a single inter-scanner CV value.

RESULTS

Phantom Study

The temperature of the phantom after imaging was $19.76^{\circ}\text{C} \pm 0.23^{\circ}\text{C}$ (mean \pm SD) on scanner α , $20.06^{\circ}\text{C} \pm 0.59^{\circ}\text{C}$ on scanner β , and $19.57^{\circ}\text{C} \pm 0.28^{\circ}\text{C}$ on scanner γ .

Figure 2 shows mean values of T1, T2, and PD acquired over 10 times on each scanner plotted against the known reference values. The regression analysis showed strong linear correlation ($R^2 = 0.973$ – 0.998 for T1; $R^2 = 0.989$ – 1.000 for T2; $R^2 = 0.982$ – 0.991 for PD).

Figure 3 shows Bland-Altman plots for the values acquired on each scanner and the reference values of the phantom. Overall, trends of biases for T1, T2, and PD showed similar patterns across different vendors. All data points were within the 95% limits of agreement, except the longest T1 value (reference value, 1838 milliseconds) on scanner α , the longest T2 value (reference value, 645.8 milliseconds) on all scanners, 1 PD point (reference value, 60%) for scanner α , and the highest PD value (reference value, 100%) for scanner β . Higher T1 and T2 values outside the range of those observed in the brain tissue (see Supplementary Table 4, Supplemental Digital Content 1, <http://links.lww.com/RLI/A400>) showed greater bias. On the other hand, PD values less than 60% (reference value), which were outside the range of values observed in the brain tissue, showed smaller bias than higher PD values, except PD 5% (reference value), which was measured as 0% on all 3 scanners.

Table 1 shows the intra-scanner and inter-scanner CV of phantom T1, T2, and PD measurements. The highest intra-scanner CV of T1 values was 2.07% (scanner β). Intra-scanner CVs of T2 values were less than 4.25% on scanners α and β , and less than 7.60% on scanner γ ; those of PD values were less than 3.71%, except the CV for a PD reference value of 10%, which was 12.86% on scanner α , and for a PD reference value of 100%, which was 5.13% on scanner β .

The inter-scanner CV was higher than intra-scanner CV for all ranges of T1 (3.25%–10.86%), T2 (4.28%–15.27%), and PD (1.35%–9.95%) values, except PD 10% (reference value). Within the range of brain tissue properties (see Supplementary Table 4, Supplemental Digital Content 1, <http://links.lww.com/RLI/A400>),

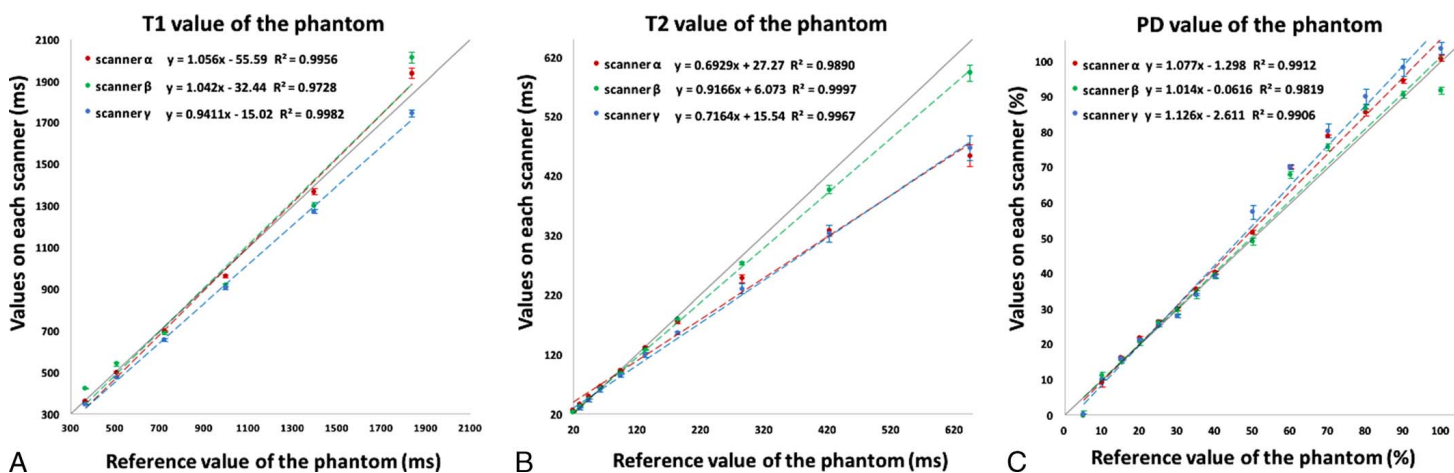


FIGURE 2. Scatterplots showing linearity of measured T1 (A), T2 (B), and proton density (C) values of the NIST/ISMRM phantom averaged across 10 acquisitions, plotted against reference values. Error bars represent one standard deviation. Dashed lines represent linear regression fits (red for scanner α , green for scanner β , and blue for scanner γ), whereas the solid lines represent identity.

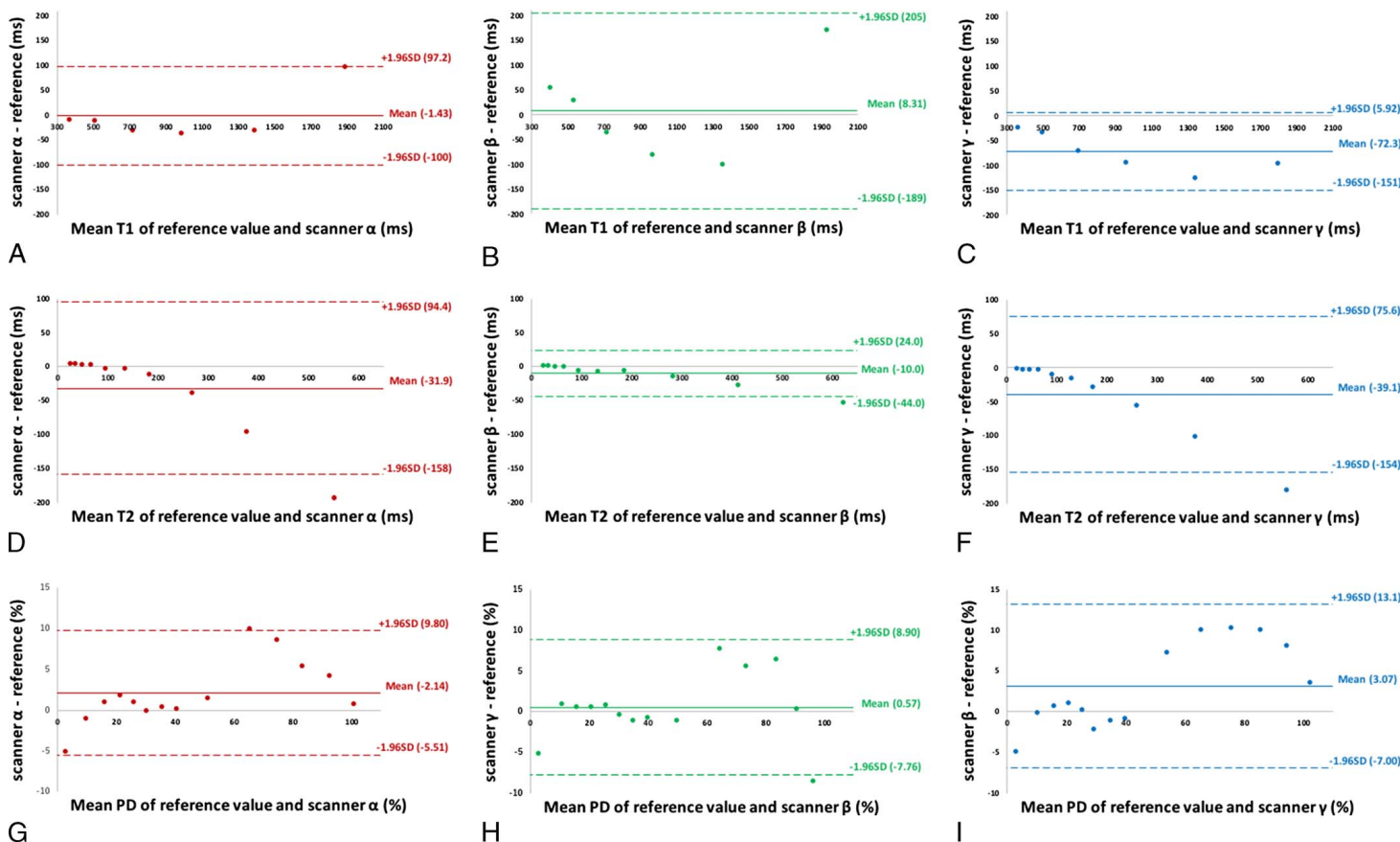


FIGURE 3. Bland-Altman plots showing bias of measurements of T1 (A, for scanner alpha; B, for scanner beta; and C, for scanner gamma), T2 (D, for scanner alpha; E, for scanner beta; and F, for scanner gamma), and proton density (G, for scanner alpha; H, for scanner beta; and I, for scanner gamma) for the NIST/ISMRM phantom.

TABLE 1. Mean Values of All Measurements and Their Intrascanner and Interscanner CV on the NIST/ISMRM Phantom for T1, T2, and PD

Sphere No.	T1	Scanner			T2	Scanner		
	Mean ± SD, ms	Scanner alpha Intrascanner CV, %	Scanner beta Intrascanner CV, %	Scanner gamma Intrascanner CV, %	Mean ± SD, ms	Scanner alpha Intrascanner CV, %	Scanner beta Intrascanner CV, %	Scanner gamma Intrascanner CV, %
1	376 ± 40.9	0.96	1.01	0.50	22.7 ± 3.25	1.26	1.18	7.60
2	506 ± 31.8	0.98	2.07	0.77	32.9 ± 3.77	1.05	0.91	5.90
3	682 ± 22.4	0.70	1.16	1.14	45.9 ± 3.25	1.05	0.95	5.27
4	930 ± 30.2	0.71	0.97	0.67	63.7 ± 2.87	1.02	0.85	4.71
5	1324 ± 49.6	1.02	1.33	0.73	89.4 ± 3.83	1.38	0.90	4.48
6	1897 ± 138	1.21	1.31	0.92	127 ± 5.81	1.69	0.90	3.71
7					171 ± 12.0	1.87	1.14	1.76
8					251 ± 21.4	2.79	1.21	4.01
9					350 ± 41.2	2.99	1.69	4.45
10					505 ± 77.0	4.25	2.45	4.64
11								
12								
13								
14								

For PD value 5% (reference value), measurement yielded 0% on all scanners, so CV was not calculated.

CV indicates coefficient of variation; PD, proton density; SD, standard deviation.

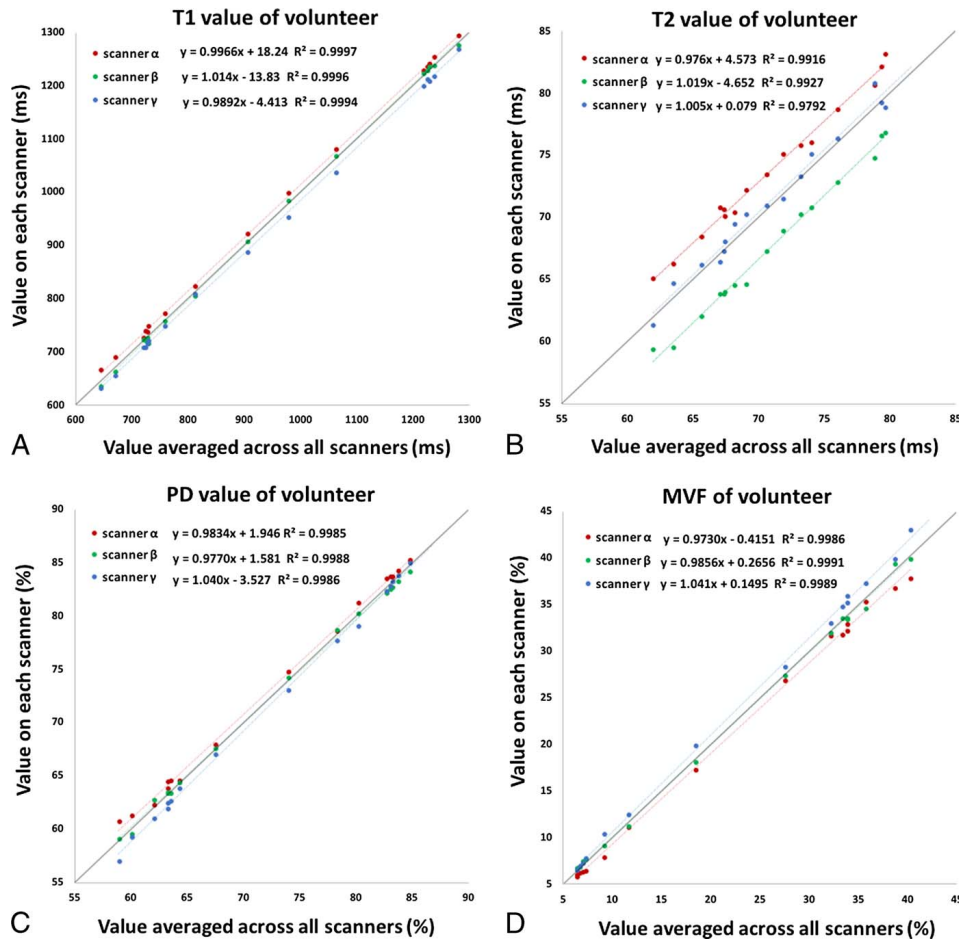


FIGURE 4. Scatterplots showing linearity of measured T1 (A), T2 (B), proton density (C), and myelin volume fraction (D) values of the brains of healthy volunteers, plotted against averaged values across all 3 scanners. Only the data of the first acquisition was used. Dashed lines represent linear regression fits (red for scanner α , green for scanner β , and blue for scanner γ), whereas the solid lines represent identity.

PD	Scanner α	Scanner β	Scanner γ	Interscanner
Mean \pm SD, %	Intrascanner CV, %	Intrascanner CV, %	Intrascanner CV, %	CV, %
0	N/A	N/A	N/A	N/A
10.0 \pm 1.00	12.86	2.38	1.37	9.95
15.9 \pm 0.21	1.24	1.05	0.66	1.35
21.2 \pm 0.60	1.09	1.03	0.86	2.83
25.8 \pm 0.45	1.84	1.41	1.05	1.75
29.2 \pm 1.10	1.68	0.40	1.52	3.76
34.5 \pm 0.89	1.49	1.45	1.11	2.59
39.6 \pm 0.56	1.31	1.37	1.32	1.42
52.7 \pm 4.27	1.06	1.11	3.71	8.11
69.4 \pm 1.26	0.76	3.50	1.11	1.82
78.3 \pm 2.31	0.62	1.36	2.72	2.95
87.4 \pm 2.36	1.23	0.73	2.56	2.70
94.3 \pm 3.83	0.73	1.20	2.59	4.06
98.7 \pm 6.26	0.98	5.13	1.73	6.35

TABLE 2. Mean Values in the GM and WM Based on the First Scan on 3 Scanners and Intrascanner and Interscanner CV of T1, T2, PD, and MVF for 3 Scanners Averaged Across 10 Subjects

VOI	T1	Scanner α		Scanner β		Scanner γ		T2	Scanner α		Scanner β		Scanner γ	
	Mean, ms	Intrascanner CV, %	Intrascanner CV, %	Intrascanner CV, %	Intrascanner CV, %	Intrascanner CV, %	Intrascanner CV, %	Mean \pm SD, ms	Intrascanner CV, %	Intrascanner CV, %	Intrascanner CV, %	Intrascanner CV, %	Intrascanner CV, %	Intrascanner CV, %
Aggregate GM VOIs	1062 \pm 23.3	0.51 \pm 0.57	0.30 \pm 0.24	0.43 \pm 0.31	1.33 \pm 0.54	73.3 \pm 2.80	0.57 \pm 0.43	0.20 \pm 0.11	0.60 \pm 0.64	4.15 \pm 0.36				
Aggregate WM VOIs	725 \pm 21.8	0.67 \pm 0.62	0.38 \pm 0.23	0.52 \pm 0.53	1.89 \pm 0.62	69.0 \pm 2.94	0.52 \pm 0.40	0.26 \pm 0.12	0.37 \pm 0.29	4.63 \pm 0.31				

Values are mean \pm SD. Size of the VOIs are also shown in the last column.

CV indicates coefficient of variation; GM, gray matter; PD, proton density; SD, standard deviation; VOI, volume of interest; WM, white matter.

interscanner CVs of T1 (645–1280 milliseconds) were less than 6.3%, interscanner CV of T2 (61.9–79.6 milliseconds) was 4.51% and interscanner CVs of PD (58.9–84.8 milliseconds) were less than 3.0%.

Volunteer Study

Figure 4 shows T1, T2, PD, and MVF values for the first acquisition on each scanner plotted against the mean of the 3 scanners. The regression analysis showed strong linear correlation ($R^2 = 0.999$ – 1.000 for T1; $R^2 = 0.979$ – 0.993 for T2; $R^2 = 0.999$ – 0.999 for PD; $R^2 = 0.999$ – 0.999 for MVF).

Supplementary Table 4 (Supplemental Digital Content 1, <http://links.lww.com/RLI/A400>) shows the intrascanner and interscanner CVs of T1, T2, PD, and MVF, and the values for aggregate GM and WM VOIs are extracted and shown in Table 2. The highest intrascanner CVs of T1, T2, PD, and MVF were 1.33%, 0.89%, 0.77%, and 4.56%, respectively, across all VOIs. The interscanner CV was higher than the intrascanner CV for all ranges of T1, T2, PD, and MVF (1.06%–3.15%, 3.61%–5.76%, 0.68%–3.21%, and 2.53%–14.6%, respectively).

Figure 5 shows volumetric data (GM, WM, CSF, NoN, BPV, ICV, MYV) for the first acquisition on each scanner plotted against the mean of the 3 scanners. The regression analysis showed strong linear correlation for GM, WM, CSF, BPV, ICV, and MYV ($R^2 = 0.966$ – 0.999). NoN showed a weaker linear correlation ($R^2 = 0.791$ – 0.856).

Table 3 shows the intrascanner and interscanner CVs of volumetric data from the 3 scanners. The intrascanner CVs were 0.11% to 1.17% for GM, WM, BPV, ICV, and MYV, 0.16 to 2.50% for CSF, and 3.43% to 10.8% for NoN. The interscanner CVs were in the range 0.42% to 5.74% for all measures except NoN (16.3%), and thus higher than the corresponding intrascanner CVs for all tissue volumes.

DISCUSSION

In this study, we evaluated linearity, bias, intrascanner repeatability, and interscanner reproducibility of multiple quantitative values acquired by the MDME sequence, with 3 scanners from different vendors, in both standardized NIST/ISMRM phantom and 10 healthy volunteers. Although the phantom study showed some bias with respect to the reference values, linearity was very strong in all the measurements, indicating that the MDME sequence can differentiate materials with different tissue properties. Trends of biases for T1, T2, and PD shown as Bland-Altman plots were similar in the 3 scanners, which could also demonstrate the robustness of the MDME sequence even across different vendors.

The T1, T2, and PD values acquired in vivo in our study fell in the same order of magnitude as those reported in previous studies using 3 T scanners,^{6,28–31} which reported a wide range of T1 and T2 values (eg, T1 600–1100 milliseconds, T2 50–80 milliseconds, and 67%–73% in the

WM) for healthy controls, largely depending on the choice of acquisition method. To date, only a few studies have investigated interscanner reproducibility of specific MR relaxometry methods for human subjects across different vendors. Bauer et al³² demonstrated that T2 values quantified with dual echo fast spin-echo on scanners from 3 different vendors showed variability up to 20%, and Deoni et al³³ validated driven equilibrium single pulse observation of T1 and T2 with interscanner CVs of approximately 6.5% and 8% for scanners from 2 different vendors. The results of our volunteer study (T1, highest CV 3.15%; T2, highest CV 5.60%) were comparable or better, even with different acquisition parameters and coils across scanners to reflect daily radiological practice.

The intrascanner and interscanner CVs in our study were lower than the changes in T1 and PD values of normal-appearing brain tissue in patients with MS^{34,35} and in the T2 values of the limbic system in patients with Alzheimer disease.³⁶ Our results suggest that MDME sequence could thus be of clinical value in multicenter and longitudinal studies, taking disease-specific within-group variation into account.³⁷

The intrascanner CVs of T1, T2, and PD measurements in volunteer data were very low (less than 1.4%) and lower than those in phantom data. However, the variation in phantom data acquired over 10 days could be partly explained by day-to-day variation in scanner performance, whereas the volunteers were scanned twice in the same session on the same day. In addition, the size of the region of interest used in phantom study was much smaller than those of the VOIs used in volunteer study. Thus, we cannot simply compare the results of the volunteers and the phantom studies. Notably, interscanner CVs of T1 and T2 values in phantom data outside the range of the volunteer data were mostly higher than those of T1 and T2 values within the volunteer data range. These results could be attributed to the fact that the MDME sequence was developed for the analysis of the brain tissue, and the commercial version of the MDME sequence may not have been fully optimized for materials with different relaxation properties.

The T2 measurements showed larger interscanner CV than those of T1. Every vendor uses their own RF pulse shapes and specific absorption rate reduction models to decrease the 180-degree refocusing pulses during the TSE readout. This could also explain the differences in the intrascanner CVs of the T2 measurements across scanners, with scanner γ showing higher values than scanners α and β . Moreover, the B1 inhomogeneity profiles differ per scanner and even per object, and imperfect gradient refocusing due to eddy currents may decrease signal intensity. These factors affect the signal amplitude during the multiecho readout, potentially resulting in an apparently altered T2 relaxation. In the postprocessing, RF pulse shape, B1 amplitude, and B1 inhomogeneity are taken into account and corrected for, but this may not be perfect. It should be noted that long T2 times were mainly affected, beyond the typical T2 values of brain tissue, suggesting that T2 measurement of CSF would be less reliable. To improve the interscanner CV of T2, more echoes than the current 2 could potentially be added to the sequence,

PD	Scanner α	Scanner β	Scanner γ		MVF	Scanner α	Scanner β	Scanner γ		
Mean \pm SD, %	Intrascanner CV, %	Intrascanner CV, %	Intrascanner CV, %	Interscanner CV, %	Mean \pm SD, %	Intrascanner CV, %	Intrascanner CV, %	Intrascanner CV, %	Interscanner CV, %	Size of VOI, cm ³
77.2 \pm 1.13	0.15 \pm 0.17	0.12 \pm 0.09	0.12 \pm 0.11	1.20 \pm 0.30	16.4 \pm 1.54	0.68 \pm 0.60	0.63 \pm 0.50	0.76 \pm 0.44	5.76 \pm 1.13	492 \pm 41.1
63.3 \pm 1.25	0.36 \pm 0.32	0.22 \pm 0.10	0.32 \pm 0.29	1.55 \pm 0.32	33.9 \pm 1.91	1.11 \pm 1.07	0.64 \pm 0.30	0.81 \pm 0.75	4.46 \pm 0.82	240 \pm 26.8

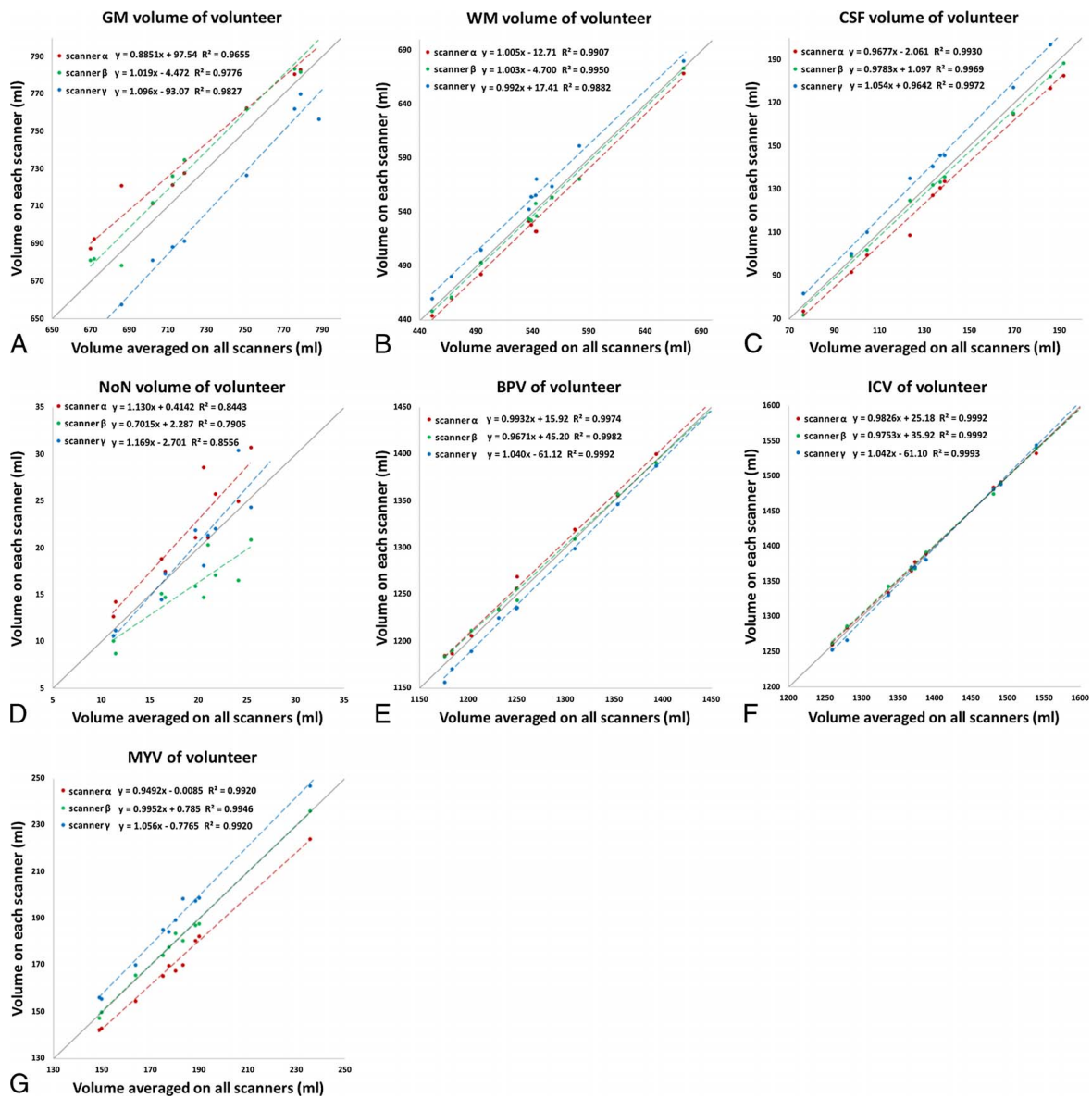


FIGURE 5. Scatterplots showing linearity of volumetric measurements of gray matter (A), white matter (B), cerebrospinal fluid (C), other brain materials (D), brain parenchymal volume (E), intracranial volume (F), and myelin volume (G) of the volunteer brains, plotted against the average of the values across all 3 scanners. Only the data of the first acquisition was used. Dashed lines represent linear regression fit (red for scanner α , green for scanner β , and blue for scanner γ), whereas the solid lines represent identity.

TABLE 3. Mean of All Volumetric Measurements Based on the First Scan, and the Intrascanner and Interscanner CV of Volunteers for GM, WM, CSF, NoN, BPV, ICV, and MVF

Tissue Type	Mean, mL	Scanner α		Scanner β		Scanner γ	
		Intrascanner CV, %	Intrascanner CV, %	Intrascanner CV, %	Intrascanner CV, %	Intrascanner CV, %	Interscanner CV, %
GM	727 \pm 48.1	1.10 \pm 0.90	0.50 \pm 0.44	0.99 \pm 0.72	2.94 \pm 1.22		
WM	537 \pm 61.3	1.15 \pm 1.04	0.54 \pm 0.52	1.11 \pm 0.69	2.40 \pm 1.30		
CSF	136 \pm 37.0	2.50 \pm 1.00	0.16 \pm 0.10	1.22 \pm 0.80	5.74 \pm 2.36		
NoN	18.2 \pm 5.3	10.8 \pm 17.4	3.43 \pm 3.39	5.63 \pm 3.62	16.3 \pm 6.76		
BPV	1282 \pm 96.1	0.40 \pm 0.64	0.11 \pm 0.10	0.25 \pm 0.16	0.73 \pm 0.40		
ICV	1418 \pm 121	0.33 \pm 0.47	0.11 \pm 0.10	0.18 \pm 0.12	0.42 \pm 0.17		
MYV	179 \pm 25.0	1.17 \pm 1.01	0.70 \pm 0.52	1.06 \pm 0.85	5.20 \pm 1.11		

Values are mean \pm SD.

CV indicates coefficient of variation; GM, gray matter; WM, white matter; CSF, cerebrospinal fluid; NoN, other brain material; BPV, brain parenchymal volume; ICV, intracranial volume; MYV, myelin volume.

but this would increase the total scan time, which would be detrimental for introduction of the sequence into clinical routine. Application of the MDME sequence to objects other than the brain has been reported for T2 measurement of musculoskeletal tissue.^{38–40} Although the MDME and multiecho spin-echo sequence showed good agreement with each other for T2 measurement of phantom, knee cartilage, and muscle, mean T2 value of bone marrow measured by multiecho spin-echo was significantly higher than that measured by the MDME sequence.³⁸ This discrepancy was assumed to be because of the varying contributions from water and lipid protons, which resulted in multiexponential decay.³⁹ The quantitative values acquired by the MDME sequence should be cautiously assessed when used to other tissues than brain.

We also observed low interscanner and intrascanner CV of tissue volumes calculated using the T1, T2, and PD maps acquired by the MDME sequence. The interscanner CVs of all tissue volumes were higher than the intrascanner CVs, reflecting the higher interscanner CVs of T1, T2, and PD measurements. Our intrascanner CVs were comparable to those reported in previous studies using 3D T1-weighted images acquired on 1.5 T and 3 T scanners based on various segmentation algorithms.^{41–44} Further, our interscanner CVs for GM, WM, CSF, BPV, and ICV were slightly lower than those shown by Huppertz et al⁴³ for a single subject using 3D T1-weighted images acquired on 6 scanners with field strength of 1.5 T and 3 T. The NoN volume, which is the smallest compartment, showed the highest variability among all types of tissue volume, consistent with previous reports.^{15,19,45} Granberg et al⁴⁵ showed lower intrascanner CV of NoN volume in MS patients than in healthy controls, indicating clinical utility of NoN volume as measures of lesion load. The algorithm implemented in the SyMRI software only uses quantitative values of each voxel for segmentation,¹⁵ and utilization of structural information, by, for example, a deep learning approach,⁴⁶ might further improve the segmentation.

The repeatability of MVF in healthy volunteer data was high, with the intrascanner CVs lower than 4.6%, but higher than those of T1, T2, and PD, probably reflecting small errors in measurement of each quantitative value. The interscanner reproducibility of MVF in the WM was overall higher than that in the GM, with the highest interscanner CVs being 6.67% and 14.60%, respectively. The intrascanner CV of MVF in WM was slightly lower than the results reported (1.3%–2.4%) by Nguyen et al⁴⁷ for the myelin water fraction in WM. To our knowledge, no previous study has evaluated the interscanner reproducibility of myelin imaging for different vendors.

There are some limitations to our study. First, we only used 3 T scanners, hence our results cannot be generalized to scanners with different field strength. Second, we did not include patients with any brain disease. A cerebral lesion would affect T1, T2, and PD values and

consequently the repeatability and reproducibility measurements. Hagiwara et al¹⁰ showed focal MS plaques in the WM to have mean T1 value of 1111 milliseconds, T2 value of 91.9 milliseconds, and PD value of 78.86% using the MDME sequence on a 3 T MR scanner. In our study using the phantom, intrascanner and interscanner CV at these T1, T2, and PD values were at the same order of magnitude as the range of T1, T2, and PD in the normal WM, indicating that the MDME sequence may reliably be used in the evaluation of WM demyelinating lesions.

In conclusion, brain quantitative values derived from the MDME sequence at 3 T are overall robust even across different scanners. Caution is warranted when applying MDME sequence to anatomies with different relaxation properties compared with brain tissue.

REFERENCES

- West J, Aalto A, Tisell A, et al. Normal appearing and diffusely abnormal white matter in patients with multiple sclerosis assessed with quantitative MR. *PLoS One*. 2014;9:e95161.
- Horsthuis K, Nederveen AJ, de Feiter MW, et al. Mapping of T1-values and gadolinium-concentrations in MRI as indicator of disease activity in luminal Crohn's disease: a feasibility study. *J Magn Reson Imaging*. 2009;29:488–493.
- Wagner MC, Lukas P, Herzog M, et al. MRI and proton-NMR relaxation times in diagnosis and therapeutic monitoring of squamous cell carcinoma. *Eur Radiol*. 1994;4:314–323.
- Ma D, Gulani V, Seiberlich N, et al. Magnetic resonance fingerprinting. *Nature*. 2013;495:187–192.
- Newbould RD, Skare ST, Alley MT, et al. Three-dimensional T(1), T(2) and proton density mapping with inversion recovery balanced SSFP. *Magn Reson Imaging*. 2010;28:1374–1382.
- Ehnes P, Seiberlich N, Ma D, et al. IR TrueFISP with a golden-ratio-based radial readout: fast quantification of T1, T2, and proton density. *Magn Reson Med*. 2013;69:71–81.
- Deoni SC, Rutt BK, Arun T, et al. Gleaning multicomponent T1 and T2 information from steady-state imaging data. *Magn Reson Med*. 2008;60:1372–1387.
- Hagiwara A, Wartjes M, Hori M, et al. SyMRI of the brain: rapid quantification of relaxation rates and proton density, with synthetic MRI, automatic brain segmentation, and myelin measurement. *Invest Radiol*. 2017;52:647–657.
- Lee SM, Choi YH, You SK, et al. Age-related changes in tissue value properties in children: simultaneous quantification of relaxation times and proton density using synthetic magnetic resonance imaging. *Invest Radiol*. 2018;53:236–245.
- Hagiwara A, Hori M, Yokoyama K, et al. Utility of a multiparametric quantitative MRI model that assesses myelin and edema for evaluating plaques, periplaque white matter, and normal-appearing white matter in patients with multiple sclerosis: a feasibility study. *AJNR Am J Neuroradiol*. 2017;38:237–242.
- Hagiwara A, Hori M, Suzuki M, et al. Contrast-enhanced synthetic MRI for the detection of brain metastases. *Acta Radiol Open*. 2016;5:2058460115626757.
- Hagiwara A, Nakazawa M, Andica C, et al. Dural enhancement in a patient with Sturge-Weber syndrome revealed by double inversion recovery contrast using synthetic MRI. *Magn Reson Med Sci*. 2016;15:151–152.

13. Andica C, Hagiwara A, Nakazawa M, et al. Synthetic MR imaging in the diagnosis of bacterial meningitis. *Magn Reson Med Sci.* 2017;16:91–92.
14. Blystad I, Wamntjes JB, Smedby O, et al. Synthetic MRI of the brain in a clinical setting. *Acta Radiol.* 2012;53:1158–1163.
15. West J, Wamntjes JB, Lundberg P. Novel whole brain segmentation and volume estimation using quantitative MRI. *Eur Radiol.* 2012;22:998–1007.
16. Wamntjes M, Engström M, Tisell A, et al. Modeling the presence of myelin and edema in the brain based on multi-parametric quantitative MRI. *Front Neurol.* 2016;7:16.
17. Jack CR Jr, Shiung MM, Gunter JL, et al. Comparison of different MRI brain atrophy rate measures with clinical disease progression in AD. *Neurology.* 2004;62:591–600.
18. Miller DH, Barkhof F, Frank JA, et al. Measurement of atrophy in multiple sclerosis: pathological basis, methodological aspects and clinical relevance. *Brain.* 2002;125(pt 8):1676–1695.
19. Andica C, Hagiwara A, Hori M, et al. Automated brain tissue and myelin volumetry based on quantitative MR imaging with various in-plane resolutions. *J Neuroradiol.* 2018;45:164–168.
20. Wamntjes JBM, Persson A, Berge J, et al. Myelin detection using rapid quantitative MR imaging correlated to macroscopically registered luxol fast blue-stained brain specimens. *AJNR Am J Neuroradiol.* 2017;38:1096–1102.
21. Hagiwara A, Hori M, Kamagata K, et al. Myelin measurement: comparison between simultaneous tissue relaxometry, magnetization transfer saturation index, and T1w/T2w ratio methods. *Sci Rep.* 2018;8:10554.
22. Raunig DL, McShane LM, Pennello G, et al. Quantitative imaging biomarkers: a review of statistical methods for technical performance assessment. *Stat Methods Med Res.* 2015;24:27–67.
23. Wamntjes JB, Leinhard OD, West J, et al. Rapid magnetic resonance quantification on the brain: optimization for clinical usage. *Magn Reson Med.* 2008;60:320–329.
24. Krauss W, Gunnarsson M, Andersson T, et al. Accuracy and reproducibility of a quantitative magnetic resonance imaging method for concurrent measurements of tissue relaxation times and proton density. *Magn Reson Imaging.* 2015;33:584–591.
25. Russek S, Boss M, Jackson E, et al. Characterization of NIST/ISMRM MRI System Phantom. In: *In Proceedings of the 20th Annual Meeting of ISMRM.* Melbourne, Victoria, Australia; 2012: Abstract 2456.
26. Keenan K, Stupic K, Boss M, et al. Multi-site, multi-vendor comparison of T1 measurement using ISMRM/NIST system phantom. In: *Proceedings of the 24th Annual Meeting of ISMRM.* Singapore; 2016: Abstract 3290.
27. Ambarki K, Lindqvist T, Wahlin A, et al. Evaluation of automatic measurement of the intracranial volume based on quantitative MR imaging. *AJNR Am J Neuroradiol.* 2012;33:1951–1956.
28. Stikov N, Boudreau M, Levesque IR, et al. On the accuracy of T1 mapping: searching for common ground. *Magn Reson Med.* 2015;73:514–522.
29. McPhee KC, Wilman AH. Transverse relaxation and flip angle mapping: evaluation of simultaneous and independent methods using multiple spin echoes. *Magn Reson Med.* 2017;77:2057–2065.
30. Whittall KP, MacKay AL, Graeb DA, et al. In vivo measurement of T2 distributions and water contents in normal human brain. *Magn Reson Med.* 1997;37:34–43.
31. Abbas Z, Gras V, Mollenhoff K, et al. Analysis of proton-density bias corrections based on T1 measurement for robust quantification of water content in the brain at 3 Tesla. *Magn Reson Med.* 2014;72:1735–1745.
32. Bauer CM, Jara H, Killiany R, et al. Whole brain quantitative T2 MRI across multiple scanners with dual echo FSE: applications to AD, MCI, and normal aging. *Neuroimage.* 2010;52:508–514.
33. Deoni SCL, Williams SCR, Jezzard P, et al. Standardized structural magnetic resonance imaging in multicentre studies using quantitative T1 and T2 imaging at 1.5 T. *Neuroimage.* 2008;40:662–671.
34. Davies GR, Hadjiprocopis A, Altmann DR, et al. Normal-appearing grey and white matter T1 abnormality in early relapsing-remitting multiple sclerosis: a longitudinal study. *Mult Scler.* 2007;13:169–177.
35. Reitz SC, Hof SM, Fleischer V, et al. Multi-parametric quantitative MRI of normal appearing white matter in multiple sclerosis, and the effect of disease activity on T2. *Brain Imaging Behav.* 2017;11:744–753.
36. Wang H, Yuan H, Shu L, et al. Prolongation of T(2) relaxation times of hippocampus and amygdala in Alzheimer's disease. *Neurosci Lett.* 2004;363:150–153.
37. Tofts PS. Measurement in MRI. In: Cercignani M, Dowell NG, Tofts PS, eds. *Quantitative MRI of the Brain.* 2nd ed. Boca Raton, FL: CRC Press; 2018:10–11.
38. Park S, Kwack KS, Lee YJ, et al. Initial experience with synthetic MRI of the knee at 3T: comparison with conventional T1 weighted imaging and T2 mapping. *Br J Radiol.* 2017;90:20170350.
39. Chougar L, Hagiwara A, Andica C, et al. Synthetic MRI of the knee: new perspectives in musculoskeletal imaging and possible applications for the assessment of bone marrow disorders. *Br J Radiol.* 2018;91:20170886.
40. Lee SH, Lee YH, Song HT, et al. Quantitative T2 mapping of knee cartilage: comparison between the synthetic MR imaging and the CPMG sequence. *Magn Reson Med Sci.* 2018. [Epub ahead of print].
41. Landman BA, Huang AJ, Gifford A, et al. Multi-parametric neuroimaging reproducibility: a 3-T resource study. *Neuroimage.* 2011;54:2854–2866.
42. Sampat MP, Healy BC, Meier DS, et al. Disease modeling in multiple sclerosis: assessment and quantification of sources of variability in brain parenchymal fraction measurements. *Neuroimage.* 2010;52:1367–1373.
43. Huppertz HJ, Kroll-Seger J, Kloppel S, et al. Intra- and interscanner variability of automated voxel-based volumetry based on a 3D probabilistic atlas of human cerebral structures. *Neuroimage.* 2010;49:2216–2224.
44. de Boer R, Vrooman HA, Ikram MA, et al. Accuracy and reproducibility study of automatic MRI brain tissue segmentation methods. *Neuroimage.* 2010;51:1047–1056.
45. Granberg T, Uppman M, Hashim F, et al. Clinical feasibility of synthetic MRI in multiple sclerosis: a diagnostic and volumetric validation study. *AJNR Am J Neuroradiol.* 2016;37:1023–1029.
46. Akkus Z, Galimzianova A, Hoogi A, et al. Deep learning for brain MRI segmentation: state of the art and future directions. *J Digit Imaging.* 2017;30:449–459.
47. Nguyen TD, Deh K, Monohan E, et al. Feasibility and reproducibility of whole brain myelin water mapping in 4 minutes using fast acquisition with spiral trajectory and adiabatic T2prep (FAST-T2) at 3T. *Magn Reson Med.* 2016;76:456–465.



Available online at
ScienceDirect
www.sciencedirect.com

Elsevier Masson France
EM|consulte
www.em-consulte.com



Editorial

Synthetic MRI and MR fingerprinting in routine neuroimaging protocol: What's the next step?

Simultaneous relaxometry techniques to map relaxation parameters in tissues are attracting widespread interest owing to the objective quantification of tissue properties and potential reduction in the scan time. So far, synthetic MRI and MR fingerprinting (MRF) are the two major simultaneous relaxometry techniques with regulatory approval. Synthetic MRI maps T1 and T2 relaxation times and proton density and synthesizes various contrast-weighted images, including T1- and T2-weighted and fluid-attenuated inversion recovery (FLAIR) images within a single 6-min acquisition [1–3]. MRF is another promising approach to simultaneously quantify tissue properties in a clinically feasible time. Instead of performing curve fitting, as in conventional relaxometry techniques, MRF adopts a unique approach in which acquisition parameters are simultaneously varied across repetition times to generate signal evolutions that characterize the various relaxation processes unique to each tissue [4]. The acquired signal is pattern-matched to a dictionary of simulated signal evolutions to acquire various quantitative metrics, such as T1 and T2 values. Both synthetic MRI and MRF show high repeatability and reproducibility of T1 and T2 values for standardized phantoms [5–7] and in vivo [6–9]. Moreover, recent efforts have enabled high-resolution three-dimensional volume coverage of the whole brain on both synthetic MRI [10,11] and MRF [12–14]. In addition, acceleration techniques, such as simultaneous multi-slice acquisition [15], have been implemented to further accelerate scanning, making these relaxometry techniques more usable in clinical settings.

In this issue of *Journal of Neuroradiology*, Ryu et al. reported their initial experience with contrast-weighted images obtained using synthetic MRI as a routine neuroimaging protocol in daily clinical practice [16]. Contrary to many previous studies that used synthetic MRI in the research protocol, this study was unique in that it implemented synthetic MRI as the routine protocol by replacing some conventional sequences, such as T1 and T2-weighted images, with synthetic MRI. Two radiologists retrospectively reviewed the imaging data of 89 patients, rated the overall image quality and anatomical delineation, and found that the image qualities of synthetic T1- and T2-weighted images were adequate for clinical use. FLAIR images showed pronounced artifacts but without any significant impact on the diagnosis. Further, they also evaluated images obtained with synthetic phase-sensitive inversion recovery (PSIR), which is a T1-weighted sequence with a greater signal intensity range, and found that the overall image quality with anatomical delineation of PSIR was superior to that of other synthetic images. They concluded that synthetic MRI can be accepted as a routine neuroimaging protocol in the clinical practice.

Then, why have synthetic MRI and MRF not been widely accepted in the clinics, despite their potential and promising performance reported in the literature? A major challenge is the generation of high-quality synthetic images from the quantitative maps. In general, the quality of FLAIR images generated from quantitative relaxation maps is inferior to that of conventional FLAIR images, which is an essential sequence in neuroradiology. Although Ryu et al. [16] and previous studies [17,18] reported that the inferior quality of synthetic FLAIR images did not affect the diagnostic ability, clinicians may not be confident regarding its use yet. The acquisition is rapid, but adding the sequence to the protocol will prolong the total scan time. To implement synthetic MRI or MRF in a time-limited clinical workflow, some existing sequences should be replaced so that the entire protocol is not elongated. Hence, improvement of the image synthesis technique to generate high-quality contrast-weighted images would be a key step for a wide clinical implementation. Approaches that rely on a multi-component model may potentially mitigate artifacts seen on synthetic FLAIR images [19]. Adopting deep learning to directly generate contrast-weighted images while bypassing T1 and T2 maps has also been gathering considerable interest for several years [20–22]. This approach improves the FLAIR image quality and, furthermore, generates MR angiography images, which are also important in the clinical practice. Implementation of these techniques is expected to further accelerate the use of synthetic MRI and MRF in the routine clinical practice.

Disclosure of interest

The authors declare that they have no competing interest.

Grant support

This work was supported by JSPS KAKENHI grant number 18H02772 and 19K17177; and AMED under grant number 19dm0307101h0001.

References

- [1]. Warntjes JB, Leinhard OD, West J, Lundberg P. Rapid magnetic resonance quantification on the brain: optimization for clinical usage. *Magn Reson Med*. 2008;60(2):320–329.
- [2]. Andica C, Hagiwara A, Hori M, Kamagata K, Koshino S, Maekawa T, et al. Review of synthetic MRI in pediatric brains: basic principle of MR quantification, its features, clinical applications, and limitations. *J Neuroradiol*. 2019;46(4):268–275.
- [3]. Hagiwara A, Warntjes M, Hori M, Andica C, Nakazawa M, Kumamaru KK, et al. SyMRI of the brain: rapid quantification of relaxation rates and proton density,

- with synthetic mri, automatic brain segmentation, and myelin measurement. *Invest Radiol.* 2017;52(10):647–657.
- [4]. Ma D, Gulani V, Seiberlich N, Liu K, Sunshine JL, Duerk JL, et al. Magnetic resonance fingerprinting. *Nature.* 2013;495(7440):187–192.
- [5]. Jiang Y, Ma D, Keenan KE, Stupic KF, Gulani V, Griswold MA. Repeatability of magnetic resonance fingerprinting T1 and T2 estimates assessed using the ISMRM/NIST MRI system phantom. *Magn Reson Med.* 2017;78(4):1452–1457.
- [6]. Kato Y, Ichikawa K, Okudaira K, Taoka T, Kawaguchi H, Murata K, et al. Comprehensive evaluation of B1(+)-corrected FISP-based magnetic resonance fingerprinting: accuracy, repeatability and reproducibility of T1 and T2 relaxation times for ISMRM/NIST system phantom and volunteers. *Magn Reson Med Sci.* 2019. <http://dx.doi.org/10.2463/mrms.mp.2019-0016> [Online ahead of print].
- [7]. Hagiwara A, Hori M, Cohen-Adad J, Nakazawa M, Suzuki Y, Kasahara A, et al. Linearity, bias, intrascanner repeatability, and interscanner reproducibility of quantitative multidynamic multiecho sequence for rapid simultaneous relaxometry at 3T: a validation study with a standardized phantom and healthy controls. *Invest Radiol.* 2019;54(1):39–47.
- [8]. Buonincontri G, Biagi L, Retico A, Cecchi P, Cosottini M, Gallagher FA, et al. Multi-site repeatability and reproducibility of MR fingerprinting of the healthy brain at 1.5 and 3.0T. *Neuroimage.* 2019;195:362–372.
- [9]. Korzdorfer G, Kirsch R, Liu K, Pfeuffer J, Hensel B, Jiang Y, et al. Reproducibility and repeatability of MR fingerprinting relaxometry in the human brain. *Radiology.* 2019;292(2):429–437.
- [10]. Fujita S, Hagiwara A, Hori M, Warntjes M, Kamagata K, Fukunaga I, et al. 3D quantitative synthetic MRI-derived cortical thickness and subcortical brain volumes: scan-rescan repeatability and comparison with conventional T1-weighted images. *J Magn Reson Imaging.* 2019;50(6):1834–1842. <http://dx.doi.org/10.1002/jmri.26744>.
- [11]. Fujita S, Hagiwara A, Hori M, Warntjes M, Kamagata K, Fukunaga I, et al. Three-dimensional high-resolution simultaneous quantitative mapping of the whole brain with 3D-QALAS: an accuracy and repeatability study. *Magn Reson Imaging.* 2019;63:235–243.
- [12]. Cao X, Ye H, Liao C, Li Q, He H, Zhong J. Fast 3D brain MR fingerprinting based on multi-axis spiral projection trajectory. *Magn Reson Med.* 2019;82(1):289–301.
- [13]. Ma D, Jiang Y, Chen Y, McGivney D, Mehta B, Gulani V, et al. Fast 3D magnetic resonance fingerprinting for a whole-brain coverage. *Magn Reson Med.* 2018;79(4):2190–2197.
- [14]. Liao C, Bilgic B, Manhard MK, Zhao B, Cao X, Zhong J, et al. 3D MR fingerprinting with accelerated stack-of-spirals and hybrid sliding-window and GRAPPA reconstruction. *Neuroimage.* 2017;162:13–22.
- [15]. Ye H, Ma D, Jiang Y, Cauley SF, Du Y, Wald LL, et al. Accelerating magnetic resonance fingerprinting (MRF) using t-blipped simultaneous multislice (SMS) acquisition. *Magn Reson Med.* 2016;75(5):2078–2085.
- [16]. Ryu KH, Baek HJ, Moon JI, Choi BH, Park SE, Ha JY, et al. Initial clinical experience of synthetic MRI as a routine neuroimaging protocol in daily practice: a single-center study. *J Neuroradiol.* 2020;47(2):151–160.
- [17]. Tanenbaum LN, Tsiouris AJ, Johnson AN, Naidich TP, DeLano MC, Melhem ER, et al. Synthetic MRI for Clinical Neuroimaging: Results of the Magnetic Resonance Image Compilation (MAGiC) Prospective, Multicenter, Multireader Trial. *AJNR Am J Neuroradiol.* 2017;38(6):1103–1110.
- [18]. Blystad I, Warntjes JB, Smedby O, Landtblom AM, Lundberg P, Larsson EM. Synthetic MRI of the brain in a clinical setting. *Acta Radiol.* 2012;53(10):1158–1163.
- [19]. Cencini M, Buonincontri G, Biagi L, Gómez PA, Schulte RF, Tosetti M. Chasing true FLAIR: a three-component magnetic resonance fingerprinting approach to synthetic MRI. *Proceedings of the 27th Annual Meeting of ISMRM.* 2019:0816.
- [20]. Hagiwara A, Otsuka Y, Hori M, Tachibana Y, Yokoyama K, Fujita S, et al. Improving the quality of synthetic FLAIR images with deep learning using a conditional generative adversarial network for pixel-by-pixel image translation. *AJNR Am J Neuroradiol.* 2019;40(2):224–230.
- [21]. Fujita S, Hagiwara A, Otsuka Y, Hori M, Takei N, Hwang K-P, et al. Deep learning approach for generating MRA images from 3D quantitative synthetic MRI without additional scans. *Invest Radiol.* 2020. <http://dx.doi.org/10.1097/RLI.0000000000000628> [Online ahead of print].
- [22]. Virtue P, Tamir JJ, Doneva M, Yu SX, Lustig M. Learning Contrast Synthesis from MR Fingerprinting. *Proceedings of the 26th Annual Meeting of ISMRM.* 2018:0676.





Shohei Fujita^{a,b,*}
Akifumi Hagiwara^b
Shigeki Aoki^b
Osamu Abe^a

^a Department of Radiology, Graduate School of Medicine, University of Tokyo, Tokyo, Japan

^b Department of Radiology, Juntendo University Hospital, Tokyo, Japan

* Corresponding author. Department of Radiology, Graduate School of Medicine, University of Tokyo, 7-3-1, Hongo, Bunkyo-ku, Tokyo 113-8655, Japan. E-mail address: shifujita-tky@umin.ac.jp (S. Fujita)

3D Quantitative Synthetic MRI-Derived Cortical Thickness and Subcortical Brain Volumes: Scan–Rescan Repeatability and Comparison With Conventional T₁-Weighted Images

Shohei Fujita, MD,¹  Akifumi Hagiwara, MD, PhD,^{1,2*}  Masaaki Hori, MD, PhD,¹ Marcel Warntjes, PhD,^{3,4} Koji Kamagata, MD, PhD,¹ Issei Fukunaga, PhD,¹ Masami Goto, PhD,⁶ Haruyama Takuya, BS,^{1,5} Kohei Takasu, BS,⁶ Christina Andica, MD,¹  Tomoko Maekawa, MD,^{1,2} Mariko Yoshida Takemura, MD, PhD,¹ Ryusuke Irie, MD,^{1,2} Akihiko Wada, MD, PhD,¹ Michimasa Suzuki, MD, PhD,¹ and Shigeki Aoki, MD, PhD¹ 

Background: Previous quantitative synthetic MRI of the brain has been solely performed in 2D.

Purpose: To evaluate the feasibility of the recently developed sequence 3D-QALAS for brain cortical thickness and volumetric analysis.

Study Type: Reproducibility/repeatability study.

Subjects: Twenty-one healthy volunteers (35.6 ± 13.8 years).

Field Strength/Sequence: 3D T₁-weighted fast spoiled gradient recalled echo (FSPGR) sequence was performed once, and 3D-QALAS sequence was performed twice with a 3T scanner.

Assessment: FreeSurfer and FIRST were used to measure cortical thickness and volume of subcortical structures, respectively. Agreement with FSPGR and scan–rescan repeatability were evaluated for 3D-QALAS.

Statistical Tests: Percent relative difference and intraclass correlation coefficient (ICC) were used to assess reproducibility and scan–rescan repeatability of the 3D-QALAS sequence-derived measurements.

Results: Percent relative difference compared with FSPGR in cortical thickness of the whole cortex was 3.1%, and 89% of the regional areas showed less than 10% relative difference in cortical thickness. The mean ICC across all regions was 0.65, and 74% of the structures showed substantial to almost perfect agreement. For volumes of subcortical structures, the median percent relative differences were lower than 10% across all subcortical structures, except for the accumbens area, and all structures showed ICCs of substantial to almost perfect agreement. For the scan–rescan test, percent relative difference in cortical thickness of the whole cortex was 2.3%, and 97% of the regional areas showed less than 10% relative difference in cortical thickness. The mean ICC across all regions was 0.73, and 80% showed substantial to almost perfect agreement. For volumes of subcortical structures, relative differences were less than 10% across all subcortical structures except for the accumbens area, and all structures showed ICCs of substantial to almost perfect agreement.

Data Conclusion: 3D-QALAS could be reliably used for measuring cortical thickness and subcortical volumes in most brain regions.

Level of Evidence: 3

Technical Efficacy: Stage 1

J. MAGN. RESON. IMAGING 2019.

View this article online at wileyonlinelibrary.com. DOI: 10.1002/jmri.26744

Received Sep 13, 2018, Accepted for publication Mar 26, 2019.

*Address reprint requests to: A.H., Department of Radiology, Juntendo University School of Medicine, 1-2-1, Hongo, Bunkyo-ku, Tokyo 113-8421, Japan.
E-mail: a-hagiwara@juntendo.ac.jp

From the ¹Department of Radiology, Juntendo University Hospital, Tokyo, Japan; ²Department of Radiology, Graduate School of Medicine, University of Tokyo, Tokyo, Japan; ³SyntheticMR AB, Sweden; ⁴Center for Medical Imaging Science and Visualization (CMIV), Sweden; ⁵Department of Radiological Sciences, Graduate School of Human Health Sciences, Tokyo Metropolitan University, Tokyo, Japan; and ⁶School of Allied Health Sciences, Kitasato University, Kanagawa, Japan

Additional supporting information may be found in the online version of this article

This is an open access article under the terms of the Creative Commons Attribution-NonCommercial License, which permits use, distribution and reproduction in any medium, provided the original work is properly cited and is not used for commercial purposes.

TISSUE RELAXOMETRY can provide quantitative values for the evaluation of diseases,¹ development,² and aging,³ as opposed to arbitrary signal intensities of conventional magnetic resonance imaging (MRI) such as T_1 -weighted, T_2 -weighted, and FLAIR images. However, its use in human brain imaging has mostly been limited to research applications because of additional lengthy scan times. Recently, quantitative synthetic MRI, enabling simultaneous quantification of T_1 and T_2 relaxation times and proton density (PD) with high reliability,⁴ has been proposed for whole brain coverage.^{5,6} The technique also allows for the creation of any contrast-weighted image that is used routinely in clinical settings,⁷ rendering its clinical application highly feasible. Quantitative synthetic MRI has been applied to a variety of diseases, such as multiple sclerosis,^{8,9} meningitis,¹⁰ and brain infarctions,¹¹ with promising results. The original sequence used for quantitative synthetic MRI was based on a multislice 2D acquisition, providing a relatively low resolution in the slice direction in comparison to conventional 3D T_1 -weighted acquisitions. Recently, however, 3D-QALAS (3D-quantification using an interleaved Look-Locker acquisition sequence with T_2 preparation pulse) has been developed for simultaneous quantification of T_1 and T_2 in cardiac imaging, showing high accuracy and precision in the heart and phantoms with various tissue properties.^{12,13}

As opposed to relaxometry, volumetric analysis of the brain has already been widely performed in clinical settings, such as for the evaluation of patients with neurodegenerative¹⁴ and demyelinating disorders.¹⁵ Additionally, regional volumetric analysis has been extensively performed in research settings. Changes in cortical thickness and subcortical volumes are related to aging^{16–18} and in a wide variety of neurological disorders.^{14,16,19} Taken together, differences in regional cortical thickness and subcortical volume may indicate the state of neurological health, and their accurate measurements may lead to a better understanding of patients' conditions.

Here, we propose application of the 3D-QALAS sequence for simultaneous acquisition of relaxometry parameters as well as for obtaining volumetric information in high-resolution 3D. Therefore, the purpose of this study was to show the validity of volumetric information acquired with 3D-QALAS by 1) evaluating the reproducibility of 3D-QALAS sequence-derived volumetric brain measurements using conventional T_1 -weighted imaging-derived measurements as reference standards, and 2) evaluating the repeatability of 3D-QALAS sequence-derived measurements by scan–rescan tests, on healthy subjects.

Materials and Methods

Subjects

This study was approved by our Institutional Review Board and written informed consent was acquired from all participants. Twenty-one healthy volunteers were included in this study (14 women and 7 men; mean age, 35.6 ± 13.8 years). None of the participants had a history of a major medical condition including neurological or psychiatric disorders. Two

radiologists (S.F. and A.H.) performed a blind examination on all volunteer exams and confirmed that all had normal structural MRI results.

Image Acquisition

All participants were scanned with a 3T scanner (Discovery 750w; GE Healthcare, Milwaukee, WI) with a 12-channel head coil. A 3D T_1 -weighted fast spoiled gradient recalled echo (FSPGR) sequence was performed once, and the 3D-QALAS sequence was performed twice (to test scan–rescan) in the same session on all the participants. Between scan–rescan of the 3D-QALAS sequence, the subjects were taken out of the MRI room and repositioned on the scanner. The scan parameters of FSPGR were as follows: sagittal acquisition; repetition time / echo time / inversion time (TR/TE/TI), 7.7/3.1/400 msec; field of view (FOV), 256×256 mm; matrix size, 256×256 ; section thickness, 1.0 mm; flip angle, 11° ; receiver bandwidth, 244.1 Hz/pixel; averages, 1; acquisition time, 5 min 45 sec. 3D-QALAS is based on a multiacquisition 3D gradient echo, with five acquisitions equally spaced in time, interleaved with a T_2 preparation pulse and an inversion pulse. Briefly, T_1 fitting was performed on four acquisitions after the inversion pulse, and T_2 fitting was performed on extrapolation of the signal intensity straddling the T_2 prep pulse. Instead of a cardiac trigger, an internal trigger started each of the five acquisitions every 900 msec, making the total cycle time 4.5 sec. Further details of the 3D-QALAS sequence and its postprocessing are available in a previous study.¹² The scan parameters of 3D-QALAS were as follows: axial acquisition; TR/TE/TI, 8.6/3.5/100 msec; FOV, 256×256 ; matrix size, 256×256 ; section thickness, 1.0 mm; flip angle, 5° ; receiver bandwidth, 97.7 Hz/pixel; averages, 1; acquisition time, 11 min 41 sec. We set the spatial resolution of the FSPGR imaging, standard reference in this study, as 1.0 mm isotropic, since the Alzheimer's Disease Neuroimaging Initiative (ADNI)²⁰ study recommended the usage of 1.0 mm isotropic data at 3T. All 3D-QALAS and FSPGR images were visually examined for artifacts such as ringing, blurring, and ghosting on site upon image acquisition. Images exhibiting these common artifacts were excluded from this study and subjects with such artifacts were rescanned.

Image Postprocessing

Images obtained from the 3D-QALAS sequence were processed on a prototype version 0.45.5 of the SyMRI software (SyntheticMR, Linköping, Sweden) to synthesize 3D synthetic T_1 -weighted images. TR and TE were virtually set to the default values of 500 msec and 10 msec, respectively. These 3D synthetic T_1 -weighted images and FSPGR images were used for subsequent analyses. Noncommercial automatic brain parcellation programs, described below, were used to measure cortical thickness and the volume of subcortical structures on the basis of 3D T_1 -weighted images for each subject.

MEASUREMENT OF CORTICAL THICKNESS AND VOLUME.

The pipeline of FreeSurfer (v. 5.3.0, <http://surfer.nmr.mgh.harvard.edu>) was used to obtain cortical thickness and volume for each sequence. FreeSurfer utilizes affine transformations and combines information about voxel intensity relative to a probability distribution for tissue classes with information about the spatial relationship of the voxel to the location of neighboring structures obtained from a manually labeled atlas.^{21,22} The Desikan-Killiany Atlas, consisting of 34 regions per hemisphere,

was used to measure average cortical thickness and volume in each area.¹⁸ Further details of FreeSurfer are available in previous articles,^{21,22} and in the documentation provided by the developers (<http://surfer.nmr.mgh.harvard.edu/>). The default analysis settings were used in running the “recon-all” command. Bilateral regional values were averaged for further analysis. Previous research has shown that brain mask cleaning was the only type of manual intervention that improved FreeSurfer-derived results.²³ Therefore, manual brain mask assessment was performed in this study. For each subject, the brain mask was visually assessed on axial, sagittal, and coronal images. Brain masks excluding brain tissue (overcropping) were manually corrected using the Freeview application. A brain mask including extracerebral tissue, such as orbit (undercropping), was not corrected because it still allowed accurate surface demarcation.

VOLUMETRY OF SUBCORTICAL STRUCTURES. Due to high variability in the spatial location and extent of subcortical gray matter segmentations produced by FreeSurfer,²¹ the volumes of subcortical gray matter structures were obtained using the pipeline of FMRIB Integrated Registration and Segmentation Tool (FIRST, <http://fsl.fmrib.ox.ac.uk/fsl/fslwiki/FIRST>) implemented in the FMRIB Software Library v. 5.0.9.²⁴ The volumes of subcortical white matter structures were obtained based on FreeSurfer using the Desikan-Killiany Atlas. Volumes of subcortical structures were measured for each sequence. All segmentation results performed on FreeSurfer and FIRST were visually screened for gross errors.

Statistical Analysis

All statistical analyses were performed with R program v. 3.3.0 (R Core Team [2016]. R: A language and environment for statistical computing. R Foundation for Statistical Computing, Vienna, Austria. URL <https://www.R-project.org/>). Agreement to measurements obtained from FSPGR and scan–rescan repeatability were evaluated for 3D-QALAS. Percent relative difference and intraclass correlation coefficient (ICC) were used to assess reproducibility and repeatability of the 3D-QALAS sequence-derived measurements. Within-subject coefficient of variation (wCV) was also used in assessing repeatability. ICC is a measure of within-subject relative to between-subject variability. The ICC estimates of agreement were categorized as the following: slight (0.01–0.20), fair (0.21–0.40), moderate (0.41–0.60), substantial (0.61–0.80), and almost perfect agreement (0.81–1.0).²⁵ Percent relative difference was calculated

by dividing the absolute difference by the mean of two measurements, defined as follows:

$$\text{percent relative difference} = \frac{2|X - Y|}{X + Y} \times 100$$

where X and Y are the measured values. The wCV was defined as follows:

$$\text{wCV} = \frac{\sigma_w}{\mu} \times 100$$

where σ_w is the within-subject standard deviation and μ is the overall mean of the measured values.

Results

Representative FreeSurfer and FIRST outputs from 3D-QALAS sequence-derived T₁-weighted images are shown in Fig. 1.

Measurement of Cortical Thickness

REPRODUCIBILITY OF 3D-QALAS SEQUENCE-DERIVED CORTICAL THICKNESS AND VOLUME: COMPARISON WITH CONVENTIONAL FSPGR. Figure 2 shows a histogram of 3D-QALAS and FSPGR sequence-derived cortical thickness estimated using FreeSurfer across all regions in the Desikan-Killiany Atlas in all subjects. The range of the cortical thicknesses in this study was consistent with previous studies, reporting cortical thickness ranging from 1–4.5 mm (both of postmortem and FreeSurfer-based findings).^{18,23,26} In Fig. 3a, regional percent relative differences between 3D-QALAS and FSPGR-derived cortical thicknesses are overlaid on an inflated brain. Figure 3b shows the boxplots for percent relative differences. Percent relative difference of the whole cortex was 3.1%, and 89% of the regional areas showed less than 10% relative difference in cortical thickness. Cortical thickness of the temporal pole, inferior temporal, pericalcarine, fusiform, and entorhinal cortex showed relatively low agreement. Table 1 shows the ICCs for 3D-QALAS and FSPGR-derived cortical thickness. The mean ICC across all regions was 0.65, and 74% of the structures showed substantial to almost perfect agreement. Cortical thickness of the temporal pole, entorhinal, lateral orbitofrontal, pars orbitalis, inferior temporal, pericalcarine, and the fusiform cortex showed particularly low

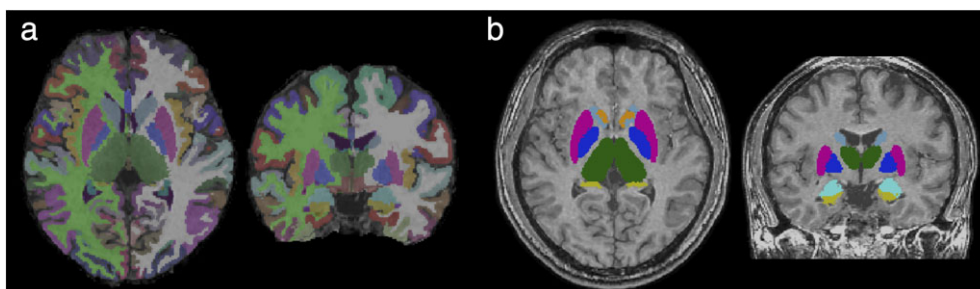


FIGURE 1: Representative labels created from automated parcellation of brain regions using (a) FreeSurfer and (b) FIRST. Results of segmentation are overlaid on synthetic T₁-weighted images.

ICC. Supplementary Table 1 shows the ICCs for 3D-QALAS and FSPGR-derived cortical volume. The mean ICC across all regions was 86%, and 97% of the structures showed substantial to almost perfect agreement. Cortical thickness of the temporal pole showed particularly low ICC.

SCAN-RESCAN REPEATABILITY OF 3D-QALAS SEQUENCE-DERIVED CORTICAL THICKNESS AND VOLUME. In Fig. 4a, regional percent relative differences between scan and rescan of 3D-QALAS-derived cortical thicknesses are overlaid on an inflated brain. Figure 4b shows the boxplots for percent relative differences. Relative percent difference in thickness of the whole cortex was 2.3%, and 97% of the regional cortical thickness showed less than 10% relative difference. Cortical thickness of the temporal pole showed relatively low agreement. Table 1 shows ICCs and wCV for scan-rescan cortical thickness. The mean ICC across all regions was 0.73, and 80% of the structures showed substantial to almost perfect agreement. Temporal pole, entorhinal, pars orbitalis, inferior temporal, and the orbitofrontal cortical thickness showed particularly low ICC and/or wCV. Supplementary Table 1 shows ICCs and wCV for scan-rescan cortical volume. The mean ICC across all regions was 87%, and 94% of the structures showed substantial to almost perfect agreement. Temporal pole and entorhinal cortical volumes showed particularly low ICC and wCV. The 3D-QALAS sequence-derived cortical volume of each region is listed in Supplementary Table 2.

Volumetry of Subcortical Structures

REPRODUCIBILITY OF 3D-QALAS SEQUENCE-DERIVED SUBCORTICAL STRUCTURAL VOLUMES: COMPARISON WITH CONVENTIONAL FSPGR. Figure 5a shows the percent relative differences between 3D-QALAS and FSPGR-derived measurements in subcortical gray matter structural volumes. The median percent relative differences were lower than 10% across

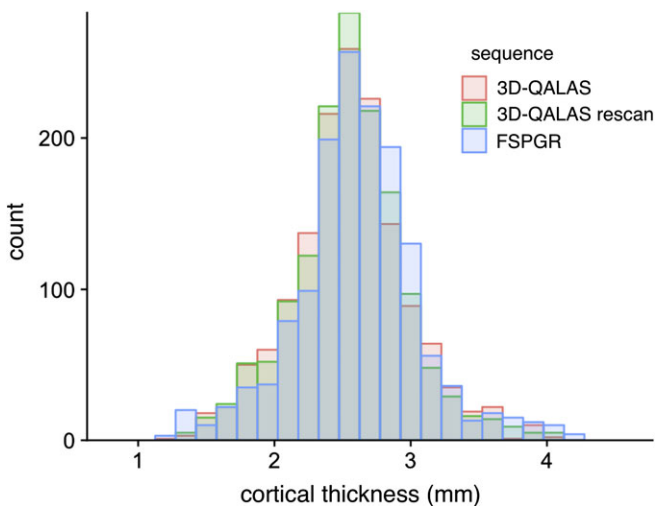


FIGURE 2: Histograms of cortical thicknesses derived from 3D-QALAS scan-rescan and FSPGR in all subjects measured using FreeSurfer.

all subcortical structures, except for the accumbens area. ICC for 3D-QALAS and FSPGR-derived measurements are shown in Table 2. All structures showed substantial or almost perfect agreement. Supplementary Table 3 shows the ICCs for 3D-QALAS and FSPGR-derived white matter volume. All structures except subcortical white matter of the temporal pole showed substantial or almost perfect agreement.

SCAN-RESCAN REPEATABILITY OF 3D-QALAS SEQUENCE-DERIVED SUBCORTICAL STRUCTURAL VOLUMES. Figure 5b shows the percent relative difference between scan and rescan of 3D-QALAS-derived measurements in subcortical gray matter structural volumes. Percent relative differences were less than 10% across all subcortical structures, except for the accumbens area. ICC and wCV for 3D-QALAS and FSPGR-derived measurements are shown in Table 2. All structures showed substantial to almost perfect agreement. The wCVs were lower than 10% across all subcortical structures, except for the accumbens area. Supplementary Table 3 shows the ICCs and wCV for scan-rescan white matter volume. All structures except subcortical white matter of entorhinal and frontal pole showed substantial or almost perfect agreement. The 3D-QALAS sequence-derived volume of each subcortical structure is listed in Supplementary Table 4.

Discussion

In this study, 3D synthetic T_1 -weighted images showed good agreement with the FSPGR 1.0 mm isotropic images in measuring regional cortical thickness and subcortical volumes in most of the brain regions. High repeatability of the 3D synthetic MRI-derived brain measurements was demonstrated in the scan-rescan test.

The 3D isotropic acquisition of 3D-QALAS allows high resolution multiplanar reconstruction, without additional scans from different directions. This capability not only provides the advantage in visual assessment and delineation of lesions, but also enables to accurately segment regional structures. With the quantification of T_1 , T_2 , and PD in these regional structures, 3D-QALAS may enable detecting and describing changes within regional structures, which could be obscured when averaging values over gross anatomic regions. Hence, 3D-QALAS has a potential to provide thorough and comprehensive characterization of brain lesions as well as the entire brain.

Cortical thickness derived from 3D synthetic T_1 -weighted and FSPGR images showed a percent relative difference of 3.1% in the whole cortex, and 89% of the regional areas showed less than 10% relative difference in cortical thickness. Although high agreements were shown in the majority of the brain regions, low agreements were found in cortical thickness of temporal pole, inferior temporal, pericalcarine, and fusiform, as shown by their median percent relative differences of more than 10%. This observation is consistent with previous studies using FreeSurfer that reported a negative relationship between cortical volume/surface

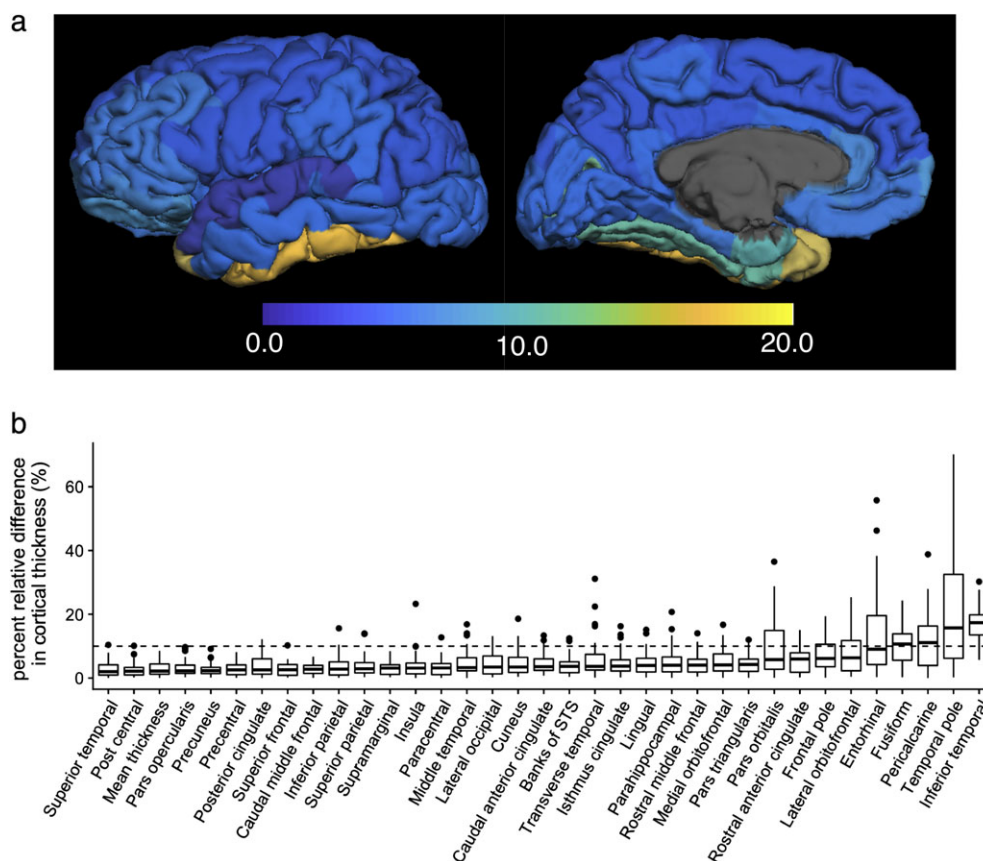


FIGURE 3: Percent relative difference in cortical thickness for 3D-QALAS and FSPGR measured using FreeSurfer. Regional percent relative difference is overlaid on an inflated brain surface (a). Median values and interquartile ranges are shown in boxplots (b). Whiskers are set at minimum and maximum, and the horizontal line marks the median. Boxes indicate the interquartile range (25–75%). Dots at the end of the boxplot represent outliers.

area and relative error of measured cortical thickness,^{23,27} which can explain low agreement in the small structures in the current study. It has also been reported that the boundaries of the temporal pole and occipital lobe were not defined precisely using FreeSurfer,²⁸ which may explain the low agreement in thickness of the temporal pole and pericalcarine.

Another possibility of the low agreements in lower parts of the brain structure is the effects of B_0 inhomogeneities due to susceptibility differences between bone and air, which could cause fitting errors upon quantifying T_1 , T_2 , and PD, and affect the subsequent synthetic T_1 -weighted images.²⁹

The cortical thickness derived from scan–rescan of 3D synthetic T_1 -weighted images showed less than a 10% relative percent difference across all regions except the thickness of the temporal pole. A previous study that included a large collection of cortical thickness data based on scan–rescan of conventional 3D magnetization prepared rapid acquisition with gradient echo (MPRAGE) images showed overall percent relative differences of 2.5–2.8% using FreeSurfer.²⁷ The median percent relative differences of 3D synthetic T_1 -weighted image-derived cortical thickness in our study was 2.9%, which is comparable to the repeatability achieved when using conventional 3D T_1 -weighted images.

Subcortical volumes derived from 3D synthetic T_1 -weighted and FSPGR images showed a percent relative difference lower than 10% across all structures except the nucleus accumbens, and the scan–rescan test of 3D synthetic T_1 -weighted images showed a percent relative difference lower than 10% across all subcortical structures. Segmentation of the accumbens and amygdala showed relatively low agreement both in scan–rescan and comparison with FSPGR in this study, which is consistent with previous studies reporting that segmentation of these area was generally unreliable compared with other subcortical regions.^{30,31} One factor that may have contributed to this lower reliability in measurements is that they are the smallest subcortical structures. Morey et al³¹ reported that the percent relative difference of the accumbens and amygdala volumes, calculated from scan–rescan of 3D T_1 -weighted images with 1.0 mm isotropic voxel based on FIRST analysis, were both higher than 10%. Taken together, 3D synthetic T_1 -weighted imaging-based subcortical volume measurement can be assumed to be as reliable as conventional 3D T_1 -weighted imaging-based measurement.

Although the in-plane resolution of 1.0 mm used in this study is low compared with that of commonly used 2D sequences, high spatial resolution in the slice-select direction enables reliable detection and reproducible measurements

TABLE 1. Intraclass Correlation Coefficients and Within-Subject Coefficients of Variation Between 3D-QALAS and FSPGR, and Scan-Rescan of 3D-QALAS for Cortical Thicknesses Measured Using FreeSurfer

Measurement	FSPGR	Rescan	ICC
	ICC	wCV (%)	
Thickness			
Mean thickness	0.79	2.1	0.81
Caudal anterior cingulate	0.75	3.9	0.73
Caudal middle frontal	0.84	2.3	0.86
Cuneus	0.63	3.5	0.75
Entorhinal	0.28	9.4	0.50
Frontal pole	0.65	8.0	0.59
Fusiform	0.44	3.2	0.68
Inferior parietal	0.73	3.0	0.79
Inferior temporal	0.47	5.0	0.36
Insula	0.66	3.9	0.65
Isthmus cingulate	0.79	3.9	0.83
Lateral occipital	0.61	2.8	0.78
Lateral orbitofrontal	0.38	6.1	0.52
Lingual	0.62	3.0	0.72
Medial orbitofrontal	0.51	4.9	0.58
Middle temporal	0.75	4.1	0.66
Parahippocampal	0.86	3.4	0.90
Paracentral	0.77	3.8	0.75
Pars opercularis	0.79	2.2	0.87
Pars orbitalis	0.38	9.7	0.43
Pars triangularis	0.76	3.5	0.80
Pericalcarine	0.49	5.5	0.68
Postcentral	0.87	2.5	0.86
Posterior cingulate	0.71	3.1	0.81
Precentral	0.70	2.3	0.77
Precuneus	0.78	1.7	0.91
Rosterior anterior cingulate	0.63	4.8	0.69
Rostral middle frontal	0.55	3.1	0.75
Superior frontal	0.80	1.9	0.87
Superior parietal	0.78	1.9	0.90
Superior temporal	0.80	2.9	0.78
Supramarginal	0.84	2.8	0.81
Temporal pole	0.00	12.3	0.48
Transverse temporal	0.62	5.0	0.70

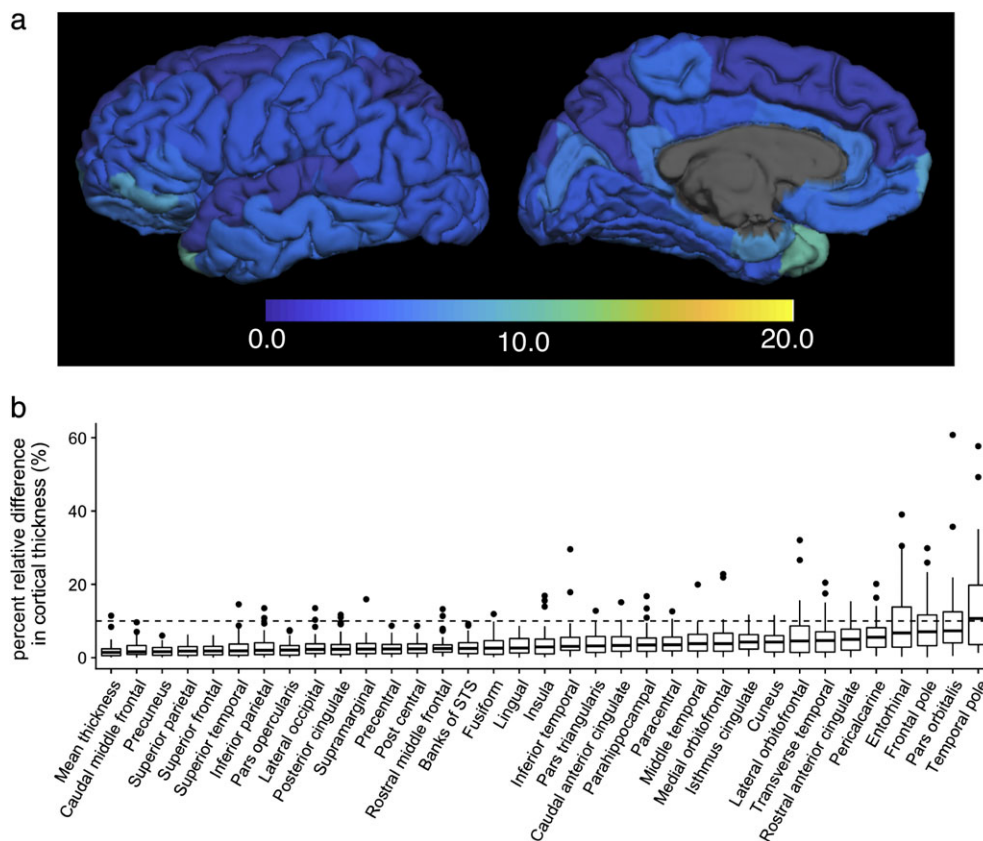


FIGURE 4: Percent relative difference in cortical thickness for 3D-QALAS scan-rescan, measured using FreeSurfer. Regional percent relative difference is overlaid on an inflated brain surface (a). Median values and interquartile ranges are shown in boxplots (b). Whiskers are set at minimum and maximum, and the horizontal line marks the median. Boxes indicate the interquartile range (25–75%). Dots at the end of the boxplot represent outliers.

among various slice positions and alignments. In fact, previous studies have shown that 3D imaging could be superior in detecting multiple sclerosis lesions and brain metastases than 2D imaging, even with lower in-plane resolutions.^{32,33}

We used T₁-weighted images only with fixed TR and TE for segmentation in this study. Using multichannel inputs (eg, T₁, T₂, and PD maps), obtained from a single 3D-QALAS sequence scan, could improve the accuracy of current segmentation algorithms that rely heavily on T₁-weighted image contrasts,

without elongating scanning times. Furthermore, even with only T₁-weighting, combining T₁-weighted images with different parameters might improve the overall segmentation, since T₁-weighted images with fixed TR and TE may not be optimal for all brain structures. An additional advantage of synthetic MRI based on relaxation parameters is that the effects of B₁ inhomogeneities and coil sensitivity profiles on the T₁-weighted images are removed.³⁴ This is expected to provide a more stable result in volumetric analysis.

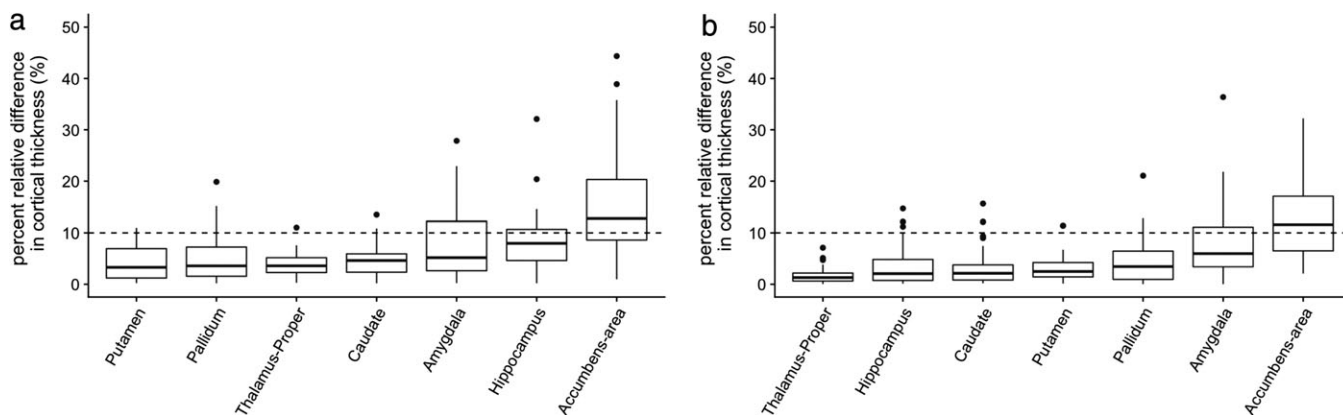


FIGURE 5: Percent relative difference of subcortical volumes measured using FIRST. (a) and (b) show comparisons between 3D-QALAS and FSPGR, and scan-rescan of 3D-QALAS, respectively. Whiskers are set at minimum and maximum, and the horizontal line marks the median. Boxes indicate the interquartile range (25–75%). Dots at the end of the boxplot represent outliers.

TABLE 2. Intraclass Correlation Coefficients and Within-Subject Coefficients of Variation Between 3D-QALAS and FSPGR, and Scan–Rescan of 3D-QALAS for Subcortical Volumes Measured Using FIRST

Measurement	FSPGR	Rescan	ICC
	ICC	wCV (%)	
Volume			
Putamen	0.86	2.9	0.91
Caudate nucleus	0.89	3.3	0.89
Nucleus accumbens	0.82	13.3	0.80
Globus pallidus	0.86	4.5	0.87
Hippocampus	0.84	3.5	0.91
Amygdala	0.66	7.6	0.72
Thalamus	0.91	1.5	0.96

Absolute quantification of tissue properties using relaxometry has been previously reported to be useful for the characterization of disease, assessment of disease activity, and monitoring of treatment.^{35,36} With accurate volumetric segmentation, 3D synthetic MRI could provide quantitative values of each brain substructure based on a single scan, which could allow for a more quantitative understanding of the brain.

The current study has several limitations. First, we only used a single 3T scanner, hence our results cannot be generalized to scanners with different field strengths. Previous studies have revealed certain biases between 1.5T and 3T for cortical thickness analysis and brain volumetry performed on FreeSurfer using 3D T₁-weighted images.^{37,38} Further research is needed to determine whether cortical thickness analysis and subcortical brain volumetry based on 3D-QALAS differ between different field strengths. Second, we used FSPGR as a standard reference, not with ground truth postmortem values. Although the ground truth for cortical thickness and subcortical volumes were not available, our results showed agreement with previous studies that compared FreeSurfer-derived measurements with postmortem values. Third, the scanning time in this study was relatively long for a routine clinical scan, making it difficult to use in clinical settings. Combining techniques such as compressed sensing³⁹ and multiband imaging⁴⁰ may further reduce scan times to a clinically applicable level. Fourth, only healthy volunteers were enrolled in this study. Although our goal in this study was not to compare patients and volunteers, future studies focusing on patients using 3D-QALAS are desired.

In conclusion, the current study may support the use of 3D quantitative synthetic MRI for reliably measuring cortical thickness and subcortical volumes in human brain, with the exceptions

of the nucleus accumbens, and thickness of temporal pole, entorhinal, inferior temporal, pericalcarine, and the fusiform.

Acknowledgment

Contract grant sponsor: Program for Brain Mapping by Integrated Neurotechnologies for Disease Studies (Brain/MINDS) from Japan Agency for Medical Research and Development, AMED; Contract grant sponsor: IMPACT Program of Council for Science, Technology and Innovation (Cabinet Office, Government of Japan); Contract grant sponsor: JSPS KAKENHI; Contract grant numbers: 16K10327, 19K17150, 19K17177, JP16H06280; Contract grant sponsor: Grant-in-Aid for Scientific Research on Innovative Areas, Resource and technical support platforms for promoting research “Advanced Bioimaging Support.”

Conflict of Interest

Marcel Warntjes is currently employed part-time at SyntheticMR and has stock in SyntheticMR.

References

- Bottomley PA, Hardy CJ, Argersinger RE, Allen-Moore G. A review of 1H nuclear magnetic resonance relaxation in pathology: Are T1 and T2 diagnostic? *Med Phys* 1987;14:1–37.
- Lee SM, Choi YH, You SK, et al. Age-related changes in tissue value properties in children: simultaneous quantification of relaxation times and proton density using synthetic magnetic resonance imaging. *Invest Radiol* 2018;53:236–245.
- Kumar R, Delshad S, Woo MA, Macey PM, Harper RM. Age-related regional brain T2-relaxation changes in healthy adults. *J Magn Reson Imaging* 2012;35:300–308.
- Hagiwara A, Hori M, Cohen-Adad J, et al. Linearity, bias, intra-scanner repeatability, and inter-scanner reproducibility of quantitative multi-echo sequence for rapid simultaneous relaxometry at 3T: A validation study with a standardized phantom and healthy controls. *Invest Radiol* 2019;54:39–47.
- Warntjes JB, Leinhard OD, West J, Lundberg P. Rapid magnetic resonance quantification on the brain: Optimization for clinical usage. *Magn Reson Med* 2008;60:320–329.
- Hagiwara A, Warntjes M, Hori M, et al. SyMRI of the brain: Rapid quantification of relaxation rates and proton density, with synthetic MRI, automatic brain segmentation, and myelin measurement. *Invest Radiol* 2017;52:647–657.
- Tanenbaum LN, Tsiouris AJ, Johnson AN, et al. Synthetic MRI for clinical neuroimaging: Results of the Magnetic Resonance Image Compilation (MAGiC) prospective, multicenter, multireader trial. *AJNR Am J Neuroradiol* 2017;38:1103–1110.
- Hagiwara A, Hori M, Yokoyama K, et al. Synthetic MRI in the detection of multiple sclerosis plaques. *AJNR Am J Neuroradiol* 2017;38:257–263.
- Granberg T, Uppman M, Hashim F, et al. Clinical feasibility of synthetic MRI in multiple sclerosis: A diagnostic and volumetric validation study. *AJNR Am J Neuroradiol* 2016;37:1023–1029.
- Andica C, Hagiwara A, Nakazawa M, et al. Synthetic MR imaging in the diagnosis of bacterial meningitis. *Magn Reson Med Sci* 2017;16:91–92.
- Wallaert L, Hagiwara A, Andica C, et al. The advantage of synthetic MRI for the visualization of anterior temporal pole lesions on double inversion recovery (DIR), phase-sensitive inversion recovery (PSIR), and myelin images in a patient with CADASIL. *Magn Reson Med Sci* 2018;17:275–276.

12. Kvernby S, Warntjes MJ, Haraldsson H, Carlhall CJ, Engvall J, Ebberts T. Simultaneous three-dimensional myocardial T1 and T2 mapping in one breath hold with 3D-QALAS. *J Cardiovasc Magn Reson* 2014;16:102.
13. Kvernby S, Warntjes M, Engvall J, Carlhall CJ, Ebberts T. Clinical feasibility of 3D-QALAS — Single breath-hold 3D myocardial T1- and T2-mapping. *Magn Reson Imaging* 2017;38:13–20.
14. Scahill RI, Schott JM, Stevens JM, Rossor MN, Fox NC. Mapping the evolution of regional atrophy in Alzheimer's disease: Unbiased analysis of fluid-registered serial MRI. *Proc Natl Acad Sci U S A* 2002;99:4703–4707.
15. Sinnecker T, Granziera C, Wuerfel J, Schlaeger R. Future brain and spinal cord volumetric imaging in the clinic for monitoring treatment response in MS. *Curr Treat Options Neurol* 2018;20:17.
16. Fotenos AF, Snyder AZ, Girton LE, Morris JC, Buckner RL. Normative estimates of cross-sectional and longitudinal brain volume decline in aging and AD. *Neurology* 2005;64:1032–1039.
17. Resnick SM, Pham DL, Kraut MA, Zonderman AB, Davatzikos C. Longitudinal magnetic resonance imaging studies of older adults: A shrinking brain. *J Neurosci* 2003;23:3295–3301.
18. Desikan RS, Segonne F, Fischl B, et al. An automated labeling system for subdividing the human cerebral cortex on MRI scans into gyral based regions of interest. *Neuroimage* 2006;31:968–980.
19. Konarski JZ, McIntyre RS, Kennedy SH, Rafi-Tari S, Soczynska JK, Ketter TA. Volumetric neuroimaging investigations in mood disorders: Bipolar disorder versus major depressive disorder. *Bipolar Disord* 2008;10:1–37.
20. Jack CR Jr, Bernstein MA, Fox NC, et al. The Alzheimer's Disease Neuroimaging Initiative (ADNI): MRI methods. *J Magn Reson Imaging* 2008;27:685–691.
21. Dale AM, Fischl B, Sereno MI. Cortical surface-based analysis. I. Segmentation and surface reconstruction. *Neuroimage* 1999;9:179–194.
22. Fischl B. *FreeSurfer*. *Neuroimage* 2012;62:774–781.
23. Iscan Z, Jin TB, Kendrick A, et al. Test-retest reliability of *FreeSurfer* measurements within and between sites: Effects of visual approval process. *Hum Brain Mapp* 2015;36:3472–3485.
24. Patenaude B, Smith SM, Kennedy DN, Jenkinson M. A Bayesian model of shape and appearance for subcortical brain segmentation. *Neuroimage* 2011;56:907–922.
25. Landis JR, Koch GG. The measurement of observer agreement for categorical data. *Biometrics* 1977;33:159–174.
26. Salat DH, Lee SY, van der Kouwe AJ, Greve DN, Fischl B, Rosas HD. Age-associated alterations in cortical gray and white matter signal intensity and gray to white matter contrast. *Neuroimage* 2009;48:21–28.
27. Tustison NJ, Cook PA, Klein A, et al. Large-scale evaluation of ANTs and *FreeSurfer* cortical thickness measurements. *Neuroimage* 2014;99:166–179.
28. Destrieux C, Fischl B, Dale A, Halgren E. Automatic parcellation of human cortical gyri and sulci using standard anatomical nomenclature. *Neuroimage* 2010;53:1–15.
29. Huang H, Ceritoglu C, Li X, et al. Correction of B0 susceptibility induced distortion in diffusion-weighted images using large-deformation diffeomorphic metric mapping. *Magn Reson Imaging* 2008;26:1294–1302.
30. Nugent AC, Luckenbaugh DA, Wood SE, Bogers W, Zarate CA Jr, Drevets WC. Automated subcortical segmentation using FIRST: Test-retest reliability, interscanner reliability, and comparison to manual segmentation. *Hum Brain Mapp* 2013;34:2313–2329.
31. Morey RA, Selgrade ES, Wagner HR 2nd, Huettel SA, Wang L, McCarthy G. Scan-rescan reliability of subcortical brain volumes derived from automated segmentation. *Hum Brain Mapp* 2010;31:1751–1762.
32. Tan IL, van Schijndel RA, Pouwels PJ, Ader HJ, Barkhof F. Serial isotropic three-dimensional fast FLAIR imaging: Using image registration and subtraction to reveal active multiple sclerosis lesions. *AJR Am J Roentgenol* 2002;179:777–782.
33. Takeda T, Takeda A, Nagaoka T, et al. Gadolinium-enhanced three-dimensional magnetization-prepared rapid gradient-echo (3D MP-RAGE) imaging is superior to spin-echo imaging in delineating brain metastases. *Acta Radiol* 2008;49:1167–1173.
34. Warntjes JB, Dahlqvist O, Lundberg P. Novel method for rapid, simultaneous T1, T2*, and proton density quantification. *Magn Reson Med* 2007;57:528–537.
35. West J, Aalto A, Tisell A, et al. Normal appearing and diffusely abnormal white matter in patients with multiple sclerosis assessed with quantitative MR. *PLoS One* 2014;9:e95161.
36. Hagiwara A, Hori M, Yokoyama K, et al. Utility of a multiparametric quantitative MRI model that assesses myelin and edema for evaluating plaques, periplaque white matter, and normal-appearing white matter in patients with multiple sclerosis: A feasibility study. *AJNR Am J Neuroradiol* 2017;38:237–242.
37. Pfefferbaum A, Rohlfing T, Rosenbloom MJ, Sullivan EV. Combining atlas-based parcellation of regional brain data acquired across scanners at 1.5 T and 3.0 T field strengths. *Neuroimage* 2012;60:940–951.
38. Han X, Jovicich J, Salat D, et al. Reliability of MRI-derived measurements of human cerebral cortical thickness: The effects of field strength, scanner upgrade and manufacturer. *Neuroimage* 2006;32:180–194.
39. Lustig M, Donoho D, Pauly JM. Sparse MRI: The application of compressed sensing for rapid MR imaging. *Magn Reson Med* 2007;58:1182–1195.
40. Feinberg DA, Moeller S, Smith SM, et al. Multiplexed echo planar imaging for sub-second whole brain fMRI and fast diffusion imaging. *PLoS One* 2010;5:e15710.



Original contribution

Three-dimensional high-resolution simultaneous quantitative mapping of the whole brain with 3D-QALAS: An accuracy and repeatability study



Shohei Fujita^{a,b}, Akifumi Hagiwara^{a,*}, Masaaki Hori^c, Marcel Warntjes^{d,e}, Koji Kamagata^a, Issei Fukunaga^a, Christina Andica^a, Tomoko Maekawa^{a,b}, Ryusuke Irie^{a,b}, Mariko Yoshida Takemura^a, Kanako Kunishima Kumamaru^a, Akihiko Wada^a, Michimasa Suzuki^a, Yutaka Ozaki^a, Osamu Abe^b, Shigeki Aoki^a

^a Department of Radiology, Juntendo University Hospital, Tokyo, Japan

^b Department of Radiology, Graduate School of Medicine, The University of Tokyo, Tokyo, Japan

^c Department of Radiology, Toho University Omori Medical Center, Tokyo, Japan

^d SyntheticMR AB, Sweden

^e Center for Medical Imaging Science and Visualization (CMIV), Sweden

ARTICLE INFO

Keywords:

Myelin
Proton density
Quantitative magnetic resonance imaging
Relaxation time
Relaxometry
Synthetic magnetic resonance imaging

ABSTRACT

Background: Previous methods for the quantification of brain tissue properties by magnetic resonance imaging were mainly based on two-dimensional acquisitions and were thus limited to a relatively low resolution in the slice direction compared to three-dimensional (3D) acquisitions. The 3D-quantification using an interleaved Look-Locker acquisition sequence with a T2 preparation pulse (3D-QALAS) sequence may allow for simultaneous acquisition of relaxometry parameters in high spatial resolution.

Purpose: To evaluate bias, linearity, and day-to-day repeatability of relaxometry parameters, as well as tissue fraction maps, acquired with 3D-QALAS.

Materials and methods: Scan-rescan test of the 3D-QALAS sequence was performed on a 1.5-T scanner with the International Society for Magnetic Resonance in Medicine/National Institute of Standards and Technology system phantom and 10 healthy volunteers (7 male, 3 female; mean age, 23.2 ± 3.6 years). Simple linear regression analysis, Bland-Altman plots, and intrasubject coefficients of variation (CV) were used to assess the reliability of 3D-QALAS sequence-derived parameters. The T1, T2, proton density (PD), and myelin volume fraction (MVF) of *in vivo* brain regions were compared with values obtained using the multidynamic multi-echo sequence.

Results: In the phantom study, the T1, T2, and PD values measured by 3D-QALAS showed strong linearity with the reference values ($R^2 = 0.998, 0.998, \text{ and } 0.960$ for T1, T2, and PD, respectively) and high repeatability (mean CV of 1.2%, 2.8%, and 2.9% for T1, T2, and PD, respectively). The T1, T2, PD, and MVF values of *in vivo* brain regions obtained with 3D-QALAS were highly consistent within subjects, with mean intrasubject CVs of 0.5%, 0.5%, 0.4%, and 1.6% for the T1, T2, PD, and MVF values, respectively.

Conclusion: 3D-QALAS enables reliable measurement of T1, T2, PD, and MVF values of the whole brain in high spatial resolution across a clinically-relevant dynamic range.

1. Introduction

Quantification of brain tissue properties using magnetic resonance imaging (MRI) has been widely used for the assessment of normal development [1,2], aging [3–5], and diseases [6–9]. Quantitative MRI

approaches allow for more objective, repeatable, and reliable evaluation of the tissue than does conventional MRI, which only allows for assessment based on the arbitrary signal contrast between tissues. Despite their potential benefits, quantitative MR techniques, such as obtaining T1, T2, and proton density (PD) values of tissue, are not

Abbreviations: BPV, Brain parenchymal volume; CSF, Cerebrospinal fluid; CV, Coefficient of variation; GM, Gray matter; ICC, Intraclass correlation coefficient; LOA, Limits of agreement; MDME, Multidynamic multi-echo; MRI, Magnetic resonance imaging; MVF, Myelin volume fraction; NoN, Other intracranial material; PD, Proton density; SD, Standard deviation; VOI, Volume of interest; WM, White matter

* Corresponding author at: Department of Radiology, Juntendo University School of Medicine, 1-2-1, Hongo, Bunkyo-ku, Tokyo 113-8421, Japan.

E-mail address: a-hagiwara@juntendo.ac.jp (A. Hagiwara).

<https://doi.org/10.1016/j.mri.2019.08.031>

Received 9 June 2019; Received in revised form 19 August 2019; Accepted 19 August 2019

0730-725X/© 2019 The Authors. Published by Elsevier Inc. This is an open access article under the CC BY-NC-ND license (<http://creativecommons.org/licenses/by-nc-nd/4.0/>).

performed in routine clinical examination, likely due to the low resolution of conventional mapping methods.

Several quantitative multiparametric approaches have been proposed to obtain high spatial resolution maps of the brain [10–13]. One such method uses a multidynamic multi-echo (MDME) sequence, which enables simultaneous tissue relaxometry of T1 and T2 relaxation times and PD, providing quantitative maps that are inherently aligned [10,14–17]. Myelin volume fraction (MVF) in a voxel can also be estimated, based on the acquired T1, T2, and PD values, assuming four compartments in brain tissues [18,19]. The MDME sequence has been used for evaluation in various brain diseases, such as multiple sclerosis [20,21], brain infarctions [22], and meningitis [23].

The MDME sequence used for quantitative synthetic MRI was based on a multi-slice 2D acquisition, which provided a relatively low resolution in the slice direction compared with 3D acquisitions. Recently, 3D-quantification using an interleaved Look-Locker acquisition sequence with a T2 preparation pulse (3D-QALAS) sequence has been developed for simultaneous quantification of T1 and T2 in cardiac imaging and showed high accuracy and precision in the heart as well as in phantoms with various tissue properties [24,25]. A previous study showed that 3D-QALAS can be reliably used for measuring cortical thickness and subcortical volumes in most brain regions [26]. However, no study to date has investigated the reliability of MR property quantification based on 3D-QALAS in the brain.

Here, we propose the application of the 3D-QALAS sequence for simultaneous acquisition of relaxometry parameters at high spatial resolution in the brain. The purpose of this study was to evaluate bias, linearity, and day-to-day repeatability of relaxometry parameters (*i.e.*, T1, T2, and PD values) of the brain acquired with 3D-QALAS by (a) evaluating T1, T2, and PD values of the International Society for Magnetic Resonance in Medicine/National Institute of Standards and Technology (ISMRM/NIST) MRI system phantom measured by 3D QALAS on different days and (b) evaluating T1, T2, PD, MVF, and tissue fraction maps of brain tissues *in vivo*.

2. Materials and methods

In phantom studies, the accuracy and repeatability of the T1, T2, and PD measurements were evaluated using an ISMRM/NIST system phantom containing spheres with standardized values [27,28]. Evaluation *in vivo* was performed with volunteers using volume of interest (VOI) analysis on T1, T2, PD, and MVF maps of the brain.

2.1. MR protocol

All scans were performed on a 1.5-T scanner (A patched R5.3.0 Ingenia, Philips Healthcare, Best, The Netherlands) with a 12-channel head coil. The 3D-QALAS sequence is based on multi-acquisition 3D gradient echo, with five acquisitions equally spaced in time, interleaved with a T2 preparation pulse and an inversion pulse. Briefly, the four acquisitions after the inversion pulse are used to determine the apparent T1* relaxation time approaching the saturated M0* magnetization. T1* and M0* must be corrected for the effect of the semi-continuous series of RF flip angles during the acquisition time to retrieve the actual T1 and M0. All M0 values are then scaled to PD such that 100% PD corresponds to the M0 of pure water. The T1 data curve is extrapolated to just prior to the T2-prep pulse. T2 relaxation is then found using the ratio of the signal intensity just prior and just after the T2-prep pulse. An internal trigger started each of the five acquisitions every 900 ms, amounting to a total cycle time of 4.5 s. Further details of the 3D-QALAS sequence have been provided by previous studies [24,25]. The substantial difference between our study and the previous cardiac 3D-QALAS studies involves the spatial and temporal resolution: imaging of the brain requires higher spatial resolution than that of the heart, but no breath hold is required. The voxel size in the cardiac study was $2 \times 2 \times 12$ mm, while that in our study was $1.2 \times 1.2 \times 1.2$ mm.

In terms of volume, the voxel size used in our study was only 3.6% ($1.728/48 \text{ mm}^3$) of that used in the cardiac study. With a longer acquisition time per beat and many more cycles, we obtained a higher resolution. Accordingly, the scan parameters of the 3D-QALAS were as follows: axial acquisition; TR/TE, 6.6/3.0 ms; inversion delay times 100, 1000, 1900, 2800 ms; T2-prep echo time 100 ms; field-of-view (FOV), $250 \times 250 \times 168$ mm; matrix size, $208 \times 208 \times 140$; section thickness, 1.20 mm; flip angle, 4°; receiver bandwidth, 230 Hz/pixel; acceleration factor = 1.7, averages, 2; acquisition time, 20 min 34 s. The scan parameters of the quantification of relaxation times and proton density by MDME [10] were as follows: axial acquisition; TR/TE1/TE2, 4000/22/99 ms; FOV, 230×230 mm; matrix size, 192×192 ; section thickness, 5 mm; flip angle, 90°; receiver bandwidth, 158.5 Hz/pixel; acceleration factor = 2, averages, 1; acquisition time, 5 min 29 s.

2.2. Phantom evaluation

The ISMRM/NIST system phantom (High Precision Devices, Inc., Boulder, Colorado, USA) consisted of multiple layers of sphere arrays that contain standardized T1 and T2 relaxation times and PD. T1 spheres consisted of different concentrations of NiCl₂ solutions, with T1 ranging from 24 to 2640 ms. T2 spheres consisted of different concentrations of MnCl₂ solutions, with T2 ranging from 8 to 1542 ms. PD spheres consisted of different concentrations of H₂O and D₂O, with PD ranging from 5 to 100% water. Reference values were measured by magnetic resonance spectroscopy at 20 °C and were provided by the Physical Measurement Laboratory at NIST [27,28]. Six T1 spheres and seven T2 spheres with T1 and T2 values within the clinically-relevant dynamic range (200–1400 ms and 50–400 ms, respectively) were evaluated in the study. All 14 PD spheres of the phantom were used. The outer and inner diameter of each sphere were 20 mm and 15 mm, respectively. The reference values of the spheres are shown in Table 1.

The NIST/ISMRM system phantom was scanned with the 3D-QALAS sequence seven times on different days over a 1-month period. The phantom was placed in position 30 min prior to each scan to reduce the effect of motion on measurements. T1, T2, and PD maps were generated using the SyMRI software (version 0.45.5) [29]. A spherical VOI with a 10-mm diameter was manually placed at the center of each sphere on the T1, T2, and PD maps, and the mean values were recorded using ITK-SNAP (version 3.6.0.).

2.3. Healthy volunteer evaluation

The local review board approved this study, and written informed consent was acquired from all participants. Ten healthy volunteers were included in this study (7 male, 3 female; mean age, 23.2 ± 3.6 [SD] years). None of the participants had a history of a major medical condition or neurological or psychiatric disorder. Two radiologists (A.H. and S.F.) blindly assessed all volunteer examinations and confirmed that none had structural abnormalities.

A scan–rescan test, as well as comparison with the 2D-MDME sequence results, was performed for each volunteer. A 2D-MDME sequence was performed once, and the 3D-QALAS sequence was performed twice (for scan–rescan) in the same session, for all volunteers. Between the scan–rescan of the 3D-QALAS sequence, the volunteers exited the scanner and were asked to rest for a few minutes T1, T2, PD, and MVF maps were generated using the SyMRI software [29] for the VOI analysis. We performed VOI analysis based on a previous study [14]. In brief, we created 16 VOIs: 8 of white matter (WM; frontal, parietal, temporal, and occipital WM; genu and splenium of the corpus callosum, internal capsules, and middle cerebellar peduncles) and 8 of gray matter (GM; frontal, parietal, temporal, and occipital GM; insula, caudate, putamen, and thalamus) VOIs in the Montreal Neurological Institute space [30–32]. VOIs of the left and right sides were combined for analysis, except for those of the splenium. For each VOI, the mean

Table 1

Mean values of 7-day measurements of T1 and T2 relaxation times and proton density (PD) and their coefficients of variation (CVs) of the International Society for Magnetic Resonance in Medicine/National institute of Standards and Technology system phantom. Reference values measured with magnetic resonance spectroscopy at 20 °C were provided by National institute of Standards and Technology.

Sphere no.	T1 (ms)			T2 (ms)			PD (%)		
	Reference	Mean ± SD	CV (%)	Reference	Mean ± SD	CV (%)	Reference	Mean ± SD	CV (%)
1	272.3	285 ± 2	0.6	43.84	42 ± 1	2.9	5	NA	NA
2	384.1	389 ± 4	1.1	62.82	61 ± 1	1.3	10	NA	NA
3	527	505 ± 5	0.9	89.52	89 ± 1	1.1	15	10.5 ± 0.4	3.5
4	751	683 ± 7	1.0	137	122 ± 1	1.0	20	14.4 ± 0.2	1.1
5	1027	934 ± 7	0.7	186.1	163 ± 3	1.8	25	16.5 ± 1.1	6.9
6	1432	1334 ± 34	2.6	258.4	212 ± 8	3.8	30	18.7 ± 0.6	3.4
7				428.3	365 ± 26	7.4	35	22.1 ± 0.5	2.1
8							40	27.2 ± 0.8	2.8
9							50	31.4 ± 0.5	1.5
10							60	38.1 ± 0.6	1.5
11							70	44.6 ± 0.5	1.1
12							80	63.5 ± 5.4	8.4
13							90	82.7 ± 1.2	1.5
14							100	89.0 ± 0.8	0.8

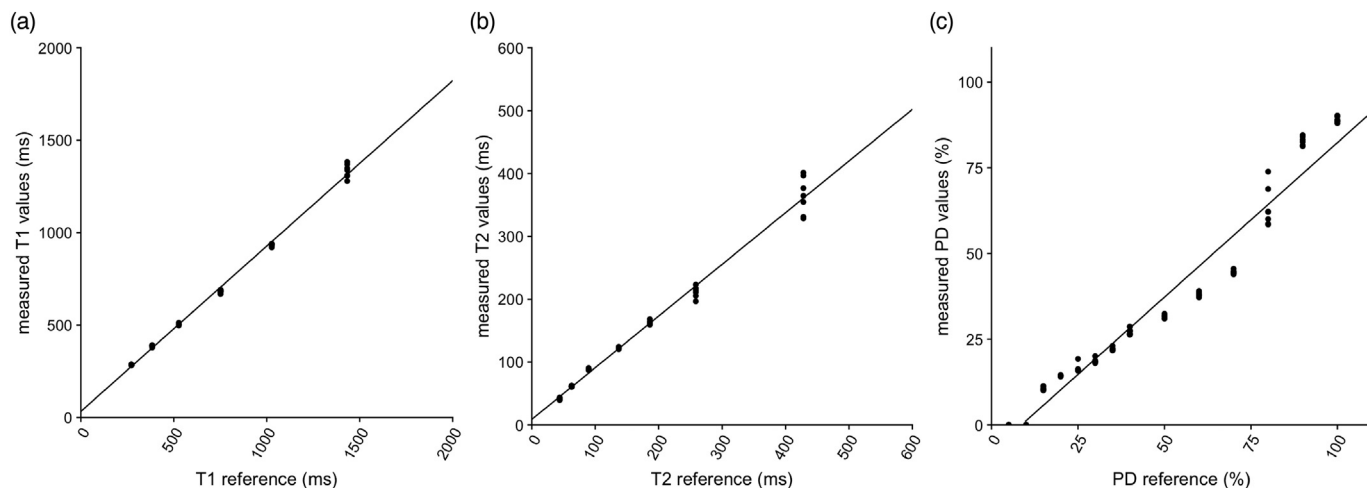


Fig. 1. Correlation plots comparing mean T1 (a), T2 (b), and PD (c) values to the reference values, showing linearity of measurements obtained with the 3D-QALAS sequence. Solid black lines represent the linear regression fit.

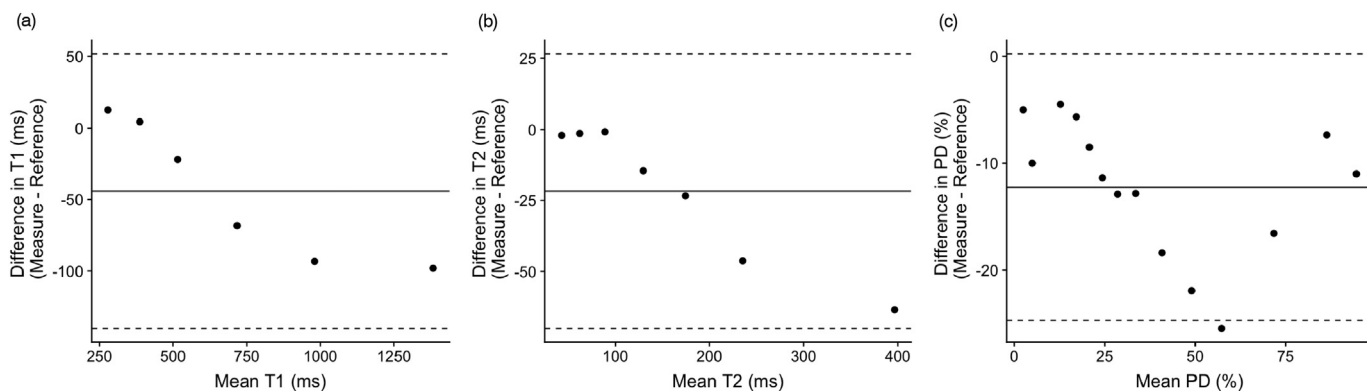


Fig. 2. Bland-Altman plots comparing T1 (a), T2 (b), and PD (c) values to the reference values, showing bias of measurements obtained with the 3D-QALAS sequence. The center solid lines represent mean differences. Upper and lower dotted lines represent the LOA, defined as the mean difference ± 1.96 × SD of the difference between the measurement and reference values. LOA, limit of agreement; SD, standard deviation.

T1, T2, PD, and MVF values were measured. *In vivo* repeatability and agreement with values obtained from MDME were evaluated for 3D-QALAS.

Based on the T1, T2, and PD values measured by the 3D-QALAS sequence, brain tissue segmentation was performed using the SymMRI

software. The details of the brain segmentation algorithm using SymMRI are described elsewhere [19]. In brief, the measured quantitative values of brain tissues were used as coordinates in a 3D feature space (*i.e.*, R1–R2–PD space). This coordinate was referred to as a lookup grid, which shows the related partial tissue volumes to the 3D space [19]. We

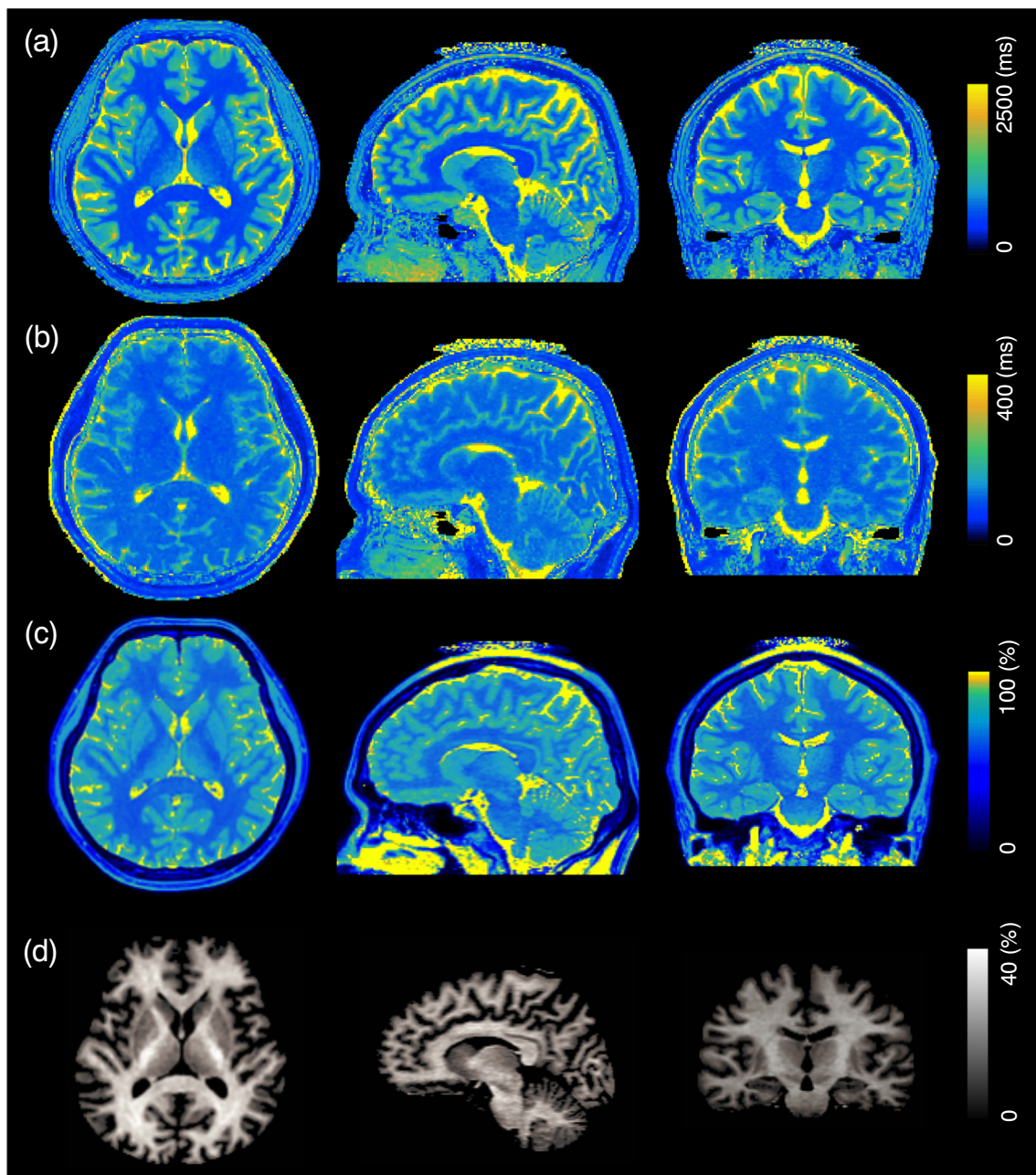


Fig. 3. Representative example of three-dimensional quantification maps of the brain. T1 maps (a), T2 maps (b), PD maps (c), and MVF maps (d) are shown in multi-planar reconstruction views. PD, proton density; MVF, myelin volume fraction.

performed brain tissue segmentation based on the same data to obtain GM, WM, and cerebrospinal fluid (CSF) volumes, and myelin volume (MYV) by multiplying the aggregated volume fraction of each tissue type in the whole brain and the voxel volume. Voxels not categorized as GM, WM, or CSF were classified as other intracranial material (NoN). The brain parenchymal volume (BPV) was calculated by summing the GM, WM, and NoN. The intracranial volume (ICV) was calculated by defining the borderline at PD = 50%. Agreement with volumes obtained from MDME and scan–rescan repeatability were evaluated for 3D-QALAS.

2.4. Statistical analysis

To assess linearity, simple linear regression analysis was performed between the mean of 7 measurements and the reference values that were provided by NIST [27,28]. For assessment of bias, Bland–Altman

plots were obtained between the measurements and the reference values. The coefficients of variation (CVs) of the 7 measurements of the spheres in the phantoms was obtained to assess day-to-day repeatability. In the volunteer study, intrasubject CVs of T1, T2, and PD based on the scan–rescan tests were calculated for each VOI per subject (based on the scan–rescan tests) and then averaged across subjects. Percentage relative difference was used to assess reproducibility of the 3D-QALAS sequence-derived brain quantitative values and tissue volumes compared with those derived from MDME. For brain tissue volumes, intraclass correlation coefficients (ICCs) were also calculated to assess reproducibility.

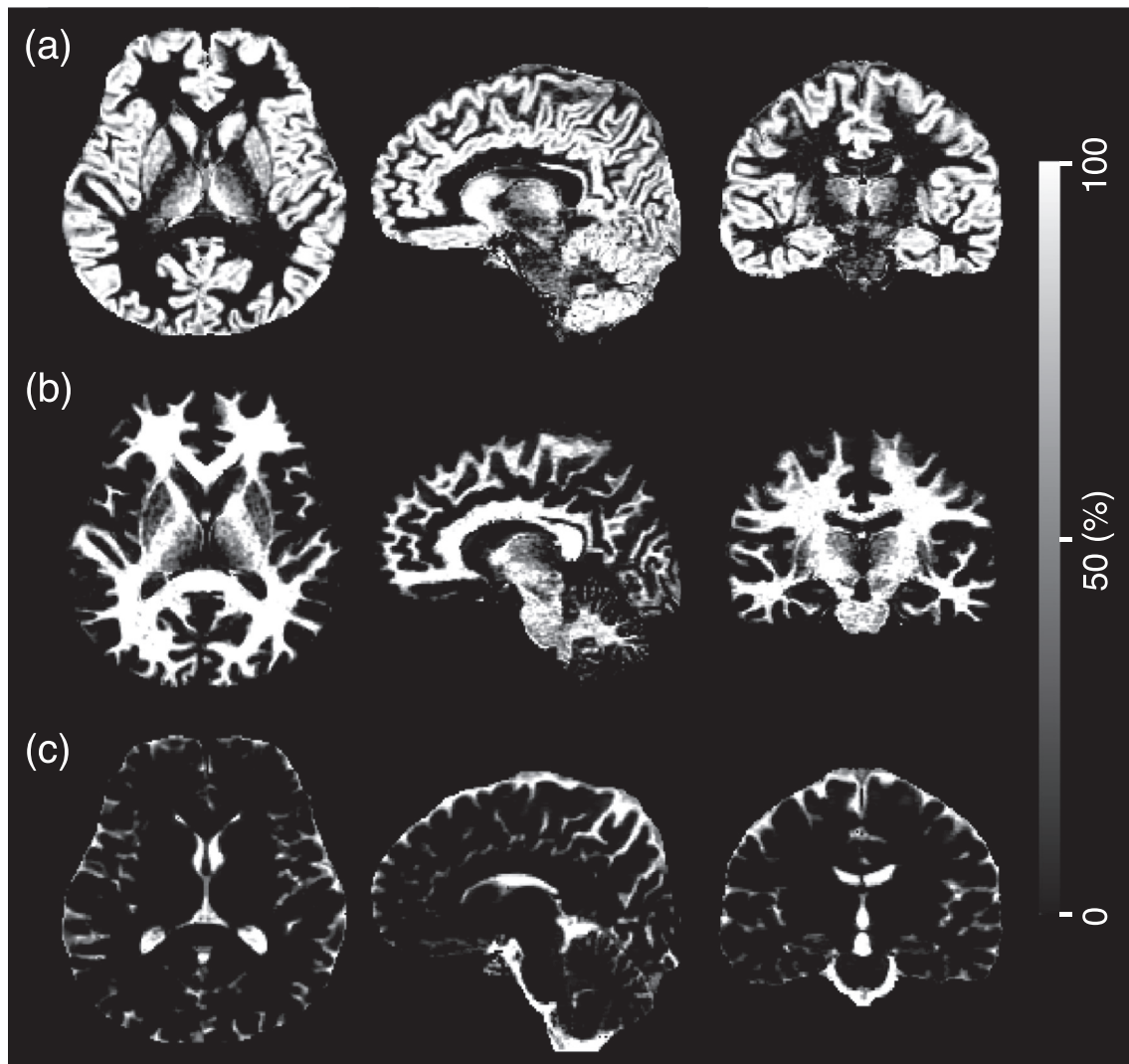


Fig. 4. Representative example of three-dimensional tissue fraction maps of the brain. GM (a), WM (b), and CSF (c) maps are shown in multi-planar reconstruction views. GM, gray matter; WM, white matter; CSF, cerebrospinal fluid.

3. Results

3.1. ISMRM/NIST MRI system phantom study

The temperature of the phantom after image acquisition was 19.1 ± 0.5 °C. The mean, SD, and CV of the repeated measurements of T1, T2, and PD of each sphere are reported in Table 1. All CVs of the T1, T2, and PD measurements based on 3D-QALAS were lower than 10% (mean CV: 1.2%, 2.8%, and 2.9%, respectively). Fig. 1 shows the simple linear regression analysis performed between the mean of the measurements and the reference values. The T1, T2, and PD values measured by 3D-QALAS all showed strong linearity with the reference values ($R^2 = 0.998, 0.998, \text{ and } 0.960$, respectively). The linear regression fit had slopes of 0.89, 0.82, and 0.90, and intercepts of 33, 9.0, and -7.8 for T1, T2, and PD, respectively. Fig. 2 shows the Bland–Altman plots obtained between the measurements and the reference values; the difference between the measurements and reference values are plotted against the mean. The mean bias was -44 ms, -22 ms, and -12% for T1, T2, and PD, respectively. The limits of agreement (LOAs), defined as the mean difference $\pm 1.96 \times$ SD of the difference between the measurements and reference values, were -140 to 51 , -70 to 27 , and -25 to 0.24 for T1, T2, and PD, respectively. All data points were within the LOAs, except for one data point of PD (reference value, 80% H₂O).

3.2. Healthy volunteer evaluation

Fig. 3 shows representative 3D T1, T2, PD, and MVF maps of the brain obtained from a healthy volunteer using 3D-QALAS. Fig. 4 illustrates tissue fraction maps obtained from a volunteer's scan. Fig. 5 shows a representative example of VOI placements in a multi-planar view.

Table 2 reports the mean, SD, and intrasubject CV of T1, T2, PD, and MVF values of each anatomic VOI across 10 healthy volunteers. Values obtained with the MDME sequence, and the relative difference between 3D-QALAS and MDME are also shown. Supplementary Table 1 shows the T1, T2, and PD values for representative anatomical parts of the brain obtained with 3D-QALAS along with values from the literature [10,11,33–38]. The T1, T2, PD, and MVF values of brain regions obtained with 3D-QALAS were highly consistent within volunteers, with mean intrasubject CVs of 0.5, 0.5, 0.4, and 1.6% for T1, T2, PD, and MVF, respectively. All *in vivo* measured values were within the dynamic range evaluated in the phantom study.

Table 3 reports the overall mean, intrasubject CV, ICC, and percentage relative difference of WM, GM, CSF, NoN, MYV, BPV, and ICV volumes based on 3D-QALAS and the 2D-MDME sequence for the 10 healthy volunteers. The WM, GM, MYV, BPV, and ICV values showed high agreement between the values obtained with 3D-QALAS and 2D-

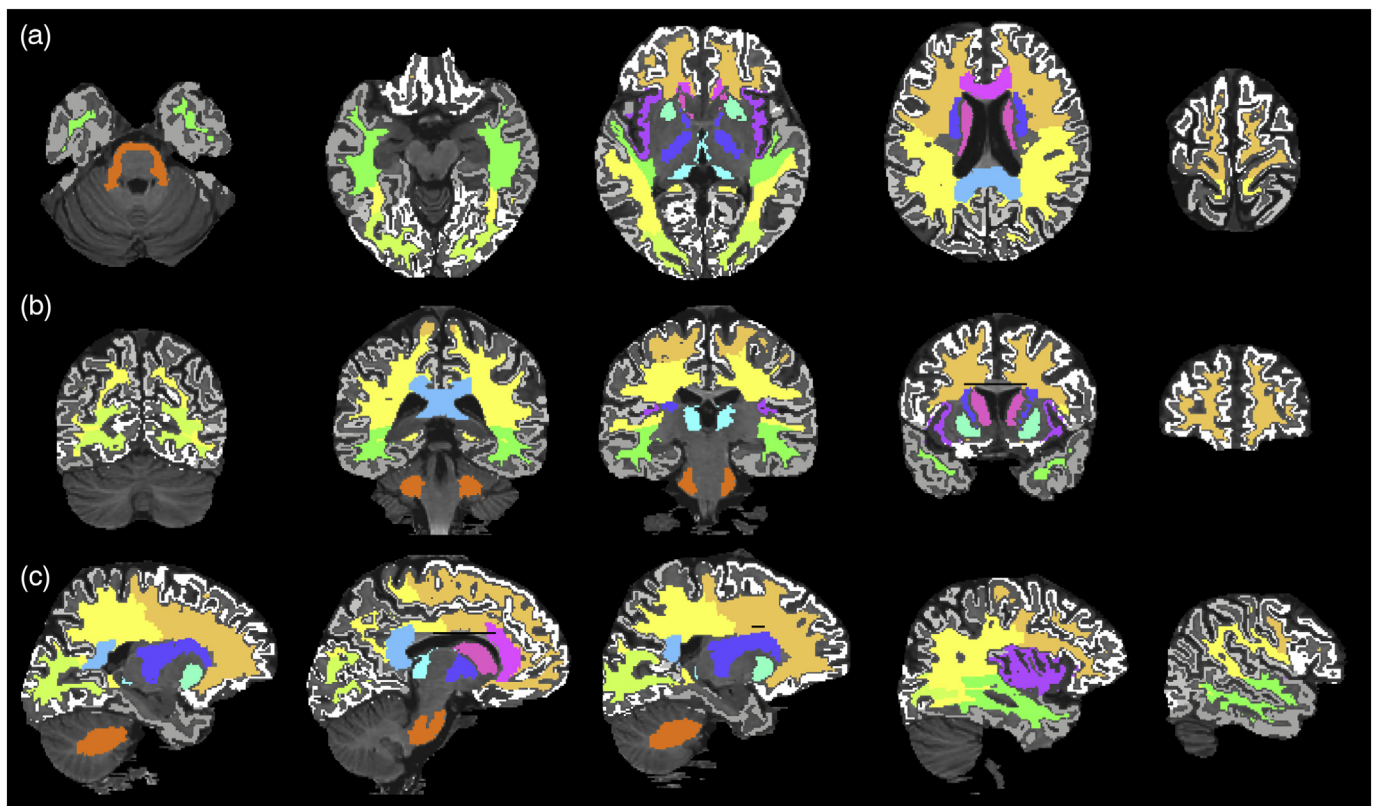


Fig. 5. Representative example of volume of interest (VOI) placement. VOIs are overlaid on a T1-weighted image in axial (a), coronal (b), and sagittal (c) views.

MDME, with percentage relative difference of 7.4%, 4.0%, 3.4%, 4.5%, and 1.3%, and ICCs of 0.97, 0.97, 0.95, 0.99, and 0.99, respectively. The CSF and NoN showed relatively low agreement between 3D-QALAS and 2D-MDME. The tissue volumes obtained with 3D-QALAS showed high repeatability, with a mean intrasubject CV of 1.9%.

4. Discussion

We presented the accuracy and repeatability of a relaxometry technique for 3D simultaneous quantification of T1, T2, PD, and MVF values of the whole brain. The T1, T2, and PD values obtained using the 3D-QALAS sequence showed high repeatability and strong linear correlation with the reference values of the standardized ISMRM/NIST system phantom. Although some biases were present with respect to the reference values, measurements were strongly linear, indicating that the 3D-QALAS sequence allows for adequate quantitative characterization. The T1, T2, and PD values of the healthy participants were in good agreement with the literature values, with high repeatability.

The 3D-QALAS sequence provides both quantitative values (*i.e.*, T1 and T2 relaxation times, PD, and MVF) and morphologic information of the whole brain in high spatial resolution. The method has the advantage that it can measure not only T1, T2, and PD values, but also MVF, which is considered to be important clinically. Another advantage of 3D-QALAS compared to other mapping techniques, which usually require multiple scans and registration, is that 3D-QALAS achieves perfect alignment among the obtained quantitative MR property maps and tissue fraction maps. Since the acquisition is performed slice-by-slice, only the effects of subject movement that occurred during the slice acquisition would be evident. The registration error should be eliminated, as long as the patient did not move during data acquisition within a slice.

Absolute quantification of MR properties using relaxometry has previously been reported to be useful for characterization of disease, assessment of disease activity, and monitoring of treatment [39–41].

The 3D isotropic acquisition with 3D-QALAS allows for generation of images from arbitrary views, without requiring additional scans from different directions. This property not only provides the advantage of visual characterization and detection of lesions, but also allows for accurate segmentation of small regional structures. This enables detecting and describing T1, T2, and PD changes within regional structures, which could be masked when averaging values over gross anatomic regions. Hence, 3D-QALAS has the potential to provide thorough and comprehensive characterization of brain lesions, as well as of the entire brain.

The validation of accuracy and repeatability of 3D-QALAS in a standardized phantom is a prerequisite for its clinical use. In our study, we compared the T1, T2, and PD values obtained using 3D-QALAS with the reference values in NIST/ISMRM phantoms across seven days. Day-to-day repeatability was lower than 3% for the T1, T2, and PD values. In the phantom study, we did not correct for temperature in T1 and T2 measurements. The correction would have lowered the reported CVs, because without the correction, the measurements would include error of the measurements and error originating from the temperature difference. However, in clinical practice, it is difficult and impractical to obtain the exact temperature of a subject. Because the CVs without temperature corrections were acceptable (mean CV of 1.2%, 2.8%, and 2.9%, for T1, T2, and PD, respectively) in our observation, we decided not to perform temperature correction.

The values acquired with 3D-QALAS showed a strong linear correlation ($R^2 = 0.98–0.99$) with the standardized values for the physiological range of structures of the brain. Our results indicate that 3D-QALAS covers the physiological range of T1, T2, and PD values in brain structures. PD values lower than 10% were estimated as 0%, suggesting that measurements of extremely low PD values would be less reliable. However, precise quantitative values of such tissues would be of less importance in the clinical setting; the PD values in the healthy human brain measured by MDME were reported to be 77% and 62% for GM and WM, respectively [14]. Further, PD values in various brain tumors

Table 2
Mean values and intrasubject coefficients of variation (CVs) of T1, T2, PD, and MVF for 10 healthy subjects, based on the 3D-QALAS sequence.

Volume of interest	T1 (ms)			T2 (ms)			PD (%)			MVF (%)						
	MDME			3D QALAS			MDME			3D QALAS						
	Overall mean (ms)	Intrasubject CV (%)	Relative difference (%)	Overall mean (ms)	Intrasubject CV (%)	Relative difference (%)	Overall mean (ms)	Intrasubject CV (%)	Relative difference (%)	Overall mean (ms)	Intrasubject CV (%)	Relative difference (%)				
Gray matter																
Frontal GM	1044 ± 21	0.4 ± 0.3	1067 ± 29	1.9 ± 1.4	93 ± 2	0.9 ± 0.8	90 ± 2	4.2 ± 1.4	81 ± 0.7	0.4 ± 0.4	83 ± 1.1	2.2 ± 1.3	8.1 ± 0.7	2.9 ± 2.5	6.7 ± 0.7	15.6 ± 10.3
Parietal GM	1028 ± 22	0.6 ± 0.5	1068 ± 25	3.0 ± 1.3	90 ± 2	0.9 ± 0.7	87 ± 2	4.3 ± 1.0	79 ± 0.7	0.3 ± 0.1	83 ± 0.6	3.5 ± 0.7	8.8 ± 0.8	3.0 ± 2.2	6.0 ± 0.4	34.9 ± 6.1
Temporal GM	1092 ± 17	0.3 ± 0.3	1123 ± 31	2.6 ± 1.8	96 ± 2	0.5 ± 0.2	90 ± 2	5.8 ± 1.8	83 ± 0.5	0.4 ± 0.3	85 ± 0.6	2.6 ± 1.0	6.5 ± 0.5	1.2 ± 1.0	5.3 ± 0.5	19.2 ± 6.4
Occipital GM	1035 ± 22	0.6 ± 0.5	1079 ± 25	3.5 ± 1.0	87 ± 1	0.5 ± 0.4	85 ± 1	2.6 ± 1.1	80 ± 0.7	0.3 ± 0.2	83 ± 0.7	2.6 ± 0.6	8.3 ± 0.8	3.5 ± 1.6	6.7 ± 0.6	18.5 ± 7.8
Insular cortex	1048 ± 21	0.3 ± 0.2	1065 ± 29	1.3 ± 1.2	96 ± 2	0.4 ± 0.5	93 ± 2	4.0 ± 2.4	79 ± 0.5	0.3 ± 0.3	83 ± 0.8	4.8 ± 1.1	8.8 ± 1.0	0.8 ± 0.8	5.8 ± 0.8	35.9 ± 8.3
Caudate	918 ± 17	0.6 ± 0.5	878 ± 28	5.3 ± 2.0	85 ± 2	0.5 ± 0.4	82 ± 1	4.1 ± 1.6	77 ± 1.1	0.4 ± 0.4	79 ± 1.4	2.4 ± 1.4	12.4 ± 1.3	2.9 ± 2.8	10.1 ± 1.9	21.5 ± 15.1
Putamen	831 ± 15	0.7 ± 0.6	795 ± 22	5.3 ± 2.0	77 ± 2	0.6 ± 0.6	75 ± 2	2.3 ± 1.3	75 ± 0.5	0.3 ± 0.2	77 ± 0.6	2.1 ± 0.8	16.5 ± 0.9	1.6 ± 1.4	13.7 ± 0.8	16.7 ± 6.1
Thalamus	780 ± 13	0.5 ± 0.3	763 ± 20	2.9 ± 1.4	81 ± 1	0.4 ± 0.3	79 ± 1	2.3 ± 1.4	73 ± 0.5	0.3 ± 0.2	73 ± 0.7	0.6 ± 0.5	19.4 ± 0.6	1.1 ± 1.0	19.8 ± 1.1	4.7 ± 2.6
Aggregate of GM	910 ± 20	0.4 ± 0.3	904 ± 18	1.6 ± 1.0	88 ± 1	0.5 ± 0.5	83 ± 1	5.8 ± 0.8	77 ± 0.7	0.3 ± 0.3	77 ± 0.7	0.9 ± 0.4	14.1 ± 0.9	1.2 ± 1.0	15.2 ± 0.6	9.4 ± 4.8
White matter																
Frontal WM	581 ± 20	0.7 ± 0.4	615 ± 15	4.4 ± 1.2	76 ± 2	0.6 ± 0.6	76 ± 1	1.0 ± 0.6	65 ± 0.4	0.3 ± 0.2	63 ± 0.9	2.6 ± 0.9	31.1 ± 0.6	1.0 ± 0.7	33.9 ± 1.3	8.2 ± 2.5
Parietal WM	575 ± 20	0.3 ± 0.3	625 ± 16	7.2 ± 1.2	79 ± 1	0.4 ± 0.5	77 ± 1	2.4 ± 0.8	64 ± 0.3	0.2 ± 0.1	64 ± 0.8	0.7 ± 0.6	32.3 ± 0.5	0.6 ± 0.4	33.2 ± 1.2	2.3 ± 2.0
Temporal WM	599 ± 20	0.7 ± 0.6	637 ± 20	5.3 ± 1.3	78 ± 2	0.6 ± 0.7	76 ± 1	2.5 ± 1.3	66 ± 0.8	0.5 ± 0.4	65 ± 1.1	2.4 ± 1.0	28.9 ± 1.1	1.5 ± 1.4	31.6 ± 1.7	9.2 ± 2.9
Occipital WM	587 ± 20	0.7 ± 0.4	667 ± 12	11.9 ± 1.2	81 ± 1	0.4 ± 0.4	79 ± 1	3.2 ± 1.0	65 ± 0.7	0.4 ± 0.2	66 ± 0.6	1.5 ± 0.7	31.1 ± 1.0	1.0 ± 0.6	30.1 ± 1.0	3.7 ± 1.9
Genu of the CC	530 ± 18	0.5 ± 0.4	539 ± 16	1.0 ± 0.9	73 ± 2	0.8 ± 0.8	75 ± 1	2.3 ± 1.4	66 ± 1.5	0.5 ± 0.4	58 ± 1.2	11.4 ± 2.4	29.0 ± 2.3	1.5 ± 1.2	41.3 ± 1.8	29.7 ± 5.8
Splenium of the CC	540 ± 17	0.2 ± 0.2	584 ± 16	6.6 ± 1.8	79 ± 1	0.4 ± 0.5	78 ± 1	2.6 ± 1.8	65 ± 0.8	0.6 ± 0.4	61 ± 0.8	5.7 ± 2.3	30.8 ± 1.1	1.4 ± 1.0	36.9 ± 1.2	16.4 ± 5.8
Internal capsule	580 ± 21	0.6 ± 0.6	615 ± 19	4.5 ± 1.6	76 ± 2	0.7 ± 0.6	75 ± 1	2.2 ± 0.9	64 ± 0.7	0.3 ± 0.3	63 ± 0.9	1.1 ± 0.8	33.0 ± 1.0	0.9 ± 0.8	34.1 ± 1.4	3.7 ± 2.3
Middle cerebellar peduncle	631 ± 16	0.3 ± 0.3	684 ± 22	7.5 ± 1.8	83 ± 1	0.3 ± 0.2	81 ± 2	2.1 ± 1.3	67 ± 0.9	0.4 ± 0.3	66 ± 0.9	2.0 ± 0.9	28.0 ± 1.2	1.3 ± 1.1	29.9 ± 1.3	7.4 ± 3.0
Aggregate of WM	580 ± 19	0.4 ± 0.3	624 ± 14	6.1 ± 1.1	78 ± 1	0.4 ± 0.6	77 ± 1	1.8 ± 0.7	65 ± 0.4	0.3 ± 0.2	64 ± 0.8	1.7 ± 0.8	31.1 ± 0.5	0.8 ± 0.5	33.2 ± 1.2	6.0 ± 2.3

GM, gray matter; WM, white matter; CC, corpus callosum; MVF, myelin volume fraction.

Table 3
Volumetric measurements of healthy volunteers based on the 3D-QALAS sequence.

Tissue type	3D QALAS		MDME		
	Overall mean (ml)	Intrasubject CV	Overall mean (ml)	Relative difference (%)	ICC
WM	618 ± 64	0.8 ± 0.7	572 ± 59	7.4 ± 2.3	0.97
GM	722 ± 75	0.7 ± 0.7	694 ± 65	4.0 ± 2.4	0.97
CSF	137 ± 35	2.0 ± 1.4	212 ± 52	43.6 ± 5.4	0.93
NoN	39 ± 6	8.2 ± 5.9	50 ± 14	33.7 ± 18.6	0.04
MYV	197 ± 23	0.8 ± 0.8	199 ± 23	3.4 ± 1.5	0.95
BPV	1378 ± 128	0.5 ± 0.4	1317 ± 131	4.5 ± 1.0	0.99
ICV	1515 ± 151	0.4 ± 0.3	1529 ± 163	1.3 ± 0.6	0.99

MDME, multidynamic multi-echo; GM, gray matter; WM, white matter; CSF, cerebrospinal fluid; NoN, other brain material; BPV, brain parenchymal volume; ICV, intracranial volume; MYV, myelin volume; ICC, intraclass correlation coefficient.

have been previously reported by Just et al., who showed that tumors have higher PD values than does WM [42].

The T1, T2, and PD values obtained with 3D-QALAS showed good overall agreement with MDME sequence-derived values, as shown by relative differences. However, the MVF values in gray matter regions differed substantially between 3D-QALAS and MDME. One possible reason may be the low absolute value of MVF in gray matter (mean MVF value of 15.2% in gray matter compared to 33.2% in white matter), which may have made the relative differences sensitive to small changes. Despite the high absolute value of the MVF in the corpus callosum, values obtained with 3D-QALAS and MDME differed substantially. One possible reason for this could be the effects of incomplete elimination of B1 inhomogeneity and coil sensitivity, because the corpus callosum is located in the center of the field-of-view that is likely to be affected by these effects. Special attention is required when applying 3D-QALAS to the corpus callosum. In spite of these discrepancies, 3D-QALAS sequence-derived T1, T2, PD, and MVF values showed high repeatability. The measured values often differ even among well-established methods and pursuing the true value may be impractical for clinical use. When performing an examination in a clinical context to monitor subtle changes in subjects' MR values, repeatability is more important than accuracy, as repeatability is associated with the smallest change that can be detected using the measurement. As long as the measurement is consistent and shows high repeatability, it could be used to depict the differences among tissues.

The 3D-QALAS sequence was constructed for analyzing brain tissue and may not be suitable for quantifying MR properties of materials that differ greatly from the brain. Our data show that 3D-QALAS slightly underestimates the values of T1, T2, and PD. However, the repeatability of these measurements was high (mean CV of 1.2%, 2.8%, and 2.9% for T1, T2, and PD values, respectively), indicating that 3D-QALAS is suitable for longitudinal studies.

We also assessed the *in vivo* repeatability of 3D-QALAS with 10 healthy volunteers. The T1, T2, and PD values acquired with 3D-QALAS showed good agreement with the results of previous studies reporting values of structures of the normal brain at 1.5 T (Supplementary Table 1) [10,11,33–38]. The CVs of T1, T2, and PD values in volunteer data were lower than those measured in the phantom study. This may be because the size of the VOIs used in the phantom study was smaller than those used in the volunteer study. The tissue volume based on 3D-QALAS showed low intrasubject CV, lower than 1%, except for NoN. NoN showed intrasubject CVs of 8.2%, which was much higher than that of the other tissue volumes. Because the CV is sensitive to small changes when the mean value used as the denominator approaches zero, the small absolute volume of NoN may have contributed to the relatively large intrasubject CV.

This study had several limitations. First, the scanning time in this study was relatively long in terms of incorporation into a routine clinical scan. Using a 3-T MRI scanner, as well as combining it with acceleration techniques, such as compressed sensing [43], may reduce

scan times to a clinically-applicable level. Second, only healthy volunteers and no patients were enrolled in the *in vivo* study. Although our goal was to validate the accuracy and repeatability of 3D-QALAS, future studies focusing on patients are required. Third, although we have validated the reliability of 3D-QALAS using the standardized phantom with reference values, the *in vivo* values were not compared with those acquired by gold-standard methods, such as IR-based T1 mapping and multi-echo T2 mapping, which requires an excessive scan time. However, the T1, T2, and PD values acquired with 3D-QALAS showed good agreement with values obtained with the well-established MDME sequence, as well as with values reported previously.

In conclusion, the three-dimensional relaxometry method, 3D-QALAS, allows for reliable measurement of T1, T2, and PD values across a clinically-relevant dynamic range, with high spatial resolution, while concurrently providing morphological information of the whole brain.

Supplementary data to this article can be found online at <https://doi.org/10.1016/j.mri.2019.08.031>.

Grant support

This work was supported by JSPS KAKENHI grant number 19K17177, 19K17150, 18K07692, 16K10327, and JP16H06280; Grant-in-Aid for Scientific Research on Innovative Areas- Resource and technical support platforms for promoting research 'Advanced Bioimaging Support'; the Budget for promotion of strategic international standardization given by the Ministry of Economy, Industry, and Trade (METI); the Japan Agency for Medical Research and Development (AMED) under grant number 18lk1010025s0101 and 19lk1010025h9902; Brain/MINDS Beyond program from AMED under Grant Number JP19dm0307024h002; and the Japanese Society for Magnetic Resonance in Medicine.

Declaration of competing interest

Marcel Warntjes is currently employed part-time at SyntheticMR and has a stock in SyntheticMR.

Acknowledgements

We gratefully appreciate the cooperation of Ukihide Tateishi (Tokyo Medical and Dental University), the chair of Japan Quantitative Imaging Biomarkers Alliance (J-QIBA), and other J-QIBA members.

References

- [1] Giedd JN, Snell JW, Lange N, Rajapakse JC, Casey BJ, Kozuch PL, et al. Quantitative magnetic resonance imaging of human brain development: ages 4–18. *Cereb Cortex* 1996;6(4):551–60.
- [2] Grossman R, Hoffman C, Mardor Y, Biegion A. Quantitative MRI measurements of human fetal brain development in utero. *Neuroimage* 2006;33(2):463–70.
- [3] Kumar R, Delshad S, Woo MA, Macey PM, Harper RM. Age-related regional brain

- T2-relaxation changes in healthy adults. *J Magn Reson Imaging* 2012;35(2):300–8.
- [4] Callaghan MF, Freund P, Draganski B, Anderson E, Cappellelli M, Chowdhury R, et al. Widespread age-related differences in the human brain microstructure revealed by quantitative magnetic resonance imaging. *Neurobiol Aging* 2014;35(8):1862–72.
- [5] Carey D, Caprini F, Allen M, Lutti A, Weiskopf N, Rees G, et al. Quantitative MRI provides markers of intra-, inter-regional, and age-related differences in young adult cortical microstructure. *Neuroimage* 2018;182:429–40.
- [6] Bottomley PA, Hardy CJ, Argersinger RE, Allen-Moore G. A review of 1H nuclear magnetic resonance relaxation in pathology: are T1 and T2 diagnostic? *Med Phys* 1987;14(1):1–37.
- [7] Manfredonia F, Ciccarello O, Khaleeli Z, Tozer DJ, Sastre-Garriga J, Miller DH, et al. Normal-appearing brain T1 relaxation time predicts disability in early primary progressive multiple sclerosis. *Arch Neurol* 2007;64(3):411–5.
- [8] Jackson GD, Connelly A, Duncan JS, Grunewald RA, Gadian DG. Detection of hippocampal pathology in intractable partial epilepsy: increased sensitivity with quantitative magnetic resonance T2 relaxometry. *Neurology* 1993;43(9):1793–9.
- [9] House MJ, St Pierre TG, Foster JK, Martins RN, Clarnette R. Quantitative MR imaging R2 relaxometry in elderly participants reporting memory loss. *AJNR Am J Neuroradiol* 2006;27(2):430–9.
- [10] Warntjes JB, Leinhard OD, West J, Lundberg P. Rapid magnetic resonance quantification on the brain: optimization for clinical usage. *Magn Reson Med* 2008;60(2):320–9.
- [11] Deoni SC, Peters TM, Rutt BK. High-resolution T1 and T2 mapping of the brain in a clinically acceptable time with DESPOT1 and DESPOT2. *Magn Reson Med* 2005;53(1):237–41.
- [12] Ehse P, Seiberlich N, Ma D, Breuer FA, Jakob PM, Griswold MA, et al. IR TrueFISP with a golden-ratio-based radial readout: fast quantification of T1, T2, and proton density. *Magn Reson Med* 2013;69(1):71–81.
- [13] Ma D, Gulani V, Seiberlich N, Liu K, Sunshine JL, Duerk JL, et al. Magnetic resonance fingerprinting. *Nature* 2013;495(7440):187–92.
- [14] Hagiwara A, Hori M, Cohen-Adad J, Nakazawa M, Suzuki Y, Kasahara A, et al. Linearity, bias, intrascanner repeatability, and interscanner reproducibility of quantitative multidynamic multiecho sequence for rapid simultaneous relaxometry at 3 T: a validation study with a standardized phantom and healthy controls. *Invest Radiol* 2019;54(1):39–47.
- [15] Hagiwara A, Warntjes M, Hori M, Andica C, Nakazawa M, Kumamaru KK, et al. SyMRI of the brain: rapid quantification of relaxation rates and proton density, with synthetic MRI, automatic brain segmentation, and myelin measurement. *Invest Radiol* 2017;52(10):647–57.
- [16] Tanenbaum LN, Tsiouris AJ, Johnson AN, Naidich TP, DeLano MC, Melhem ER, et al. Synthetic MRI for clinical neuroimaging: results of the magnetic resonance image compilation (MAGiC) prospective, multicenter, multireader trial. *AJNR Am J Neuroradiol* 2017;38(6):1103–10.
- [17] Blystad I, Warntjes JB, Smedby O, Landtblom AM, Lundberg P, Larsson EM. Synthetic MRI of the brain in a clinical setting. *Acta Radiol* 2012;53(10):1158–63.
- [18] Warntjes M, Engstrom M, Tisell A, Lundberg P. Modeling the presence of myelin and edema in the brain based on multi-parametric quantitative MRI. *Front Neurol* 2016;7:16.
- [19] West J, Warntjes JB, Lundberg P. Novel whole brain segmentation and volume estimation using quantitative MRI. *Eur Radiol* 2012;22(5):998–1007.
- [20] Hagiwara A, Hori M, Yokoyama K, Takemura MY, Andica C, Tabata T, et al. Synthetic MRI in the detection of multiple sclerosis plaques. *AJNR Am J Neuroradiol* 2017;38(2):257–63.
- [21] Granberg T, Uppman M, Hashim F, Cananau C, Nordin LE, Shams S, et al. Clinical feasibility of synthetic MRI in multiple sclerosis: a diagnostic and volumetric validation study. *AJNR Am J Neuroradiol* 2016;37(6):1023–9.
- [22] Wallaert L, Hagiwara A, Andica C, Hori M, Yamashiro K, Koshino S, et al. The advantage of synthetic MRI for the visualization of anterior temporal pole lesions on double inversion recovery (DIR), phase-sensitive inversion recovery (PSIR), and myelin images in a patient with CADASIL. *Magn Reson Med* 2018;17(4):275–6.
- [23] Andica C, Hagiwara A, Nakazawa M, Kumamaru KK, Hori M, Ikeno M, et al. Synthetic MR imaging in the diagnosis of bacterial meningitis. *Magn Reson Med* 2017;16(2):91–2.
- [24] Kvernby S, Warntjes MJ, Haraldsson H, Carlhall CJ, Engvall J, Ebberts T. Simultaneous three-dimensional myocardial T1 and T2 mapping in one breath hold with 3D-QALAS. *J Cardiovasc Magn Reson* 2014;16:102.
- [25] Kvernby S, Warntjes M, Engvall J, Carlhall CJ, Ebberts T. Clinical feasibility of 3D-QALAS - single breath-hold 3D myocardial T1- and T2-mapping. *Magn Reson Imaging* 2017;38:13–20.
- [26] Fujita S, Hagiwara A, Hori M, Warntjes M, Kamagata K, Fukunaga I, et al. 3D quantitative synthetic MRI-derived cortical thickness and subcortical brain volumes: scan-rescan repeatability and comparison with conventional T1-weighted images. *J Magn Reson Imaging* 2019. (Epub ahead of print).
- [27] Russek SBM, Jackson E, et al. Characterization of NIST/ISMRM MRI system phantom. Proceedings of the 20th annual meeting of ISMRM Melbourne, Victoria, Australia. 2456. 2012.
- [28] Keenan KSK, Boss M, et al. Multi-site, multi-vendor comparison of T1 measurement using ISMRM/NIST system phantom. Proceedings of the 24th annual meeting of ISMRM. 3290. 2016.
- [29] User manual, version 8.0.0, SyMRI 8. Linko'ping: SyntheticMR AB. 2016.
- [30] Mazziotta J, Toga A, Evans A, Fox P, Lancaster J, Zilles K, et al. A probabilistic atlas and reference system for the human brain: International Consortium for Brain Mapping (ICBM). *Philos Trans R Soc Lond B Biol Sci* 2001;356(1412):1293–322.
- [31] Mazziotta J, Toga A, Evans A, Fox P, Lancaster J, Zilles K, et al. A four-dimensional probabilistic atlas of the human brain. *J Am Med Inform Assoc* 2001;8(5):401–30.
- [32] Maintz JB, Viergever MA. A survey of medical image registration. *Med Image Anal* 1998;2(1):1–36.
- [33] Neeb H, Zilles K, Shah NJ. A new method for fast quantitative mapping of absolute water content in vivo. *Neuroimage* 2006;31(3):1156–68.
- [34] McKenzie CA, Chen Z, Drost DJ, Prato FS. Fast acquisition of quantitative T2 maps. *Magn Reson Med* 1999;41(1):208–12.
- [35] Deichmann R. Fast high-resolution T1 mapping of the human brain. *Magn Reson Med* 2005;54(1):20–7.
- [36] Whittall KP, MacKay AL, Graeb DA, Nugent RA, Li DK, Paty DW. In vivo measurement of T2 distributions and water contents in normal human brain. *Magn Reson Med* 1997;37(1):34–43.
- [37] Oh J, Cha S, Aiken AH, Han ET, Crane JC, Stainsby JA, et al. Quantitative apparent diffusion coefficients and T2 relaxation times in characterizing contrast enhancing brain tumors and regions of peritumoral edema. *J Magn Reson Imaging* 2005;21(6):701–8.
- [38] Ernst T, Kreis R, Ross BD. Absolute quantitation of water and metabolites in the human brain. I. Compartments and water. *J Magn Reson* 1993;102(1):1–8.
- [39] West J, Aalto A, Tisell A, Leinhard OD, Landtblom AM, Smedby O, et al. Normal appearing and diffusely abnormal white matter in patients with multiple sclerosis assessed with quantitative MR. *PLoS One* 2014;9(4):e95161.
- [40] Hagiwara A, Hori M, Yokoyama K, Takemura MY, Andica C, Kumamaru KK, et al. Utility of a multiparametric quantitative MRI model that assesses myelin and edema for evaluating plaques, periplaque white matter, and normal-appearing white matter in patients with multiple sclerosis: a feasibility study. *AJNR Am J Neuroradiol* 2017;38(2):237–42.
- [41] Wang H, Yuan H, Shu L, Xie J, Zhang D. Prolongation of T(2) relaxation times of hippocampus and amygdala in Alzheimer's disease. *Neurosci Lett* 2004;363(2):150–3.
- [42] Just M, Thelen M. Tissue characterization with T1, T2, and proton density values: results in 160 patients with brain tumors. *Radiology* 1988;169(3):779–85.
- [43] Lustig M, Donoho D, Pauly JM. Sparse MRI: the application of compressed sensing for rapid MR imaging. *Magn Reson Med* 2007;58(6):1182–95.



Available online at
ScienceDirect
www.sciencedirect.com

Elsevier Masson France
EM|consulte
www.em-consulte.com



Editorial

Synthetic MRI and MR fingerprinting in routine neuroimaging protocol: What's the next step?

Simultaneous relaxometry techniques to map relaxation parameters in tissues are attracting widespread interest owing to the objective quantification of tissue properties and potential reduction in the scan time. So far, synthetic MRI and MR fingerprinting (MRF) are the two major simultaneous relaxometry techniques with regulatory approval. Synthetic MRI maps T1 and T2 relaxation times and proton density and synthesizes various contrast-weighted images, including T1- and T2-weighted and fluid-attenuated inversion recovery (FLAIR) images within a single 6-min acquisition [1–3]. MRF is another promising approach to simultaneously quantify tissue properties in a clinically feasible time. Instead of performing curve fitting, as in conventional relaxometry techniques, MRF adopts a unique approach in which acquisition parameters are simultaneously varied across repetition times to generate signal evolutions that characterize the various relaxation processes unique to each tissue [4]. The acquired signal is pattern-matched to a dictionary of simulated signal evolutions to acquire various quantitative metrics, such as T1 and T2 values. Both synthetic MRI and MRF show high repeatability and reproducibility of T1 and T2 values for standardized phantoms [5–7] and in vivo [6–9]. Moreover, recent efforts have enabled high-resolution three-dimensional volume coverage of the whole brain on both synthetic MRI [10,11] and MRF [12–14]. In addition, acceleration techniques, such as simultaneous multi-slice acquisition [15], have been implemented to further accelerate scanning, making these relaxometry techniques more usable in clinical settings.

In this issue of *Journal of Neuroradiology*, Ryu et al. reported their initial experience with contrast-weighted images obtained using synthetic MRI as a routine neuroimaging protocol in daily clinical practice [16]. Contrary to many previous studies that used synthetic MRI in the research protocol, this study was unique in that it implemented synthetic MRI as the routine protocol by replacing some conventional sequences, such as T1 and T2-weighted images, with synthetic MRI. Two radiologists retrospectively reviewed the imaging data of 89 patients, rated the overall image quality and anatomical delineation, and found that the image qualities of synthetic T1- and T2-weighted images were adequate for clinical use. FLAIR images showed pronounced artifacts but without any significant impact on the diagnosis. Further, they also evaluated images obtained with synthetic phase-sensitive inversion recovery (PSIR), which is a T1-weighted sequence with a greater signal intensity range, and found that the overall image quality with anatomical delineation of PSIR was superior to that of other synthetic images. They concluded that synthetic MRI can be accepted as a routine neuroimaging protocol in the clinical practice.

Then, why have synthetic MRI and MRF not been widely accepted in the clinics, despite their potential and promising performance reported in the literature? A major challenge is the generation of high-quality synthetic images from the quantitative maps. In general, the quality of FLAIR images generated from quantitative relaxation maps is inferior to that of conventional FLAIR images, which is an essential sequence in neuroradiology. Although Ryu et al. [16] and previous studies [17,18] reported that the inferior quality of synthetic FLAIR images did not affect the diagnostic ability, clinicians may not be confident regarding its use yet. The acquisition is rapid, but adding the sequence to the protocol will prolong the total scan time. To implement synthetic MRI or MRF in a time-limited clinical workflow, some existing sequences should be replaced so that the entire protocol is not elongated. Hence, improvement of the image synthesis technique to generate high-quality contrast-weighted images would be a key step for a wide clinical implementation. Approaches that rely on a multi-component model may potentially mitigate artifacts seen on synthetic FLAIR images [19]. Adopting deep learning to directly generate contrast-weighted images while bypassing T1 and T2 maps has also been gathering considerable interest for several years [20–22]. This approach improves the FLAIR image quality and, furthermore, generates MR angiography images, which are also important in the clinical practice. Implementation of these techniques is expected to further accelerate the use of synthetic MRI and MRF in the routine clinical practice.

Disclosure of interest

The authors declare that they have no competing interest.

Grant support

This work was supported by JSPS KAKENHI grant number 18H02772 and 19K17177; and AMED under grant number 19dm0307101h0001.

References

- [1]. Warntjes JB, Leinhard OD, West J, Lundberg P. Rapid magnetic resonance quantification on the brain: optimization for clinical usage. *Magn Reson Med*. 2008;60(2):320–329.
- [2]. Andica C, Hagiwara A, Hori M, Kamagata K, Koshino S, Maekawa T, et al. Review of synthetic MRI in pediatric brains: basic principle of MR quantification, its features, clinical applications, and limitations. *J Neuroradiol*. 2019;46(4):268–275.
- [3]. Hagiwara A, Warntjes M, Hori M, Andica C, Nakazawa M, Kumamaru KK, et al. SyMRI of the brain: rapid quantification of relaxation rates and proton density,

- with synthetic mri, automatic brain segmentation, and myelin measurement. *Invest Radiol.* 2017;52(10):647–657.
- [4]. Ma D, Gulani V, Seiberlich N, Liu K, Sunshine JL, Duerk JL, et al. Magnetic resonance fingerprinting. *Nature.* 2013;495(7440):187–192.
- [5]. Jiang Y, Ma D, Keenan KE, Stupic KF, Gulani V, Griswold MA. Repeatability of magnetic resonance fingerprinting T1 and T2 estimates assessed using the ISMRM/NIST MRI system phantom. *Magn Reson Med.* 2017;78(4):1452–1457.
- [6]. Kato Y, Ichikawa K, Okudaira K, Taoka T, Kawaguchi H, Murata K, et al. Comprehensive evaluation of B1(+)-corrected FISP-based magnetic resonance fingerprinting: accuracy, repeatability and reproducibility of T1 and T2 relaxation times for ISMRM/NIST system phantom and volunteers. *Magn Reson Med Sci.* 2019. <http://dx.doi.org/10.2463/mrms.mp.2019-0016> [Online ahead of print].
- [7]. Hagiwara A, Hori M, Cohen-Adad J, Nakazawa M, Suzuki Y, Kasahara A, et al. Linearity, bias, intrascanner repeatability, and interscanner reproducibility of quantitative multidynamic multiecho sequence for rapid simultaneous relaxometry at 3T: a validation study with a standardized phantom and healthy controls. *Invest Radiol.* 2019;54(1):39–47.
- [8]. Buonincontri G, Biagi L, Retico A, Cecchi P, Cosottini M, Gallagher FA, et al. Multi-site repeatability and reproducibility of MR fingerprinting of the healthy brain at 1.5 and 3.0T. *Neuroimage.* 2019;195:362–372.
- [9]. Korzdorfer G, Kirsch R, Liu K, Pfeuffer J, Hensel B, Jiang Y, et al. Reproducibility and repeatability of MR fingerprinting relaxometry in the human brain. *Radiology.* 2019;292(2):429–437.
- [10]. Fujita S, Hagiwara A, Hori M, Warntjes M, Kamagata K, Fukunaga I, et al. 3D quantitative synthetic MRI-derived cortical thickness and subcortical brain volumes: scan-rescan repeatability and comparison with conventional T1-weighted images. *J Magn Reson Imaging.* 2019;50(6):1834–1842. <http://dx.doi.org/10.1002/jmri.26744>.
- [11]. Fujita S, Hagiwara A, Hori M, Warntjes M, Kamagata K, Fukunaga I, et al. Three-dimensional high-resolution simultaneous quantitative mapping of the whole brain with 3D-QALAS: an accuracy and repeatability study. *Magn Reson Imaging.* 2019;63:235–243.
- [12]. Cao X, Ye H, Liao C, Li Q, He H, Zhong J. Fast 3D brain MR fingerprinting based on multi-axis spiral projection trajectory. *Magn Reson Med.* 2019;82(1):289–301.
- [13]. Ma D, Jiang Y, Chen Y, McGivney D, Mehta B, Gulani V, et al. Fast 3D magnetic resonance fingerprinting for a whole-brain coverage. *Magn Reson Med.* 2018;79(4):2190–2197.
- [14]. Liao C, Bilgic B, Manhard MK, Zhao B, Cao X, Zhong J, et al. 3D MR fingerprinting with accelerated stack-of-spirals and hybrid sliding-window and GRAPPA reconstruction. *Neuroimage.* 2017;162:13–22.
- [15]. Ye H, Ma D, Jiang Y, Cauley SF, Du Y, Wald LL, et al. Accelerating magnetic resonance fingerprinting (MRF) using t-blipped simultaneous multislice (SMS) acquisition. *Magn Reson Med.* 2016;75(5):2078–2085.
- [16]. Ryu KH, Baek HJ, Moon JI, Choi BH, Park SE, Ha JY, et al. Initial clinical experience of synthetic MRI as a routine neuroimaging protocol in daily practice: a single-center study. *J Neuroradiol.* 2020;47(2):151–160.
- [17]. Tanenbaum LN, Tsiouris AJ, Johnson AN, Naidich TP, DeLano MC, Melhem ER, et al. Synthetic MRI for Clinical Neuroimaging: Results of the Magnetic Resonance Image Compilation (MAGiC) Prospective, Multicenter, Multireader Trial. *AJNR Am J Neuroradiol.* 2017;38(6):1103–1110.
- [18]. Blystad I, Warntjes JB, Smedby O, Landtblom AM, Lundberg P, Larsson EM. Synthetic MRI of the brain in a clinical setting. *Acta Radiol.* 2012;53(10):1158–1163.
- [19]. Cencini M, Buonincontri G, Biagi L, Gómez PA, Schulte RF, Tosetti M. Chasing true FLAIR: a three-component magnetic resonance fingerprinting approach to synthetic MRI. *Proceedings of the 27th Annual Meeting of ISMRM.* 2019:0816.
- [20]. Hagiwara A, Otsuka Y, Hori M, Tachibana Y, Yokoyama K, Fujita S, et al. Improving the quality of synthetic FLAIR images with deep learning using a conditional generative adversarial network for pixel-by-pixel image translation. *AJNR Am J Neuroradiol.* 2019;40(2):224–230.
- [21]. Fujita S, Hagiwara A, Otsuka Y, Hori M, Takei N, Hwang K-P, et al. Deep learning approach for generating MRA images from 3D quantitative synthetic MRI without additional scans. *Invest Radiol.* 2020. <http://dx.doi.org/10.1097/RLI.0000000000000628> [Online ahead of print].
- [22]. Virtue P, Tamir JJ, Doneva M, Yu SX, Lustig M. Learning Contrast Synthesis from MR Fingerprinting. *Proceedings of the 26th Annual Meeting of ISMRM.* 2018:0676.





Shohei Fujita^{a,b,*}
Akifumi Hagiwara^b
Shigeki Aoki^b
Osamu Abe^a

^a Department of Radiology, Graduate School of Medicine, University of Tokyo, Tokyo, Japan

^b Department of Radiology, Juntendo University Hospital, Tokyo, Japan

* Corresponding author. Department of Radiology, Graduate School of Medicine, University of Tokyo, 7-3-1, Hongo, Bunkyo-ku, Tokyo 113-8655, Japan. E-mail address: shifujita-tky@umin.ac.jp (S. Fujita)

3D Quantitative Synthetic MRI-Derived Cortical Thickness and Subcortical Brain Volumes: Scan–Rescan Repeatability and Comparison With Conventional T₁-Weighted Images

Shohei Fujita, MD,¹  Akifumi Hagiwara, MD, PhD,^{1,2*}  Masaaki Hori, MD, PhD,¹ Marcel Warntjes, PhD,^{3,4} Koji Kamagata, MD, PhD,¹ Issei Fukunaga, PhD,¹ Masami Goto, PhD,⁶ Haruyama Takuya, BS,^{1,5} Kohei Takasu, BS,⁶ Christina Andica, MD,¹  Tomoko Maekawa, MD,^{1,2} Mariko Yoshida Takemura, MD, PhD,¹ Ryusuke Irie, MD,^{1,2} Akihiko Wada, MD, PhD,¹ Michimasa Suzuki, MD, PhD,¹ and Shigeki Aoki, MD, PhD¹ 

Background: Previous quantitative synthetic MRI of the brain has been solely performed in 2D.

Purpose: To evaluate the feasibility of the recently developed sequence 3D-QALAS for brain cortical thickness and volumetric analysis.

Study Type: Reproducibility/repeatability study.

Subjects: Twenty-one healthy volunteers (35.6 ± 13.8 years).

Field Strength/Sequence: 3D T₁-weighted fast spoiled gradient recalled echo (FSPGR) sequence was performed once, and 3D-QALAS sequence was performed twice with a 3T scanner.

Assessment: FreeSurfer and FIRST were used to measure cortical thickness and volume of subcortical structures, respectively. Agreement with FSPGR and scan–rescan repeatability were evaluated for 3D-QALAS.

Statistical Tests: Percent relative difference and intraclass correlation coefficient (ICC) were used to assess reproducibility and scan–rescan repeatability of the 3D-QALAS sequence-derived measurements.

Results: Percent relative difference compared with FSPGR in cortical thickness of the whole cortex was 3.1%, and 89% of the regional areas showed less than 10% relative difference in cortical thickness. The mean ICC across all regions was 0.65, and 74% of the structures showed substantial to almost perfect agreement. For volumes of subcortical structures, the median percent relative differences were lower than 10% across all subcortical structures, except for the accumbens area, and all structures showed ICCs of substantial to almost perfect agreement. For the scan–rescan test, percent relative difference in cortical thickness of the whole cortex was 2.3%, and 97% of the regional areas showed less than 10% relative difference in cortical thickness. The mean ICC across all regions was 0.73, and 80% showed substantial to almost perfect agreement. For volumes of subcortical structures, relative differences were less than 10% across all subcortical structures except for the accumbens area, and all structures showed ICCs of substantial to almost perfect agreement.

Data Conclusion: 3D-QALAS could be reliably used for measuring cortical thickness and subcortical volumes in most brain regions.

Level of Evidence: 3

Technical Efficacy: Stage 1

J. MAGN. RESON. IMAGING 2019.

View this article online at wileyonlinelibrary.com. DOI: 10.1002/jmri.26744

Received Sep 13, 2018, Accepted for publication Mar 26, 2019.

*Address reprint requests to: A.H., Department of Radiology, Juntendo University School of Medicine, 1-2-1, Hongo, Bunkyo-ku, Tokyo 113-8421, Japan.
E-mail: a-hagiwara@juntendo.ac.jp

From the ¹Department of Radiology, Juntendo University Hospital, Tokyo, Japan; ²Department of Radiology, Graduate School of Medicine, University of Tokyo, Tokyo, Japan; ³SyntheticMR AB, Sweden; ⁴Center for Medical Imaging Science and Visualization (CMIV), Sweden; ⁵Department of Radiological Sciences, Graduate School of Human Health Sciences, Tokyo Metropolitan University, Tokyo, Japan; and ⁶School of Allied Health Sciences, Kitasato University, Kanagawa, Japan

Additional supporting information may be found in the online version of this article

This is an open access article under the terms of the Creative Commons Attribution-NonCommercial License, which permits use, distribution and reproduction in any medium, provided the original work is properly cited and is not used for commercial purposes.

TISSUE RELAXOMETRY can provide quantitative values for the evaluation of diseases,¹ development,² and aging,³ as opposed to arbitrary signal intensities of conventional magnetic resonance imaging (MRI) such as T₁-weighted, T₂-weighted, and FLAIR images. However, its use in human brain imaging has mostly been limited to research applications because of additional lengthy scan times. Recently, quantitative synthetic MRI, enabling simultaneous quantification of T₁ and T₂ relaxation times and proton density (PD) with high reliability,⁴ has been proposed for whole brain coverage.^{5,6} The technique also allows for the creation of any contrast-weighted image that is used routinely in clinical settings,⁷ rendering its clinical application highly feasible. Quantitative synthetic MRI has been applied to a variety of diseases, such as multiple sclerosis,^{8,9} meningitis,¹⁰ and brain infarctions,¹¹ with promising results. The original sequence used for quantitative synthetic MRI was based on a multislice 2D acquisition, providing a relatively low resolution in the slice direction in comparison to conventional 3D T₁-weighted acquisitions. Recently, however, 3D-QALAS (3D-quantification using an interleaved Look-Locker acquisition sequence with T₂ preparation pulse) has been developed for simultaneous quantification of T₁ and T₂ in cardiac imaging, showing high accuracy and precision in the heart and phantoms with various tissue properties.^{12,13}

As opposed to relaxometry, volumetric analysis of the brain has already been widely performed in clinical settings, such as for the evaluation of patients with neurodegenerative¹⁴ and demyelinating disorders.¹⁵ Additionally, regional volumetric analysis has been extensively performed in research settings. Changes in cortical thickness and subcortical volumes are related to aging^{16–18} and in a wide variety of neurological disorders.^{14,16,19} Taken together, differences in regional cortical thickness and subcortical volume may indicate the state of neurological health, and their accurate measurements may lead to a better understanding of patients' conditions.

Here, we propose application of the 3D-QALAS sequence for simultaneous acquisition of relaxometry parameters as well as for obtaining volumetric information in high-resolution 3D. Therefore, the purpose of this study was to show the validity of volumetric information acquired with 3D-QALAS by 1) evaluating the reproducibility of 3D-QALAS sequence-derived volumetric brain measurements using conventional T₁-weighted imaging-derived measurements as reference standards, and 2) evaluating the repeatability of 3D-QALAS sequence-derived measurements by scan–rescan tests, on healthy subjects.

Materials and Methods

Subjects

This study was approved by our Institutional Review Board and written informed consent was acquired from all participants. Twenty-one healthy volunteers were included in this study (14 women and 7 men; mean age, 35.6 ± 13.8 years). None of the participants had a history of a major medical condition including neurological or psychiatric disorders. Two

radiologists (S.F. and A.H.) performed a blind examination on all volunteer exams and confirmed that all had normal structural MRI results.

Image Acquisition

All participants were scanned with a 3T scanner (Discovery 750w; GE Healthcare, Milwaukee, WI) with a 12-channel head coil. A 3D T₁-weighted fast spoiled gradient recalled echo (FSPGR) sequence was performed once, and the 3D-QALAS sequence was performed twice (to test scan–rescan) in the same session on all the participants. Between scan–rescan of the 3D-QALAS sequence, the subjects were taken out of the MRI room and repositioned on the scanner. The scan parameters of FSPGR were as follows: sagittal acquisition; repetition time / echo time / inversion time (TR/TE/TI), 7.7/3.1/400 msec; field of view (FOV), 256 × 256 mm; matrix size, 256 × 256; section thickness, 1.0 mm; flip angle, 11°; receiver bandwidth, 244.1 Hz/pixel; averages, 1; acquisition time, 5 min 45 sec. 3D-QALAS is based on a multiacquisition 3D gradient echo, with five acquisitions equally spaced in time, interleaved with a T₂ preparation pulse and an inversion pulse. Briefly, T₁ fitting was performed on four acquisitions after the inversion pulse, and T₂ fitting was performed on extrapolation of the signal intensity straddling the T₂ prep pulse. Instead of a cardiac trigger, an internal trigger started each of the five acquisitions every 900 msec, making the total cycle time 4.5 sec. Further details of the 3D-QALAS sequence and its postprocessing are available in a previous study.¹² The scan parameters of 3D-QALAS were as follows: axial acquisition; TR/TE/TI, 8.6/3.5/100 msec; FOV, 256 × 256; matrix size, 256 × 256; section thickness, 1.0 mm; flip angle, 5°; receiver bandwidth, 97.7 Hz/pixel; averages, 1; acquisition time, 11 min 41 sec. We set the spatial resolution of the FSPGR imaging, standard reference in this study, as 1.0 mm isotropic, since the Alzheimer's Disease Neuroimaging Initiative (ADNI)²⁰ study recommended the usage of 1.0 mm isotropic data at 3T. All 3D-QALAS and FSPGR images were visually examined for artifacts such as ringing, blurring, and ghosting on site upon image acquisition. Images exhibiting these common artifacts were excluded from this study and subjects with such artifacts were rescanned.

Image Postprocessing

Images obtained from the 3D-QALAS sequence were processed on a prototype version 0.45.5 of the SyMRI software (SyntheticMR, Linköping, Sweden) to synthesize 3D synthetic T₁-weighted images. TR and TE were virtually set to the default values of 500 msec and 10 msec, respectively. These 3D synthetic T₁-weighted images and FSPGR images were used for subsequent analyses. Noncommercial automatic brain parcellation programs, described below, were used to measure cortical thickness and the volume of subcortical structures on the basis of 3D T₁-weighted images for each subject.

MEASUREMENT OF CORTICAL THICKNESS AND VOLUME.

The pipeline of FreeSurfer (v. 5.3.0, <http://surfer.nmr.mgh.harvard.edu>) was used to obtain cortical thickness and volume for each sequence. FreeSurfer utilizes affine transformations and combines information about voxel intensity relative to a probability distribution for tissue classes with information about the spatial relationship of the voxel to the location of neighboring structures obtained from a manually labeled atlas.^{21,22} The Desikan-Killiany Atlas, consisting of 34 regions per hemisphere,

was used to measure average cortical thickness and volume in each area.¹⁸ Further details of FreeSurfer are available in previous articles,^{21,22} and in the documentation provided by the developers (<http://surfer.nmr.mgh.harvard.edu/>). The default analysis settings were used in running the “recon-all” command. Bilateral regional values were averaged for further analysis. Previous research has shown that brain mask cleaning was the only type of manual intervention that improved FreeSurfer-derived results.²³ Therefore, manual brain mask assessment was performed in this study. For each subject, the brain mask was visually assessed on axial, sagittal, and coronal images. Brain masks excluding brain tissue (overcropping) were manually corrected using the Freeview application. A brain mask including extracerebral tissue, such as orbit (undercropping), was not corrected because it still allowed accurate surface demarcation.

VOLUMETRY OF SUBCORTICAL STRUCTURES. Due to high variability in the spatial location and extent of subcortical gray matter segmentations produced by FreeSurfer,²¹ the volumes of subcortical gray matter structures were obtained using the pipeline of FMRIB Integrated Registration and Segmentation Tool (FIRST, <http://fsl.fmrib.ox.ac.uk/fsl/fslwiki/FIRST>) implemented in the FMRIB Software Library v. 5.0.9.²⁴ The volumes of subcortical white matter structures were obtained based on FreeSurfer using the Desikan-Killiany Atlas. Volumes of subcortical structures were measured for each sequence. All segmentation results performed on FreeSurfer and FIRST were visually screened for gross errors.

Statistical Analysis

All statistical analyses were performed with R program v. 3.3.0 (R Core Team [2016]. R: A language and environment for statistical computing. R Foundation for Statistical Computing, Vienna, Austria. URL <https://www.R-project.org/>). Agreement to measurements obtained from FSPGR and scan–rescan repeatability were evaluated for 3D-QALAS. Percent relative difference and intraclass correlation coefficient (ICC) were used to assess reproducibility and repeatability of the 3D-QALAS sequence-derived measurements. Within-subject coefficient of variation (wCV) was also used in assessing repeatability. ICC is a measure of within-subject relative to between-subject variability. The ICC estimates of agreement were categorized as the following: slight (0.01–0.20), fair (0.21–0.40), moderate (0.41–0.60), substantial (0.61–0.80), and almost perfect agreement (0.81–1.0).²⁵ Percent relative difference was calculated

by dividing the absolute difference by the mean of two measurements, defined as follows:

$$\text{percent relative difference} = \frac{2|X - Y|}{X + Y} \times 100$$

where X and Y are the measured values. The wCV was defined as follows:

$$\text{wCV} = \frac{\sigma_w}{\mu} \times 100$$

where σ_w is the within-subject standard deviation and μ is the overall mean of the measured values.

Results

Representative FreeSurfer and FIRST outputs from 3D-QALAS sequence-derived T₁-weighted images are shown in Fig. 1.

Measurement of Cortical Thickness

REPRODUCIBILITY OF 3D-QALAS SEQUENCE-DERIVED CORTICAL THICKNESS AND VOLUME: COMPARISON WITH CONVENTIONAL FSPGR. Figure 2 shows a histogram of 3D-QALAS and FSPGR sequence-derived cortical thickness estimated using FreeSurfer across all regions in the Desikan-Killiany Atlas in all subjects. The range of the cortical thicknesses in this study was consistent with previous studies, reporting cortical thickness ranging from 1–4.5 mm (both of postmortem and FreeSurfer-based findings).^{18,23,26} In Fig. 3a, regional percent relative differences between 3D-QALAS and FSPGR-derived cortical thicknesses are overlaid on an inflated brain. Figure 3b shows the boxplots for percent relative differences. Percent relative difference of the whole cortex was 3.1%, and 89% of the regional areas showed less than 10% relative difference in cortical thickness. Cortical thickness of the temporal pole, inferior temporal, pericalcarine, fusiform, and entorhinal cortex showed relatively low agreement. Table 1 shows the ICCs for 3D-QALAS and FSPGR-derived cortical thickness. The mean ICC across all regions was 0.65, and 74% of the structures showed substantial to almost perfect agreement. Cortical thickness of the temporal pole, entorhinal, lateral orbitofrontal, pars orbitalis, inferior temporal, pericalcarine, and the fusiform cortex showed particularly low

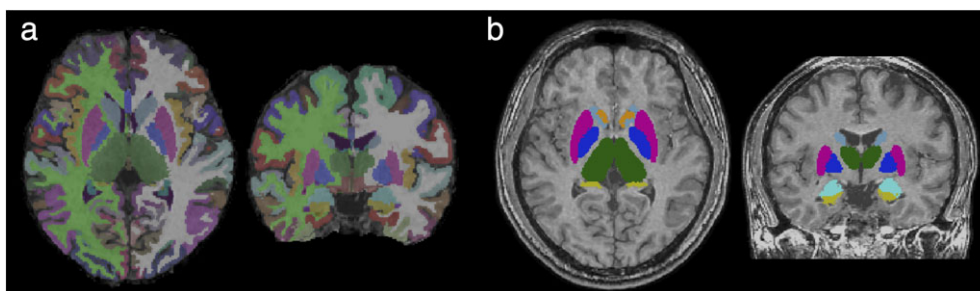


FIGURE 1: Representative labels created from automated parcellation of brain regions using (a) FreeSurfer and (b) FIRST. Results of segmentation are overlaid on synthetic T₁-weighted images.

ICC. Supplementary Table 1 shows the ICCs for 3D-QALAS and FSPGR-derived cortical volume. The mean ICC across all regions was 86%, and 97% of the structures showed substantial to almost perfect agreement. Cortical thickness of the temporal pole showed particularly low ICC.

SCAN-RESCAN REPEATABILITY OF 3D-QALAS SEQUENCE-DERIVED CORTICAL THICKNESS AND VOLUME. In Fig. 4a, regional percent relative differences between scan and rescan of 3D-QALAS-derived cortical thicknesses are overlaid on an inflated brain. Figure 4b shows the boxplots for percent relative differences. Relative percent difference in thickness of the whole cortex was 2.3%, and 97% of the regional cortical thickness showed less than 10% relative difference. Cortical thickness of the temporal pole showed relatively low agreement. Table 1 shows ICCs and wCV for scan-rescan cortical thickness. The mean ICC across all regions was 0.73, and 80% of the structures showed substantial to almost perfect agreement. Temporal pole, entorhinal, pars orbitalis, inferior temporal, and the orbitofrontal cortical thickness showed particularly low ICC and/or wCV. Supplementary Table 1 shows ICCs and wCV for scan-rescan cortical volume. The mean ICC across all regions was 87%, and 94% of the structures showed substantial to almost perfect agreement. Temporal pole and entorhinal cortical volumes showed particularly low ICC and wCV. The 3D-QALAS sequence-derived cortical volume of each region is listed in Supplementary Table 2.

Volumetry of Subcortical Structures

REPRODUCIBILITY OF 3D-QALAS SEQUENCE-DERIVED SUBCORTICAL STRUCTURAL VOLUMES: COMPARISON WITH CONVENTIONAL FSPGR. Figure 5a shows the percent relative differences between 3D-QALAS and FSPGR-derived measurements in subcortical gray matter structural volumes. The median percent relative differences were lower than 10% across

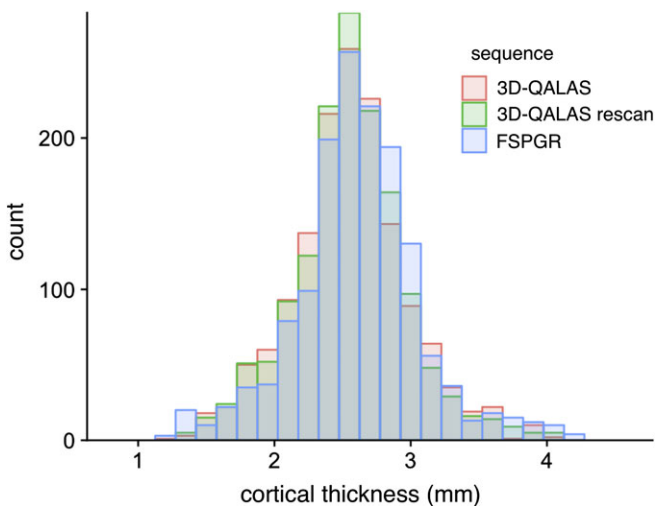


FIGURE 2: Histograms of cortical thicknesses derived from 3D-QALAS scan-rescan and FSPGR in all subjects measured using FreeSurfer.

all subcortical structures, except for the accumbens area. ICC for 3D-QALAS and FSPGR-derived measurements are shown in Table 2. All structures showed substantial or almost perfect agreement. Supplementary Table 3 shows the ICCs for 3D-QALAS and FSPGR-derived white matter volume. All structures except subcortical white matter of the temporal pole showed substantial or almost perfect agreement.

SCAN-RESCAN REPEATABILITY OF 3D-QALAS SEQUENCE-DERIVED SUBCORTICAL STRUCTURAL VOLUMES. Figure 5b shows the percent relative difference between scan and rescan of 3D-QALAS-derived measurements in subcortical gray matter structural volumes. Percent relative differences were less than 10% across all subcortical structures, except for the accumbens area. ICC and wCV for 3D-QALAS and FSPGR-derived measurements are shown in Table 2. All structures showed substantial to almost perfect agreement. The wCVs were lower than 10% across all subcortical structures, except for the accumbens area. Supplementary Table 3 shows the ICCs and wCV for scan-rescan white matter volume. All structures except subcortical white matter of entorhinal and frontal pole showed substantial or almost perfect agreement. The 3D-QALAS sequence-derived volume of each subcortical structure is listed in Supplementary Table 4.

Discussion

In this study, 3D synthetic T_1 -weighted images showed good agreement with the FSPGR 1.0 mm isotropic images in measuring regional cortical thickness and subcortical volumes in most of the brain regions. High repeatability of the 3D synthetic MRI-derived brain measurements was demonstrated in the scan-rescan test.

The 3D isotropic acquisition of 3D-QALAS allows high resolution multiplanar reconstruction, without additional scans from different directions. This capability not only provides the advantage in visual assessment and delineation of lesions, but also enables to accurately segment regional structures. With the quantification of T_1 , T_2 , and PD in these regional structures, 3D-QALAS may enable detecting and describing changes within regional structures, which could be obscured when averaging values over gross anatomic regions. Hence, 3D-QALAS has a potential to provide thorough and comprehensive characterization of brain lesions as well as the entire brain.

Cortical thickness derived from 3D synthetic T_1 -weighted and FSPGR images showed a percent relative difference of 3.1% in the whole cortex, and 89% of the regional areas showed less than 10% relative difference in cortical thickness. Although high agreements were shown in the majority of the brain regions, low agreements were found in cortical thickness of temporal pole, inferior temporal, pericalcarine, and fusiform, as shown by their median percent relative differences of more than 10%. This observation is consistent with previous studies using FreeSurfer that reported a negative relationship between cortical volume/surface

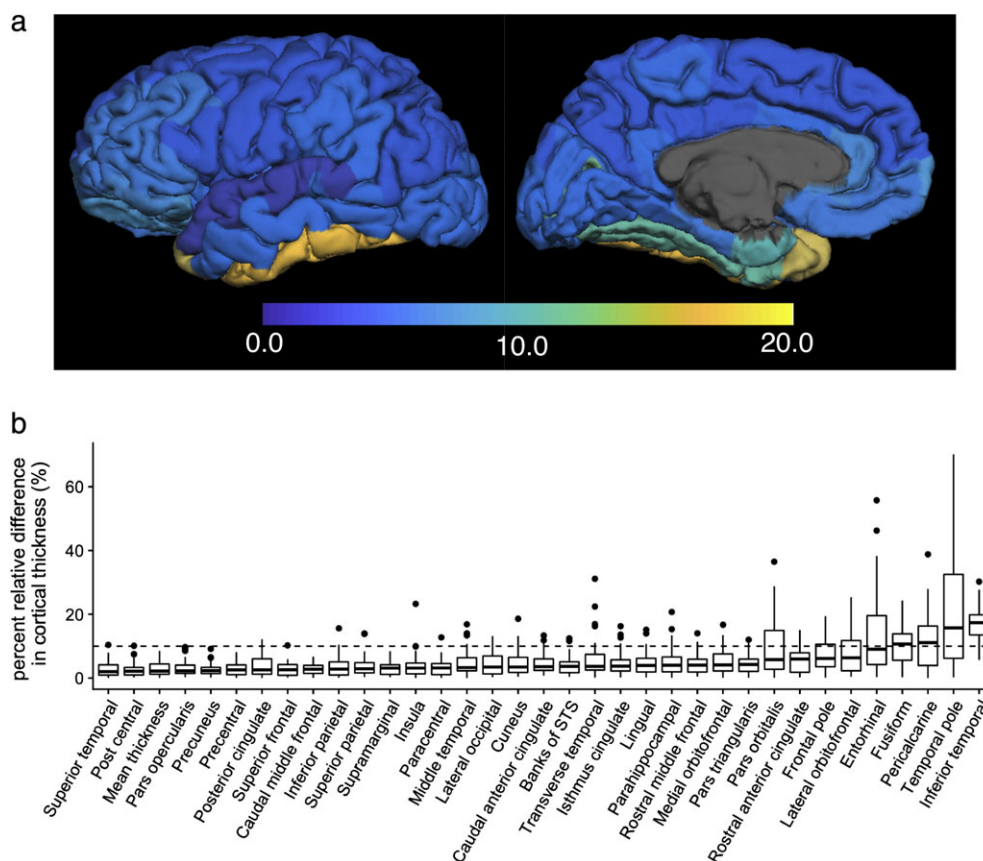


FIGURE 3: Percent relative difference in cortical thickness for 3D-QALAS and FSPGR measured using FreeSurfer. Regional percent relative difference is overlaid on an inflated brain surface (a). Median values and interquartile ranges are shown in boxplots (b). Whiskers are set at minimum and maximum, and the horizontal line marks the median. Boxes indicate the interquartile range (25–75%). Dots at the end of the boxplot represent outliers.

area and relative error of measured cortical thickness,^{23,27} which can explain low agreement in the small structures in the current study. It has also been reported that the boundaries of the temporal pole and occipital lobe were not defined precisely using FreeSurfer,²⁸ which may explain the low agreement in thickness of the temporal pole and pericalcarine.

Another possibility of the low agreements in lower parts of the brain structure is the effects of B_0 inhomogeneities due to susceptibility differences between bone and air, which could cause fitting errors upon quantifying T_1 , T_2 , and PD, and affect the subsequent synthetic T_1 -weighted images.²⁹

The cortical thickness derived from scan–rescan of 3D synthetic T_1 -weighted images showed less than a 10% relative percent difference across all regions except the thickness of the temporal pole. A previous study that included a large collection of cortical thickness data based on scan–rescan of conventional 3D magnetization prepared rapid acquisition with gradient echo (MPRAGE) images showed overall percent relative differences of 2.5–2.8% using FreeSurfer.²⁷ The median percent relative differences of 3D synthetic T_1 -weighted image-derived cortical thickness in our study was 2.9%, which is comparable to the repeatability achieved when using conventional 3D T_1 -weighted images.

Subcortical volumes derived from 3D synthetic T_1 -weighted and FSPGR images showed a percent relative difference lower than 10% across all structures except the nucleus accumbens, and the scan–rescan test of 3D synthetic T_1 -weighted images showed a percent relative difference lower than 10% across all subcortical structures. Segmentation of the accumbens and amygdala showed relatively low agreement both in scan–rescan and comparison with FSPGR in this study, which is consistent with previous studies reporting that segmentation of these area was generally unreliable compared with other subcortical regions.^{30,31} One factor that may have contributed to this lower reliability in measurements is that they are the smallest subcortical structures. Morey et al³¹ reported that the percent relative difference of the accumbens and amygdala volumes, calculated from scan–rescan of 3D T_1 -weighted images with 1.0 mm isotropic voxel based on FIRST analysis, were both higher than 10%. Taken together, 3D synthetic T_1 -weighted imaging-based subcortical volume measurement can be assumed to be as reliable as conventional 3D T_1 -weighted imaging-based measurement.

Although the in-plane resolution of 1.0 mm used in this study is low compared with that of commonly used 2D sequences, high spatial resolution in the slice-select direction enables reliable detection and reproducible measurements

TABLE 1. Intraclass Correlation Coefficients and Within-Subject Coefficients of Variation Between 3D-QALAS and FSPGR, and Scan-Rescan of 3D-QALAS for Cortical Thicknesses Measured Using FreeSurfer

Measurement	FSPGR	Rescan	ICC
	ICC	wCV (%)	
Thickness			
Mean thickness	0.79	2.1	0.81
Caudal anterior cingulate	0.75	3.9	0.73
Caudal middle frontal	0.84	2.3	0.86
Cuneus	0.63	3.5	0.75
Entorhinal	0.28	9.4	0.50
Frontal pole	0.65	8.0	0.59
Fusiform	0.44	3.2	0.68
Inferior parietal	0.73	3.0	0.79
Inferior temporal	0.47	5.0	0.36
Insula	0.66	3.9	0.65
Isthmus cingulate	0.79	3.9	0.83
Lateral occipital	0.61	2.8	0.78
Lateral orbitofrontal	0.38	6.1	0.52
Lingual	0.62	3.0	0.72
Medial orbitofrontal	0.51	4.9	0.58
Middle temporal	0.75	4.1	0.66
Parahippocampal	0.86	3.4	0.90
Paracentral	0.77	3.8	0.75
Pars opercularis	0.79	2.2	0.87
Pars orbitalis	0.38	9.7	0.43
Pars triangularis	0.76	3.5	0.80
Pericalcarine	0.49	5.5	0.68
Postcentral	0.87	2.5	0.86
Posterior cingulate	0.71	3.1	0.81
Precentral	0.70	2.3	0.77
Precuneus	0.78	1.7	0.91
Rosterior anterior cingulate	0.63	4.8	0.69
Rostral middle frontal	0.55	3.1	0.75
Superior frontal	0.80	1.9	0.87
Superior parietal	0.78	1.9	0.90
Superior temporal	0.80	2.9	0.78
Supramarginal	0.84	2.8	0.81
Temporal pole	0.00	12.3	0.48
Transverse temporal	0.62	5.0	0.70

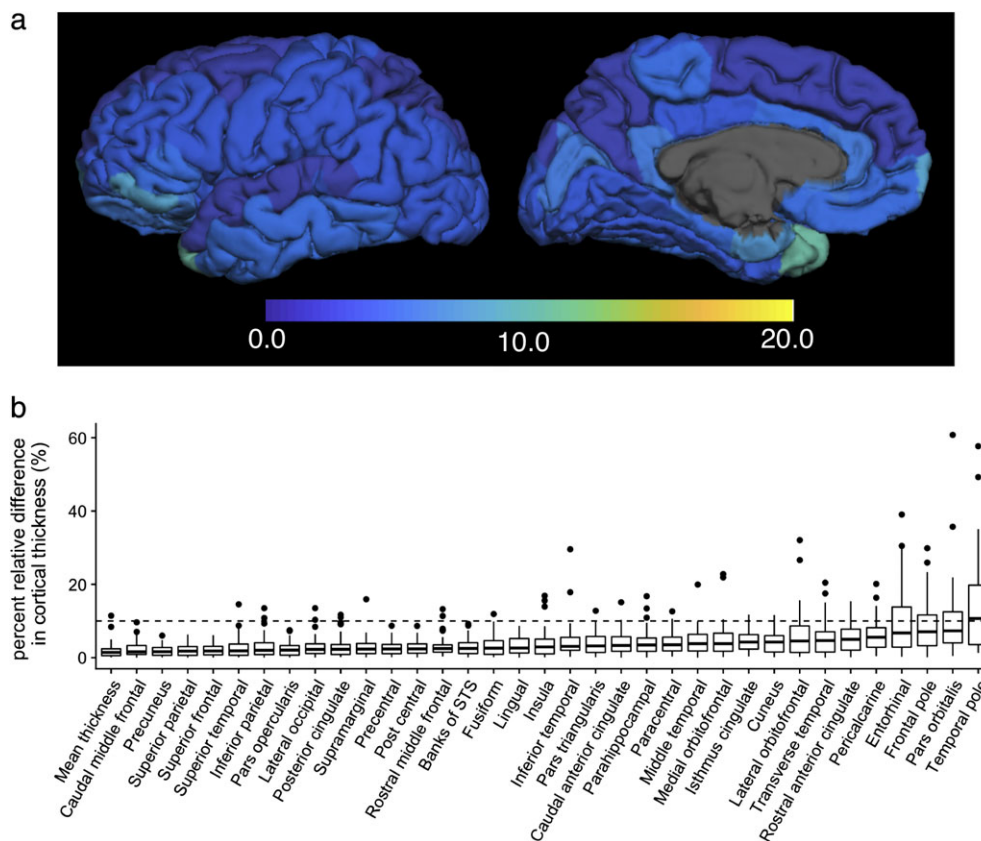


FIGURE 4: Percent relative difference in cortical thickness for 3D-QALAS scan-rescan, measured using FreeSurfer. Regional percent relative difference is overlaid on an inflated brain surface (a). Median values and interquartile ranges are shown in boxplots (b). Whiskers are set at minimum and maximum, and the horizontal line marks the median. Boxes indicate the interquartile range (25–75%). Dots at the end of the boxplot represent outliers.

among various slice positions and alignments. In fact, previous studies have shown that 3D imaging could be superior in detecting multiple sclerosis lesions and brain metastases than 2D imaging, even with lower in-plane resolutions.^{32,33}

We used T_1 -weighted images only with fixed TR and TE for segmentation in this study. Using multichannel inputs (eg, T_1 , T_2 , and PD maps), obtained from a single 3D-QALAS sequence scan, could improve the accuracy of current segmentation algorithms that rely heavily on T_1 -weighted image contrasts,

without elongating scanning times. Furthermore, even with only T_1 -weighting, combining T_1 -weighted images with different parameters might improve the overall segmentation, since T_1 -weighted images with fixed TR and TE may not be optimal for all brain structures. An additional advantage of synthetic MRI based on relaxation parameters is that the effects of B_1 inhomogeneities and coil sensitivity profiles on the T_1 -weighted images are removed.³⁴ This is expected to provide a more stable result in volumetric analysis.

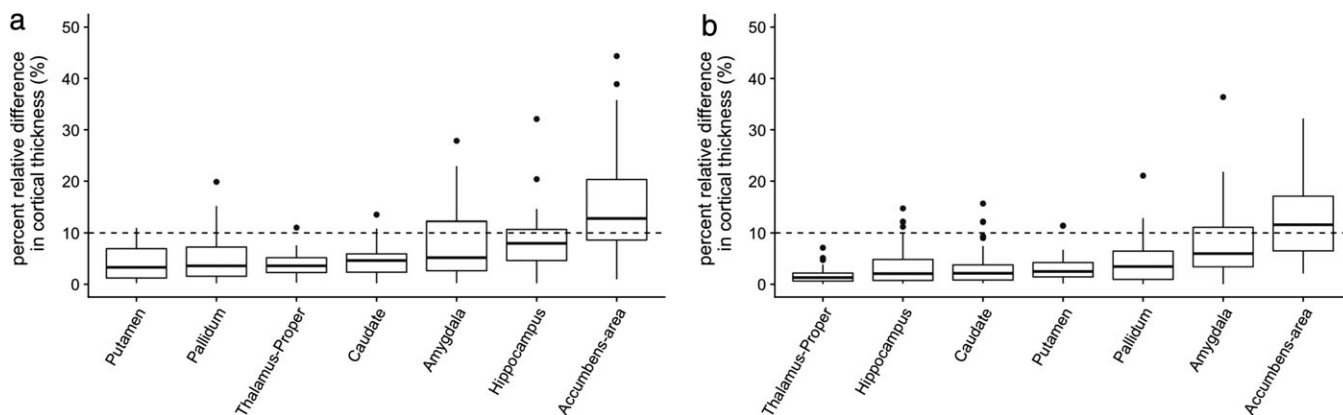


FIGURE 5: Percent relative difference of subcortical volumes measured using FIRST. (a) and (b) show comparisons between 3D-QALAS and FSPGR, and scan-rescan of 3D-QALAS, respectively. Whiskers are set at minimum and maximum, and the horizontal line marks the median. Boxes indicate the interquartile range (25–75%). Dots at the end of the boxplot represent outliers.

TABLE 2. Intraclass Correlation Coefficients and Within-Subject Coefficients of Variation Between 3D-QALAS and FSPGR, and Scan–Rescan of 3D-QALAS for Subcortical Volumes Measured Using FIRST

Measurement	FSPGR	Rescan	ICC
	ICC	wCV (%)	
Volume			
Putamen	0.86	2.9	0.91
Caudate nucleus	0.89	3.3	0.89
Nucleus accumbens	0.82	13.3	0.80
Globus pallidus	0.86	4.5	0.87
Hippocampus	0.84	3.5	0.91
Amygdala	0.66	7.6	0.72
Thalamus	0.91	1.5	0.96

Absolute quantification of tissue properties using relaxometry has been previously reported to be useful for the characterization of disease, assessment of disease activity, and monitoring of treatment.^{35,36} With accurate volumetric segmentation, 3D synthetic MRI could provide quantitative values of each brain substructure based on a single scan, which could allow for a more quantitative understanding of the brain.

The current study has several limitations. First, we only used a single 3T scanner, hence our results cannot be generalized to scanners with different field strengths. Previous studies have revealed certain biases between 1.5T and 3T for cortical thickness analysis and brain volumetry performed on FreeSurfer using 3D T₁-weighted images.^{37,38} Further research is needed to determine whether cortical thickness analysis and subcortical brain volumetry based on 3D-QALAS differ between different field strengths. Second, we used FSPGR as a standard reference, not with ground truth postmortem values. Although the ground truth for cortical thickness and subcortical volumes were not available, our results showed agreement with previous studies that compared FreeSurfer-derived measurements with postmortem values. Third, the scanning time in this study was relatively long for a routine clinical scan, making it difficult to use in clinical settings. Combining techniques such as compressed sensing³⁹ and multiband imaging⁴⁰ may further reduce scan times to a clinically applicable level. Fourth, only healthy volunteers were enrolled in this study. Although our goal in this study was not to compare patients and volunteers, future studies focusing on patients using 3D-QALAS are desired.

In conclusion, the current study may support the use of 3D quantitative synthetic MRI for reliably measuring cortical thickness and subcortical volumes in human brain, with the exceptions

of the nucleus accumbens, and thickness of temporal pole, entorhinal, inferior temporal, pericalcarine, and the fusiform.

Acknowledgment

Contract grant sponsor: Program for Brain Mapping by Integrated Neurotechnologies for Disease Studies (Brain/MINDS) from Japan Agency for Medical Research and Development, AMED; Contract grant sponsor: IMPACT Program of Council for Science, Technology and Innovation (Cabinet Office, Government of Japan); Contract grant sponsor: JSPS KAKENHI; Contract grant numbers: 16K10327, 19K17150, 19K17177, JP16H06280; Contract grant sponsor: Grant-in-Aid for Scientific Research on Innovative Areas, Resource and technical support platforms for promoting research “Advanced Bioimaging Support.”

Conflict of Interest

Marcel Wartjes is currently employed part-time at SyntheticMR and has stock in SyntheticMR.

References

- Bottomley PA, Hardy CJ, Argersinger RE, Allen-Moore G. A review of 1H nuclear magnetic resonance relaxation in pathology: Are T1 and T2 diagnostic? *Med Phys* 1987;14:1–37.
- Lee SM, Choi YH, You SK, et al. Age-related changes in tissue value properties in children: simultaneous quantification of relaxation times and proton density using synthetic magnetic resonance imaging. *Invest Radiol* 2018;53:236–245.
- Kumar R, Delshad S, Woo MA, Macey PM, Harper RM. Age-related regional brain T2-relaxation changes in healthy adults. *J Magn Reson Imaging* 2012;35:300–308.
- Hagiwara A, Hori M, Cohen-Adad J, et al. Linearity, bias, intra-scanner repeatability, and inter-scanner reproducibility of quantitative multi-echo sequence for rapid simultaneous relaxometry at 3T: A validation study with a standardized phantom and healthy controls. *Invest Radiol* 2019;54:39–47.
- Wartjes JB, Leinhard OD, West J, Lundberg P. Rapid magnetic resonance quantification on the brain: Optimization for clinical usage. *Magn Reson Med* 2008;60:320–329.
- Hagiwara A, Wartjes M, Hori M, et al. SyMRI of the brain: Rapid quantification of relaxation rates and proton density, with synthetic MRI, automatic brain segmentation, and myelin measurement. *Invest Radiol* 2017;52:647–657.
- Tanenbaum LN, Tsiouris AJ, Johnson AN, et al. Synthetic MRI for clinical neuroimaging: Results of the Magnetic Resonance Image Compilation (MAGiC) prospective, multicenter, multireader trial. *AJNR Am J Neuroradiol* 2017;38:1103–1110.
- Hagiwara A, Hori M, Yokoyama K, et al. Synthetic MRI in the detection of multiple sclerosis plaques. *AJNR Am J Neuroradiol* 2017;38:257–263.
- Granberg T, Uppman M, Hashim F, et al. Clinical feasibility of synthetic MRI in multiple sclerosis: A diagnostic and volumetric validation study. *AJNR Am J Neuroradiol* 2016;37:1023–1029.
- Andica C, Hagiwara A, Nakazawa M, et al. Synthetic MR imaging in the diagnosis of bacterial meningitis. *Magn Reson Med Sci* 2017;16:91–92.
- Wallaert L, Hagiwara A, Andica C, et al. The advantage of synthetic MRI for the visualization of anterior temporal pole lesions on double inversion recovery (DIR), phase-sensitive inversion recovery (PSIR), and myelin images in a patient with CADASIL. *Magn Reson Med Sci* 2018;17:275–276.

12. Kvernby S, Warntjes MJ, Haraldsson H, Carlhall CJ, Engvall J, Ebberts T. Simultaneous three-dimensional myocardial T1 and T2 mapping in one breath hold with 3D-QALAS. *J Cardiovasc Magn Reson* 2014;16:102.
13. Kvernby S, Warntjes M, Engvall J, Carlhall CJ, Ebberts T. Clinical feasibility of 3D-QALAS — Single breath-hold 3D myocardial T1- and T2-mapping. *Magn Reson Imaging* 2017;38:13–20.
14. Scahill RI, Schott JM, Stevens JM, Rossor MN, Fox NC. Mapping the evolution of regional atrophy in Alzheimer's disease: Unbiased analysis of fluid-registered serial MRI. *Proc Natl Acad Sci U S A* 2002;99:4703–4707.
15. Sinnecker T, Granziera C, Wuerfel J, Schlaeger R. Future brain and spinal cord volumetric imaging in the clinic for monitoring treatment response in MS. *Curr Treat Options Neurol* 2018;20:17.
16. Fotenos AF, Snyder AZ, Girton LE, Morris JC, Buckner RL. Normative estimates of cross-sectional and longitudinal brain volume decline in aging and AD. *Neurology* 2005;64:1032–1039.
17. Resnick SM, Pham DL, Kraut MA, Zonderman AB, Davatzikos C. Longitudinal magnetic resonance imaging studies of older adults: A shrinking brain. *J Neurosci* 2003;23:3295–3301.
18. Desikan RS, Segonne F, Fischl B, et al. An automated labeling system for subdividing the human cerebral cortex on MRI scans into gyral based regions of interest. *Neuroimage* 2006;31:968–980.
19. Konarski JZ, McIntyre RS, Kennedy SH, Rafi-Tari S, Soczynska JK, Ketter TA. Volumetric neuroimaging investigations in mood disorders: Bipolar disorder versus major depressive disorder. *Bipolar Disord* 2008;10:1–37.
20. Jack CR Jr, Bernstein MA, Fox NC, et al. The Alzheimer's Disease Neuroimaging Initiative (ADNI): MRI methods. *J Magn Reson Imaging* 2008;27:685–691.
21. Dale AM, Fischl B, Sereno MI. Cortical surface-based analysis. I. Segmentation and surface reconstruction. *Neuroimage* 1999;9:179–194.
22. Fischl B. *FreeSurfer*. *Neuroimage* 2012;62:774–781.
23. Iscan Z, Jin TB, Kendrick A, et al. Test-retest reliability of *FreeSurfer* measurements within and between sites: Effects of visual approval process. *Hum Brain Mapp* 2015;36:3472–3485.
24. Patenaude B, Smith SM, Kennedy DN, Jenkinson M. A Bayesian model of shape and appearance for subcortical brain segmentation. *Neuroimage* 2011;56:907–922.
25. Landis JR, Koch GG. The measurement of observer agreement for categorical data. *Biometrics* 1977;33:159–174.
26. Salat DH, Lee SY, van der Kouwe AJ, Greve DN, Fischl B, Rosas HD. Age-associated alterations in cortical gray and white matter signal intensity and gray to white matter contrast. *Neuroimage* 2009;48:21–28.
27. Tustison NJ, Cook PA, Klein A, et al. Large-scale evaluation of ANTs and *FreeSurfer* cortical thickness measurements. *Neuroimage* 2014;99:166–179.
28. Destrieux C, Fischl B, Dale A, Halgren E. Automatic parcellation of human cortical gyri and sulci using standard anatomical nomenclature. *Neuroimage* 2010;53:1–15.
29. Huang H, Ceritoglu C, Li X, et al. Correction of B0 susceptibility induced distortion in diffusion-weighted images using large-deformation diffeomorphic metric mapping. *Magn Reson Imaging* 2008;26:1294–1302.
30. Nugent AC, Luckenbaugh DA, Wood SE, Bogers W, Zarate CA Jr, Drevets WC. Automated subcortical segmentation using FIRST: Test-retest reliability, interscanner reliability, and comparison to manual segmentation. *Hum Brain Mapp* 2013;34:2313–2329.
31. Morey RA, Selgrade ES, Wagner HR 2nd, Huettel SA, Wang L, McCarthy G. Scan-rescan reliability of subcortical brain volumes derived from automated segmentation. *Hum Brain Mapp* 2010;31:1751–1762.
32. Tan IL, van Schijndel RA, Pouwels PJ, Ader HJ, Barkhof F. Serial isotropic three-dimensional fast FLAIR imaging: Using image registration and subtraction to reveal active multiple sclerosis lesions. *AJR Am J Roentgenol* 2002;179:777–782.
33. Takeda T, Takeda A, Nagaoka T, et al. Gadolinium-enhanced three-dimensional magnetization-prepared rapid gradient-echo (3D MP-RAGE) imaging is superior to spin-echo imaging in delineating brain metastases. *Acta Radiol* 2008;49:1167–1173.
34. Warntjes JB, Dahlqvist O, Lundberg P. Novel method for rapid, simultaneous T1, T2*, and proton density quantification. *Magn Reson Med* 2007;57:528–537.
35. West J, Aalto A, Tisell A, et al. Normal appearing and diffusely abnormal white matter in patients with multiple sclerosis assessed with quantitative MR. *PLoS One* 2014;9:e95161.
36. Hagiwara A, Hori M, Yokoyama K, et al. Utility of a multiparametric quantitative MRI model that assesses myelin and edema for evaluating plaques, periplaque white matter, and normal-appearing white matter in patients with multiple sclerosis: A feasibility study. *AJNR Am J Neuroradiol* 2017;38:237–242.
37. Pfefferbaum A, Rohlfing T, Rosenbloom MJ, Sullivan EV. Combining atlas-based parcellation of regional brain data acquired across scanners at 1.5 T and 3.0 T field strengths. *Neuroimage* 2012;60:940–951.
38. Han X, Jovicich J, Salat D, et al. Reliability of MRI-derived measurements of human cerebral cortical thickness: The effects of field strength, scanner upgrade and manufacturer. *Neuroimage* 2006;32:180–194.
39. Lustig M, Donoho D, Pauly JM. Sparse MRI: The application of compressed sensing for rapid MR imaging. *Magn Reson Med* 2007;58:1182–1195.
40. Feinberg DA, Moeller S, Smith SM, et al. Multiplexed echo planar imaging for sub-second whole brain fMRI and fast diffusion imaging. *PLoS One* 2010;5:e15710.



Original contribution

Three-dimensional high-resolution simultaneous quantitative mapping of the whole brain with 3D-QALAS: An accuracy and repeatability study



Shohei Fujita^{a,b}, Akifumi Hagiwara^{a,*}, Masaaki Hori^c, Marcel Warntjes^{d,e}, Koji Kamagata^a, Issei Fukunaga^a, Christina Andica^a, Tomoko Maekawa^{a,b}, Ryusuke Irie^{a,b}, Mariko Yoshida Takemura^a, Kanako Kunishima Kumamaru^a, Akihiko Wada^a, Michimasa Suzuki^a, Yutaka Ozaki^a, Osamu Abe^b, Shigeki Aoki^a

^a Department of Radiology, Juntendo University Hospital, Tokyo, Japan

^b Department of Radiology, Graduate School of Medicine, The University of Tokyo, Tokyo, Japan

^c Department of Radiology, Toho University Omori Medical Center, Tokyo, Japan

^d SyntheticMR AB, Sweden

^e Center for Medical Imaging Science and Visualization (CMIV), Sweden

ARTICLE INFO

Keywords:

Myelin
Proton density
Quantitative magnetic resonance imaging
Relaxation time
Relaxometry
Synthetic magnetic resonance imaging

ABSTRACT

Background: Previous methods for the quantification of brain tissue properties by magnetic resonance imaging were mainly based on two-dimensional acquisitions and were thus limited to a relatively low resolution in the slice direction compared to three-dimensional (3D) acquisitions. The 3D-quantification using an interleaved Look-Locker acquisition sequence with a T2 preparation pulse (3D-QALAS) sequence may allow for simultaneous acquisition of relaxometry parameters in high spatial resolution.

Purpose: To evaluate bias, linearity, and day-to-day repeatability of relaxometry parameters, as well as tissue fraction maps, acquired with 3D-QALAS.

Materials and methods: Scan-rescan test of the 3D-QALAS sequence was performed on a 1.5-T scanner with the International Society for Magnetic Resonance in Medicine/National Institute of Standards and Technology system phantom and 10 healthy volunteers (7 male, 3 female; mean age, 23.2 ± 3.6 years). Simple linear regression analysis, Bland-Altman plots, and intrasubject coefficients of variation (CV) were used to assess the reliability of 3D-QALAS sequence-derived parameters. The T1, T2, proton density (PD), and myelin volume fraction (MVF) of *in vivo* brain regions were compared with values obtained using the multidynamic multi-echo sequence.

Results: In the phantom study, the T1, T2, and PD values measured by 3D-QALAS showed strong linearity with the reference values ($R^2 = 0.998, 0.998, \text{ and } 0.960$ for T1, T2, and PD, respectively) and high repeatability (mean CV of 1.2%, 2.8%, and 2.9% for T1, T2, and PD, respectively). The T1, T2, PD, and MVF values of *in vivo* brain regions obtained with 3D-QALAS were highly consistent within subjects, with mean intrasubject CVs of 0.5%, 0.5%, 0.4%, and 1.6% for the T1, T2, PD, and MVF values, respectively.

Conclusion: 3D-QALAS enables reliable measurement of T1, T2, PD, and MVF values of the whole brain in high spatial resolution across a clinically-relevant dynamic range.

1. Introduction

Quantification of brain tissue properties using magnetic resonance imaging (MRI) has been widely used for the assessment of normal development [1,2], aging [3–5], and diseases [6–9]. Quantitative MRI

approaches allow for more objective, repeatable, and reliable evaluation of the tissue than does conventional MRI, which only allows for assessment based on the arbitrary signal contrast between tissues. Despite their potential benefits, quantitative MR techniques, such as obtaining T1, T2, and proton density (PD) values of tissue, are not

Abbreviations: BPV, Brain parenchymal volume; CSF, Cerebrospinal fluid; CV, Coefficient of variation; GM, Gray matter; ICC, Intraclass correlation coefficient; LOA, Limits of agreement; MDME, Multidynamic multi-echo; MRI, Magnetic resonance imaging; MVF, Myelin volume fraction; NoN, Other intracranial material; PD, Proton density; SD, Standard deviation; VOI, Volume of interest; WM, White matter

* Corresponding author at: Department of Radiology, Juntendo University School of Medicine, 1-2-1, Hongo, Bunkyo-ku, Tokyo 113-8421, Japan.

E-mail address: a-hagiwara@juntendo.ac.jp (A. Hagiwara).

<https://doi.org/10.1016/j.mri.2019.08.031>

Received 9 June 2019; Received in revised form 19 August 2019; Accepted 19 August 2019

0730-725X/© 2019 The Authors. Published by Elsevier Inc. This is an open access article under the CC BY-NC-ND license (<http://creativecommons.org/licenses/by-nc-nd/4.0/>).

performed in routine clinical examination, likely due to the low resolution of conventional mapping methods.

Several quantitative multiparametric approaches have been proposed to obtain high spatial resolution maps of the brain [10–13]. One such method uses a multidynamic multi-echo (MDME) sequence, which enables simultaneous tissue relaxometry of T1 and T2 relaxation times and PD, providing quantitative maps that are inherently aligned [10,14–17]. Myelin volume fraction (MVF) in a voxel can also be estimated, based on the acquired T1, T2, and PD values, assuming four compartments in brain tissues [18,19]. The MDME sequence has been used for evaluation in various brain diseases, such as multiple sclerosis [20,21], brain infarctions [22], and meningitis [23].

The MDME sequence used for quantitative synthetic MRI was based on a multi-slice 2D acquisition, which provided a relatively low resolution in the slice direction compared with 3D acquisitions. Recently, 3D-quantification using an interleaved Look-Locker acquisition sequence with a T2 preparation pulse (3D-QALAS) sequence has been developed for simultaneous quantification of T1 and T2 in cardiac imaging and showed high accuracy and precision in the heart as well as in phantoms with various tissue properties [24,25]. A previous study showed that 3D-QALAS can be reliably used for measuring cortical thickness and subcortical volumes in most brain regions [26]. However, no study to date has investigated the reliability of MR property quantification based on 3D-QALAS in the brain.

Here, we propose the application of the 3D-QALAS sequence for simultaneous acquisition of relaxometry parameters at high spatial resolution in the brain. The purpose of this study was to evaluate bias, linearity, and day-to-day repeatability of relaxometry parameters (*i.e.*, T1, T2, and PD values) of the brain acquired with 3D-QALAS by (a) evaluating T1, T2, and PD values of the International Society for Magnetic Resonance in Medicine/National Institute of Standards and Technology (ISMRM/NIST) MRI system phantom measured by 3D QALAS on different days and (b) evaluating T1, T2, PD, MVF, and tissue fraction maps of brain tissues *in vivo*.

2. Materials and methods

In phantom studies, the accuracy and repeatability of the T1, T2, and PD measurements were evaluated using an ISMRM/NIST system phantom containing spheres with standardized values [27,28]. Evaluation *in vivo* was performed with volunteers using volume of interest (VOI) analysis on T1, T2, PD, and MVF maps of the brain.

2.1. MR protocol

All scans were performed on a 1.5-T scanner (A patched R5.3.0 Ingenia, Philips Healthcare, Best, The Netherlands) with a 12-channel head coil. The 3D-QALAS sequence is based on multi-acquisition 3D gradient echo, with five acquisitions equally spaced in time, interleaved with a T2 preparation pulse and an inversion pulse. Briefly, the four acquisitions after the inversion pulse are used to determine the apparent T1* relaxation time approaching the saturated M0* magnetization. T1* and M0* must be corrected for the effect of the semi-continuous series of RF flip angles during the acquisition time to retrieve the actual T1 and M0. All M0 values are then scaled to PD such that 100% PD corresponds to the M0 of pure water. The T1 data curve is extrapolated to just prior to the T2-prep pulse. T2 relaxation is then found using the ratio of the signal intensity just prior and just after the T2-prep pulse. An internal trigger started each of the five acquisitions every 900 ms, amounting to a total cycle time of 4.5 s. Further details of the 3D-QALAS sequence have been provided by previous studies [24,25]. The substantial difference between our study and the previous cardiac 3D-QALAS studies involves the spatial and temporal resolution: imaging of the brain requires higher spatial resolution than that of the heart, but no breath hold is required. The voxel size in the cardiac study was $2 \times 2 \times 12$ mm, while that in our study was $1.2 \times 1.2 \times 1.2$ mm.

In terms of volume, the voxel size used in our study was only 3.6% ($1.728/48 \text{ mm}^3$) of that used in the cardiac study. With a longer acquisition time per beat and many more cycles, we obtained a higher resolution. Accordingly, the scan parameters of the 3D-QALAS were as follows: axial acquisition; TR/TE, 6.6/3.0 ms; inversion delay times 100, 1000, 1900, 2800 ms; T2-prep echo time 100 ms; field-of-view (FOV), $250 \times 250 \times 168$ mm; matrix size, $208 \times 208 \times 140$; section thickness, 1.20 mm; flip angle, 4°; receiver bandwidth, 230 Hz/pixel; acceleration factor = 1.7, averages, 2; acquisition time, 20 min 34 s. The scan parameters of the quantification of relaxation times and proton density by MDME [10] were as follows: axial acquisition; TR/TE1/TE2, 4000/22/99 ms; FOV, 230×230 mm; matrix size, 192×192 ; section thickness, 5 mm; flip angle, 90°; receiver bandwidth, 158.5 Hz/pixel; acceleration factor = 2, averages, 1; acquisition time, 5 min 29 s.

2.2. Phantom evaluation

The ISMRM/NIST system phantom (High Precision Devices, Inc., Boulder, Colorado, USA) consisted of multiple layers of sphere arrays that contain standardized T1 and T2 relaxation times and PD. T1 spheres consisted of different concentrations of NiCl₂ solutions, with T1 ranging from 24 to 2640 ms. T2 spheres consisted of different concentrations of MnCl₂ solutions, with T2 ranging from 8 to 1542 ms. PD spheres consisted of different concentrations of H₂O and D₂O, with PD ranging from 5 to 100% water. Reference values were measured by magnetic resonance spectroscopy at 20 °C and were provided by the Physical Measurement Laboratory at NIST [27,28]. Six T1 spheres and seven T2 spheres with T1 and T2 values within the clinically-relevant dynamic range (200–1400 ms and 50–400 ms, respectively) were evaluated in the study. All 14 PD spheres of the phantom were used. The outer and inner diameter of each sphere were 20 mm and 15 mm, respectively. The reference values of the spheres are shown in Table 1.

The NIST/ISMRM system phantom was scanned with the 3D-QALAS sequence seven times on different days over a 1-month period. The phantom was placed in position 30 min prior to each scan to reduce the effect of motion on measurements. T1, T2, and PD maps were generated using the SyMRI software (version 0.45.5) [29]. A spherical VOI with a 10-mm diameter was manually placed at the center of each sphere on the T1, T2, and PD maps, and the mean values were recorded using ITK-SNAP (version 3.6.0.).

2.3. Healthy volunteer evaluation

The local review board approved this study, and written informed consent was acquired from all participants. Ten healthy volunteers were included in this study (7 male, 3 female; mean age, 23.2 ± 3.6 [SD] years). None of the participants had a history of a major medical condition or neurological or psychiatric disorder. Two radiologists (A.H. and S.F.) blindly assessed all volunteer examinations and confirmed that none had structural abnormalities.

A scan–rescan test, as well as comparison with the 2D-MDME sequence results, was performed for each volunteer. A 2D-MDME sequence was performed once, and the 3D-QALAS sequence was performed twice (for scan–rescan) in the same session, for all volunteers. Between the scan–rescan of the 3D-QALAS sequence, the volunteers exited the scanner and were asked to rest for a few minutes T1, T2, PD, and MVF maps were generated using the SyMRI software [29] for the VOI analysis. We performed VOI analysis based on a previous study [14]. In brief, we created 16 VOIs: 8 of white matter (WM; frontal, parietal, temporal, and occipital WM; genu and splenium of the corpus callosum, internal capsules, and middle cerebellar peduncles) and 8 of gray matter (GM; frontal, parietal, temporal, and occipital GM; insula, caudate, putamen, and thalamus) VOIs in the Montreal Neurological Institute space [30–32]. VOIs of the left and right sides were combined for analysis, except for those of the splenium. For each VOI, the mean

Table 1

Mean values of 7-day measurements of T1 and T2 relaxation times and proton density (PD) and their coefficients of variation (CVs) of the International Society for Magnetic Resonance in Medicine/National institute of Standards and Technology system phantom. Reference values measured with magnetic resonance spectroscopy at 20 °C were provided by National institute of Standards and Technology.

Sphere no.	T1 (ms)			T2 (ms)			PD (%)		
	Reference	Mean ± SD	CV (%)	Reference	Mean ± SD	CV (%)	Reference	Mean ± SD	CV (%)
1	272.3	285 ± 2	0.6	43.84	42 ± 1	2.9	5	NA	NA
2	384.1	389 ± 4	1.1	62.82	61 ± 1	1.3	10	NA	NA
3	527	505 ± 5	0.9	89.52	89 ± 1	1.1	15	10.5 ± 0.4	3.5
4	751	683 ± 7	1.0	137	122 ± 1	1.0	20	14.4 ± 0.2	1.1
5	1027	934 ± 7	0.7	186.1	163 ± 3	1.8	25	16.5 ± 1.1	6.9
6	1432	1334 ± 34	2.6	258.4	212 ± 8	3.8	30	18.7 ± 0.6	3.4
7				428.3	365 ± 26	7.4	35	22.1 ± 0.5	2.1
8							40	27.2 ± 0.8	2.8
9							50	31.4 ± 0.5	1.5
10							60	38.1 ± 0.6	1.5
11							70	44.6 ± 0.5	1.1
12							80	63.5 ± 5.4	8.4
13							90	82.7 ± 1.2	1.5
14							100	89.0 ± 0.8	0.8

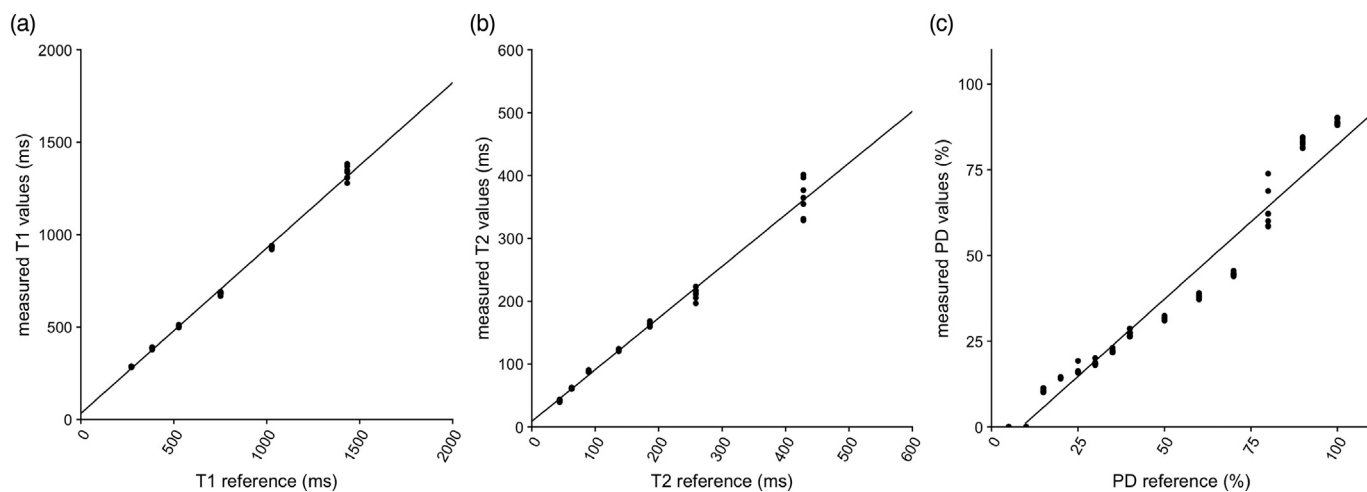


Fig. 1. Correlation plots comparing mean T1 (a), T2 (b), and PD (c) values to the reference values, showing linearity of measurements obtained with the 3D-QALAS sequence. Solid black lines represent the linear regression fit.

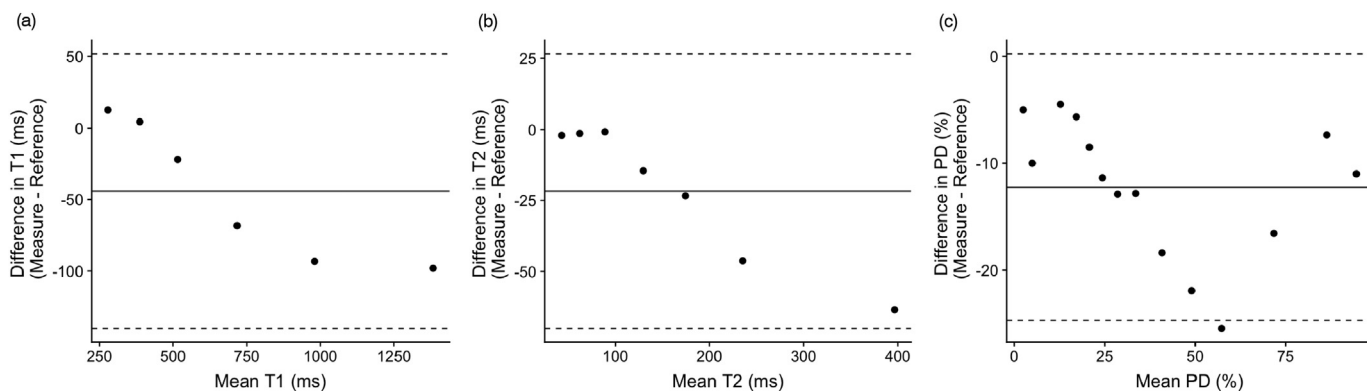


Fig. 2. Bland-Altman plots comparing T1 (a), T2 (b), and PD (c) values to the reference values, showing bias of measurements obtained with the 3D-QALAS sequence. The center solid lines represent mean differences. Upper and lower dotted lines represent the LOA, defined as the mean difference ± 1.96 × SD of the difference between the measurement and reference values. LOA, limit of agreement; SD, standard deviation.

T1, T2, PD, and MVF values were measured. *In vivo* repeatability and agreement with values obtained from MDME were evaluated for 3D-QALAS.

Based on the T1, T2, and PD values measured by the 3D-QALAS sequence, brain tissue segmentation was performed using the SymMRI

software. The details of the brain segmentation algorithm using SymMRI are described elsewhere [19]. In brief, the measured quantitative values of brain tissues were used as coordinates in a 3D feature space (*i.e.*, R1–R2–PD space). This coordinate was referred to as a lookup grid, which shows the related partial tissue volumes to the 3D space [19]. We

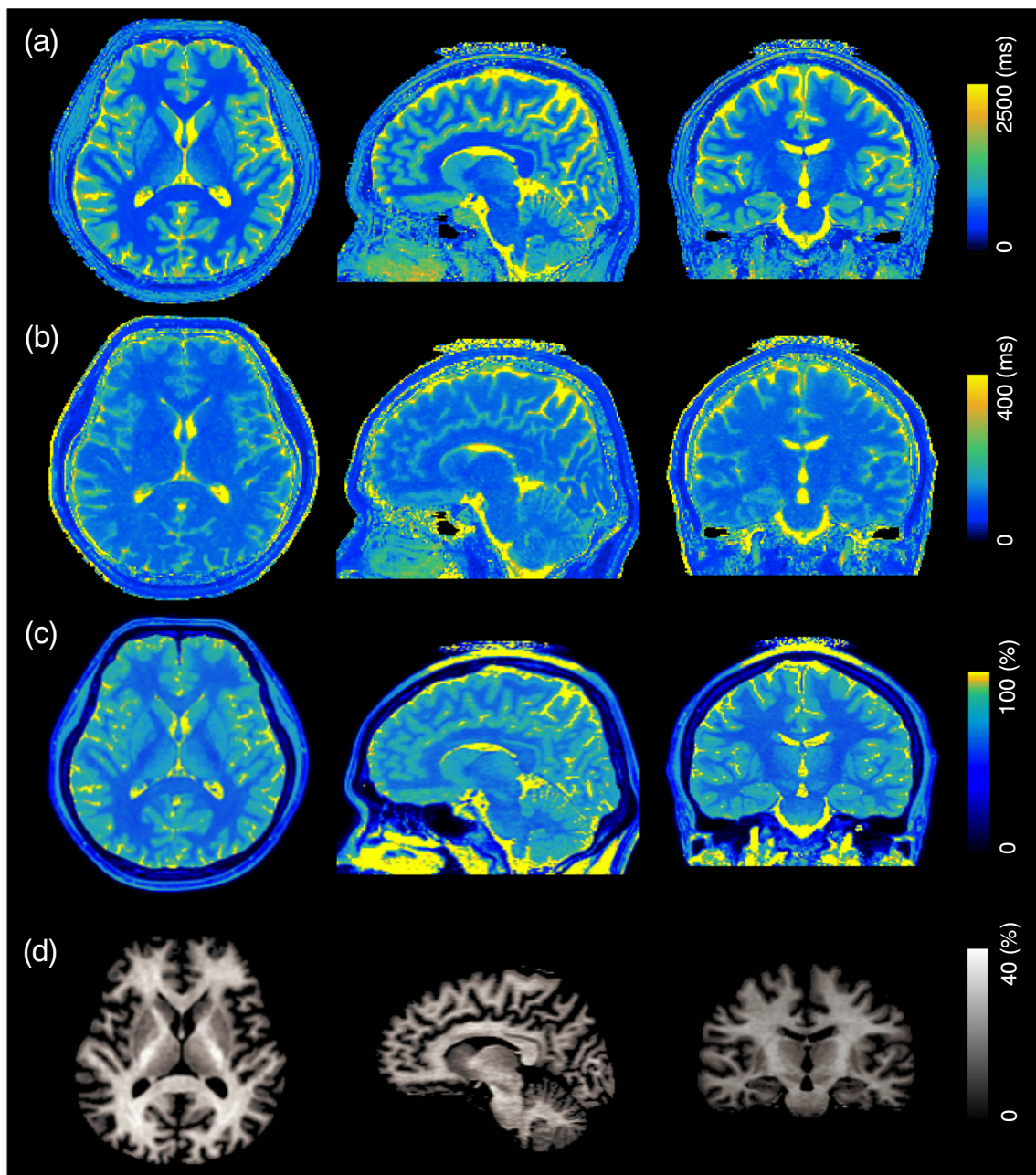


Fig. 3. Representative example of three-dimensional quantification maps of the brain. T1 maps (a), T2 maps (b), PD maps (c), and MVF maps (d) are shown in multi-planar reconstruction views. PD, proton density; MVF, myelin volume fraction.

performed brain tissue segmentation based on the same data to obtain GM, WM, and cerebrospinal fluid (CSF) volumes, and myelin volume (MYV) by multiplying the aggregated volume fraction of each tissue type in the whole brain and the voxel volume. Voxels not categorized as GM, WM, or CSF were classified as other intracranial material (NoN). The brain parenchymal volume (BPV) was calculated by summing the GM, WM, and NoN. The intracranial volume (ICV) was calculated by defining the borderline at PD = 50%. Agreement with volumes obtained from MDME and scan–rescan repeatability were evaluated for 3D-QALAS.

2.4. Statistical analysis

To assess linearity, simple linear regression analysis was performed between the mean of 7 measurements and the reference values that were provided by NIST [27,28]. For assessment of bias, Bland–Altman

plots were obtained between the measurements and the reference values. The coefficients of variation (CVs) of the 7 measurements of the spheres in the phantoms was obtained to assess day-to-day repeatability. In the volunteer study, intrasubject CVs of T1, T2, and PD based on the scan–rescan tests were calculated for each VOI per subject (based on the scan–rescan tests) and then averaged across subjects. Percentage relative difference was used to assess reproducibility of the 3D-QALAS sequence-derived brain quantitative values and tissue volumes compared with those derived from MDME. For brain tissue volumes, intraclass correlation coefficients (ICCs) were also calculated to assess reproducibility.

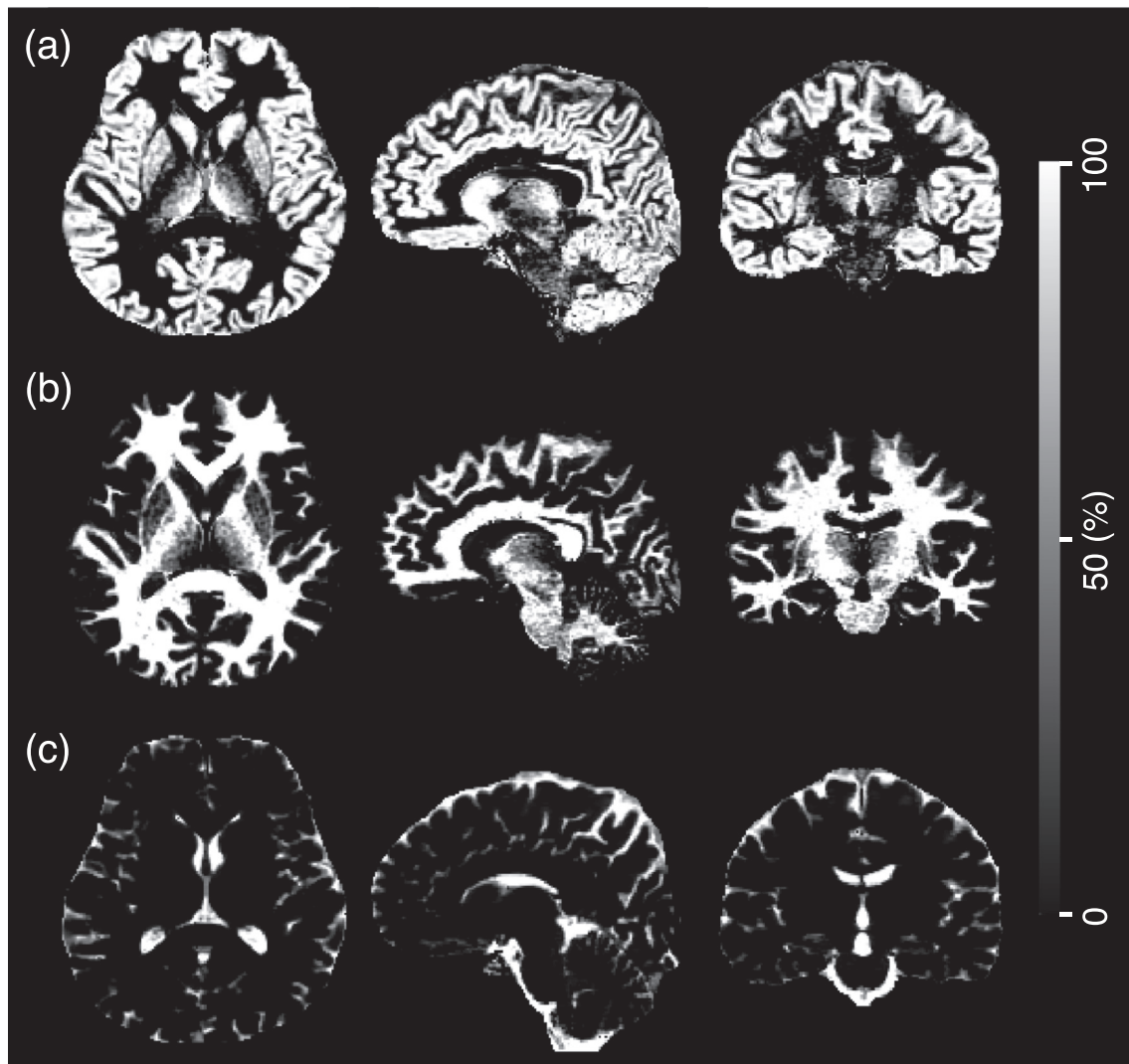


Fig. 4. Representative example of three-dimensional tissue fraction maps of the brain. GM (a), WM (b), and CSF (c) maps are shown in multi-planar reconstruction views. GM, gray matter; WM, white matter; CSF, cerebrospinal fluid.

3. Results

3.1. ISMRM/NIST MRI system phantom study

The temperature of the phantom after image acquisition was 19.1 ± 0.5 °C. The mean, SD, and CV of the repeated measurements of T1, T2, and PD of each sphere are reported in Table 1. All CVs of the T1, T2, and PD measurements based on 3D-QALAS were lower than 10% (mean CV: 1.2%, 2.8%, and 2.9%, respectively). Fig. 1 shows the simple linear regression analysis performed between the mean of the measurements and the reference values. The T1, T2, and PD values measured by 3D-QALAS all showed strong linearity with the reference values ($R^2 = 0.998, 0.998, \text{ and } 0.960$, respectively). The linear regression fit had slopes of 0.89, 0.82, and 0.90, and intercepts of 33, 9.0, and -7.8 for T1, T2, and PD, respectively. Fig. 2 shows the Bland–Altman plots obtained between the measurements and the reference values; the difference between the measurements and reference values are plotted against the mean. The mean bias was -44 ms, -22 ms, and -12% for T1, T2, and PD, respectively. The limits of agreement (LOAs), defined as the mean difference $\pm 1.96 \times$ SD of the difference between the measurements and reference values, were -140 to 51 , -70 to 27 , and -25 to 0.24 for T1, T2, and PD, respectively. All data points were within the LOAs, except for one data point of PD (reference value, 80% H₂O).

3.2. Healthy volunteer evaluation

Fig. 3 shows representative 3D T1, T2, PD, and MVF maps of the brain obtained from a healthy volunteer using 3D-QALAS. Fig. 4 illustrates tissue fraction maps obtained from a volunteer's scan. Fig. 5 shows a representative example of VOI placements in a multi-planar view.

Table 2 reports the mean, SD, and intrasubject CV of T1, T2, PD, and MVF values of each anatomic VOI across 10 healthy volunteers. Values obtained with the MDME sequence, and the relative difference between 3D-QALAS and MDME are also shown. Supplementary Table 1 shows the T1, T2, and PD values for representative anatomical parts of the brain obtained with 3D-QALAS along with values from the literature [10,11,33–38]. The T1, T2, PD, and MVF values of brain regions obtained with 3D-QALAS were highly consistent within volunteers, with mean intrasubject CVs of 0.5, 0.5, 0.4, and 1.6% for T1, T2, PD, and MVF, respectively. All *in vivo* measured values were within the dynamic range evaluated in the phantom study.

Table 3 reports the overall mean, intrasubject CV, ICC, and percentage relative difference of WM, GM, CSF, NoN, MYV, BPV, and ICV volumes based on 3D-QALAS and the 2D-MDME sequence for the 10 healthy volunteers. The WM, GM, MYV, BPV, and ICV values showed high agreement between the values obtained with 3D-QALAS and 2D-

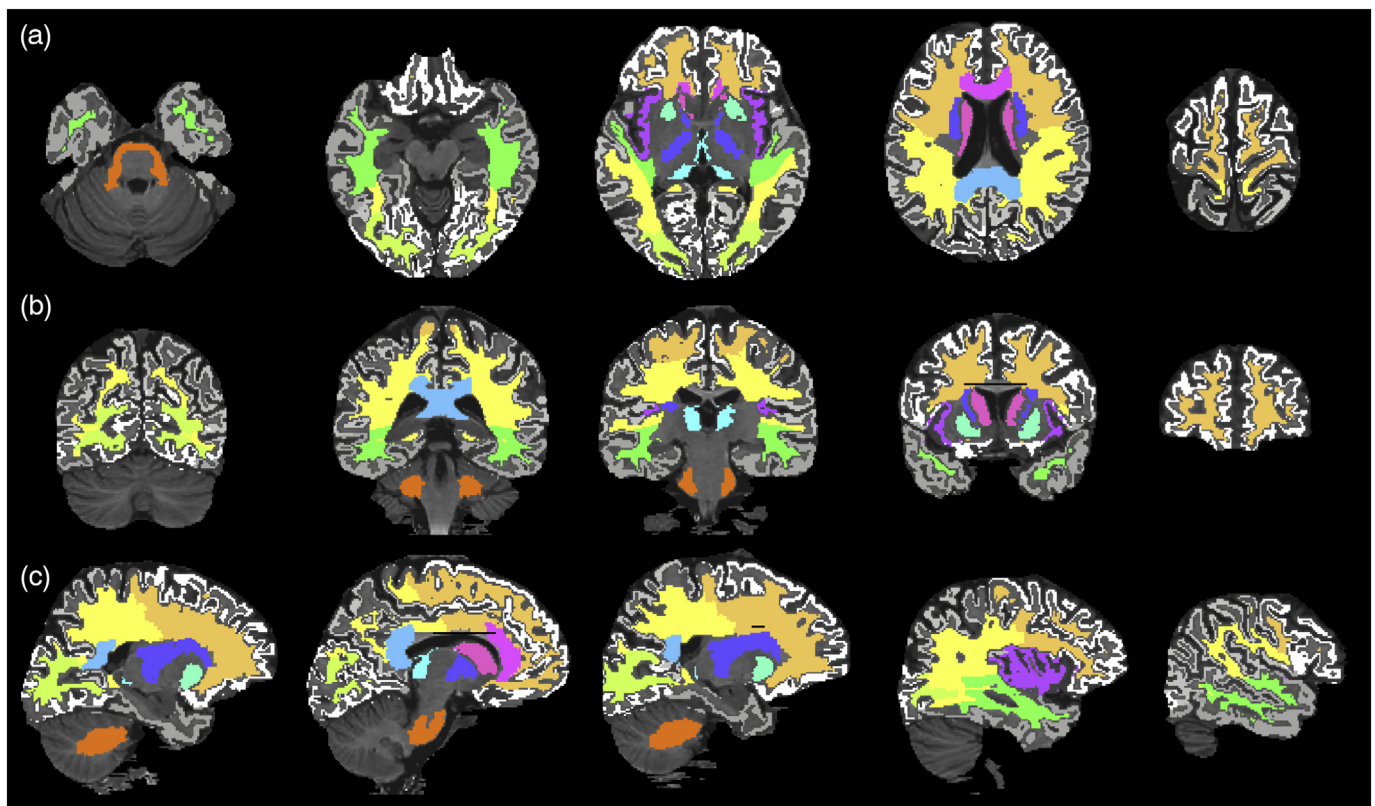


Fig. 5. Representative example of volume of interest (VOI) placement. VOIs are overlaid on a T1-weighted image in axial (a), coronal (b), and sagittal (c) views.

MDME, with percentage relative difference of 7.4%, 4.0%, 3.4%, 4.5%, and 1.3%, and ICCs of 0.97, 0.97, 0.95, 0.99, and 0.99, respectively. The CSF and NoN showed relatively low agreement between 3D-QALAS and 2D-MDME. The tissue volumes obtained with 3D-QALAS showed high repeatability, with a mean intrasubject CV of 1.9%.

4. Discussion

We presented the accuracy and repeatability of a relaxometry technique for 3D simultaneous quantification of T1, T2, PD, and MVF values of the whole brain. The T1, T2, and PD values obtained using the 3D-QALAS sequence showed high repeatability and strong linear correlation with the reference values of the standardized ISMRM/NIST system phantom. Although some biases were present with respect to the reference values, measurements were strongly linear, indicating that the 3D-QALAS sequence allows for adequate quantitative characterization. The T1, T2, and PD values of the healthy participants were in good agreement with the literature values, with high repeatability.

The 3D-QALAS sequence provides both quantitative values (*i.e.*, T1 and T2 relaxation times, PD, and MVF) and morphologic information of the whole brain in high spatial resolution. The method has the advantage that it can measure not only T1, T2, and PD values, but also MVF, which is considered to be important clinically. Another advantage of 3D-QALAS compared to other mapping techniques, which usually require multiple scans and registration, is that 3D-QALAS achieves perfect alignment among the obtained quantitative MR property maps and tissue fraction maps. Since the acquisition is performed slice-by-slice, only the effects of subject movement that occurred during the slice acquisition would be evident. The registration error should be eliminated, as long as the patient did not move during data acquisition within a slice.

Absolute quantification of MR properties using relaxometry has previously been reported to be useful for characterization of disease, assessment of disease activity, and monitoring of treatment [39–41].

The 3D isotropic acquisition with 3D-QALAS allows for generation of images from arbitrary views, without requiring additional scans from different directions. This property not only provides the advantage of visual characterization and detection of lesions, but also allows for accurate segmentation of small regional structures. This enables detecting and describing T1, T2, and PD changes within regional structures, which could be masked when averaging values over gross anatomic regions. Hence, 3D-QALAS has the potential to provide thorough and comprehensive characterization of brain lesions, as well as of the entire brain.

The validation of accuracy and repeatability of 3D-QALAS in a standardized phantom is a prerequisite for its clinical use. In our study, we compared the T1, T2, and PD values obtained using 3D-QALAS with the reference values in NIST/ISMRM phantoms across seven days. Day-to-day repeatability was lower than 3% for the T1, T2, and PD values. In the phantom study, we did not correct for temperature in T1 and T2 measurements. The correction would have lowered the reported CVs, because without the correction, the measurements would include error of the measurements and error originating from the temperature difference. However, in clinical practice, it is difficult and impractical to obtain the exact temperature of a subject. Because the CVs without temperature corrections were acceptable (mean CV of 1.2%, 2.8%, and 2.9%, for T1, T2, and PD, respectively) in our observation, we decided not to perform temperature correction.

The values acquired with 3D-QALAS showed a strong linear correlation ($R^2 = 0.98–0.99$) with the standardized values for the physiological range of structures of the brain. Our results indicate that 3D-QALAS covers the physiological range of T1, T2, and PD values in brain structures. PD values lower than 10% were estimated as 0%, suggesting that measurements of extremely low PD values would be less reliable. However, precise quantitative values of such tissues would be of less importance in the clinical setting; the PD values in the healthy human brain measured by MDME were reported to be 77% and 62% for GM and WM, respectively [14]. Further, PD values in various brain tumors

Table 2
Mean values and intrasubject coefficients of variation (CVs) of T1, T2, PD, and MVF for 10 healthy subjects, based on the 3D-QALAS sequence.

Volume of interest	T1 (ms)			T2 (ms)			PD (%)			MVF (%)						
	MDME			3D QALAS			MDME			3D QALAS						
	Overall mean (ms)	Intrasubject CV (%)	Relative difference (%)	Overall mean (ms)	Intrasubject CV (%)	Relative difference (%)	Overall mean (ms)	Intrasubject CV (%)	Relative difference (%)	Overall mean (ms)	Intrasubject CV (%)	Relative difference (%)				
Gray matter																
Frontal GM	1044 ± 21	0.4 ± 0.3	1067 ± 29	1.9 ± 1.4	93 ± 2	0.9 ± 0.8	90 ± 2	4.2 ± 1.4	81 ± 0.7	0.4 ± 0.4	83 ± 1.1	2.2 ± 1.3	8.1 ± 0.7	2.9 ± 2.5	6.7 ± 0.7	15.6 ± 10.3
Parietal GM	1028 ± 22	0.6 ± 0.5	1068 ± 25	3.0 ± 1.3	90 ± 2	0.9 ± 0.7	87 ± 2	4.3 ± 1.0	79 ± 0.7	0.3 ± 0.1	83 ± 0.6	3.5 ± 0.7	8.8 ± 0.8	3.0 ± 2.2	6.0 ± 0.4	34.9 ± 6.1
Temporal GM	1092 ± 17	0.3 ± 0.3	1123 ± 31	2.6 ± 1.8	96 ± 2	0.5 ± 0.2	90 ± 2	5.8 ± 1.8	83 ± 0.5	0.4 ± 0.3	85 ± 0.6	2.6 ± 1.0	6.5 ± 0.5	1.2 ± 1.0	5.3 ± 0.5	19.2 ± 6.4
Occipital GM	1035 ± 22	0.6 ± 0.5	1079 ± 25	3.5 ± 1.0	87 ± 1	0.5 ± 0.4	85 ± 1	2.6 ± 1.1	80 ± 0.7	0.3 ± 0.2	83 ± 0.7	2.6 ± 0.6	8.3 ± 0.8	3.5 ± 1.6	6.7 ± 0.6	18.5 ± 7.8
Insular cortex	1048 ± 21	0.3 ± 0.2	1065 ± 29	1.3 ± 1.2	96 ± 2	0.4 ± 0.5	93 ± 2	4.0 ± 2.4	79 ± 0.5	0.3 ± 0.3	83 ± 0.8	4.8 ± 1.1	8.8 ± 1.0	0.8 ± 0.8	5.8 ± 0.8	35.9 ± 8.3
Caudate	918 ± 17	0.6 ± 0.5	878 ± 28	5.3 ± 2.0	85 ± 2	0.5 ± 0.4	82 ± 1	4.1 ± 1.6	77 ± 1.1	0.4 ± 0.4	79 ± 1.4	2.4 ± 1.4	12.4 ± 1.3	2.9 ± 2.8	10.1 ± 1.9	21.5 ± 15.1
Putamen	831 ± 15	0.7 ± 0.6	795 ± 22	5.3 ± 2.0	77 ± 2	0.6 ± 0.6	75 ± 2	2.3 ± 1.3	75 ± 0.5	0.3 ± 0.2	77 ± 0.6	2.1 ± 0.8	16.5 ± 0.9	1.6 ± 1.4	13.7 ± 0.8	16.7 ± 6.1
Thalamus	780 ± 13	0.5 ± 0.3	763 ± 20	2.9 ± 1.4	81 ± 1	0.4 ± 0.3	79 ± 1	2.3 ± 1.4	73 ± 0.5	0.3 ± 0.2	73 ± 0.7	0.6 ± 0.5	19.4 ± 0.6	1.1 ± 1.0	19.8 ± 1.1	4.7 ± 2.6
Aggregate of GM	910 ± 20	0.4 ± 0.3	904 ± 18	1.6 ± 1.0	88 ± 1	0.5 ± 0.5	83 ± 1	5.8 ± 0.8	77 ± 0.7	0.3 ± 0.3	77 ± 0.7	0.9 ± 0.4	14.1 ± 0.9	1.2 ± 1.0	15.2 ± 0.6	9.4 ± 4.8
White matter																
Frontal WM	581 ± 20	0.7 ± 0.4	615 ± 15	4.4 ± 1.2	76 ± 2	0.6 ± 0.6	76 ± 1	1.0 ± 0.6	65 ± 0.4	0.3 ± 0.2	63 ± 0.9	2.6 ± 0.9	31.1 ± 0.6	1.0 ± 0.7	33.9 ± 1.3	8.2 ± 2.5
Parietal WM	575 ± 20	0.3 ± 0.3	625 ± 16	7.2 ± 1.2	79 ± 1	0.4 ± 0.5	77 ± 1	2.4 ± 0.8	64 ± 0.3	0.2 ± 0.1	64 ± 0.8	0.7 ± 0.6	32.3 ± 0.5	0.6 ± 0.4	33.2 ± 1.2	2.3 ± 2.0
Temporal WM	599 ± 20	0.7 ± 0.6	637 ± 20	5.3 ± 1.3	78 ± 2	0.6 ± 0.7	76 ± 1	2.5 ± 1.3	66 ± 0.8	0.5 ± 0.4	65 ± 1.1	2.4 ± 1.0	28.9 ± 1.1	1.5 ± 1.4	31.6 ± 1.7	9.2 ± 2.9
Occipital WM	587 ± 20	0.7 ± 0.4	667 ± 12	11.9 ± 1.2	81 ± 1	0.4 ± 0.4	79 ± 1	3.2 ± 1.0	65 ± 0.7	0.4 ± 0.2	66 ± 0.6	1.5 ± 0.7	31.1 ± 1.0	1.0 ± 0.6	30.1 ± 1.0	3.7 ± 1.9
Genu of the CC	530 ± 18	0.5 ± 0.4	539 ± 16	1.0 ± 0.9	73 ± 2	0.8 ± 0.8	75 ± 1	2.3 ± 1.4	66 ± 1.5	0.5 ± 0.4	58 ± 1.2	11.4 ± 2.4	29.0 ± 2.3	1.5 ± 1.2	41.3 ± 1.8	29.7 ± 5.8
Splenium of the CC	540 ± 17	0.2 ± 0.2	584 ± 16	6.6 ± 1.8	79 ± 1	0.4 ± 0.5	78 ± 1	2.6 ± 1.8	65 ± 0.8	0.6 ± 0.4	61 ± 0.8	5.7 ± 2.3	30.8 ± 1.1	1.4 ± 1.0	36.9 ± 1.2	16.4 ± 5.8
Internal capsule	580 ± 21	0.6 ± 0.6	615 ± 19	4.5 ± 1.6	76 ± 2	0.7 ± 0.6	75 ± 1	2.2 ± 0.9	64 ± 0.7	0.3 ± 0.3	63 ± 0.9	1.1 ± 0.8	33.0 ± 1.0	0.9 ± 0.8	34.1 ± 1.4	3.7 ± 2.3
Middle cerebellar peduncle	631 ± 16	0.3 ± 0.3	684 ± 22	7.5 ± 1.8	83 ± 1	0.3 ± 0.2	81 ± 2	2.1 ± 1.3	67 ± 0.9	0.4 ± 0.3	66 ± 0.9	2.0 ± 0.9	28.0 ± 1.2	1.3 ± 1.1	29.9 ± 1.3	7.4 ± 3.0
Aggregate of WM	580 ± 19	0.4 ± 0.3	624 ± 14	6.1 ± 1.1	78 ± 1	0.4 ± 0.6	77 ± 1	1.8 ± 0.7	65 ± 0.4	0.3 ± 0.2	64 ± 0.8	1.7 ± 0.8	31.1 ± 0.5	0.8 ± 0.5	33.2 ± 1.2	6.0 ± 2.3

GM, gray matter; WM, white matter; CC, corpus callosum; MVF, myelin volume fraction.

Table 3
Volumetric measurements of healthy volunteers based on the 3D-QALAS sequence.

Tissue type	3D QALAS		MDME		
	Overall mean (ml)	Intrasubject CV	Overall mean (ml)	Relative difference (%)	ICC
WM	618 ± 64	0.8 ± 0.7	572 ± 59	7.4 ± 2.3	0.97
GM	722 ± 75	0.7 ± 0.7	694 ± 65	4.0 ± 2.4	0.97
CSF	137 ± 35	2.0 ± 1.4	212 ± 52	43.6 ± 5.4	0.93
NoN	39 ± 6	8.2 ± 5.9	50 ± 14	33.7 ± 18.6	0.04
MYV	197 ± 23	0.8 ± 0.8	199 ± 23	3.4 ± 1.5	0.95
BPV	1378 ± 128	0.5 ± 0.4	1317 ± 131	4.5 ± 1.0	0.99
ICV	1515 ± 151	0.4 ± 0.3	1529 ± 163	1.3 ± 0.6	0.99

MDME, multidynamic multi-echo; GM, gray matter; WM, white matter; CSF, cerebrospinal fluid; NoN, other brain material; BPV, brain parenchymal volume; ICV, intracranial volume; MYV, myelin volume; ICC, intraclass correlation coefficient.

have been previously reported by Just et al., who showed that tumors have higher PD values than does WM [42].

The T1, T2, and PD values obtained with 3D-QALAS showed good overall agreement with MDME sequence-derived values, as shown by relative differences. However, the MVF values in gray matter regions differed substantially between 3D-QALAS and MDME. One possible reason may be the low absolute value of MVF in gray matter (mean MVF value of 15.2% in gray matter compared to 33.2% in white matter), which may have made the relative differences sensitive to small changes. Despite the high absolute value of the MVF in the corpus callosum, values obtained with 3D-QALAS and MDME differed substantially. One possible reason for this could be the effects of incomplete elimination of B1 inhomogeneity and coil sensitivity, because the corpus callosum is located in the center of the field-of-view that is likely to be affected by these effects. Special attention is required when applying 3D-QALAS to the corpus callosum. In spite of these discrepancies, 3D-QALAS sequence-derived T1, T2, PD, and MVF values showed high repeatability. The measured values often differ even among well-established methods and pursuing the true value may be impractical for clinical use. When performing an examination in a clinical context to monitor subtle changes in subjects' MR values, repeatability is more important than accuracy, as repeatability is associated with the smallest change that can be detected using the measurement. As long as the measurement is consistent and shows high repeatability, it could be used to depict the differences among tissues.

The 3D-QALAS sequence was constructed for analyzing brain tissue and may not be suitable for quantifying MR properties of materials that differ greatly from the brain. Our data show that 3D-QALAS slightly underestimates the values of T1, T2, and PD. However, the repeatability of these measurements was high (mean CV of 1.2%, 2.8%, and 2.9% for T1, T2, and PD values, respectively), indicating that 3D-QALAS is suitable for longitudinal studies.

We also assessed the *in vivo* repeatability of 3D-QALAS with 10 healthy volunteers. The T1, T2, and PD values acquired with 3D-QALAS showed good agreement with the results of previous studies reporting values of structures of the normal brain at 1.5 T (Supplementary Table 1) [10,11,33–38]. The CVs of T1, T2, and PD values in volunteer data were lower than those measured in the phantom study. This may be because the size of the VOIs used in the phantom study was smaller than those used in the volunteer study. The tissue volume based on 3D-QALAS showed low intrasubject CV, lower than 1%, except for NoN. NoN showed intrasubject CVs of 8.2%, which was much higher than that of the other tissue volumes. Because the CV is sensitive to small changes when the mean value used as the denominator approaches zero, the small absolute volume of NoN may have contributed to the relatively large intrasubject CV.

This study had several limitations. First, the scanning time in this study was relatively long in terms of incorporation into a routine clinical scan. Using a 3-T MRI scanner, as well as combining it with acceleration techniques, such as compressed sensing [43], may reduce

scan times to a clinically-applicable level. Second, only healthy volunteers and no patients were enrolled in the *in vivo* study. Although our goal was to validate the accuracy and repeatability of 3D-QALAS, future studies focusing on patients are required. Third, although we have validated the reliability of 3D-QALAS using the standardized phantom with reference values, the *in vivo* values were not compared with those acquired by gold-standard methods, such as IR-based T1 mapping and multi-echo T2 mapping, which requires an excessive scan time. However, the T1, T2, and PD values acquired with 3D-QALAS showed good agreement with values obtained with the well-established MDME sequence, as well as with values reported previously.

In conclusion, the three-dimensional relaxometry method, 3D-QALAS, allows for reliable measurement of T1, T2, and PD values across a clinically-relevant dynamic range, with high spatial resolution, while concurrently providing morphological information of the whole brain.

Supplementary data to this article can be found online at <https://doi.org/10.1016/j.mri.2019.08.031>.

Grant support

This work was supported by JSPS KAKENHI grant number 19K17177, 19K17150, 18K07692, 16K10327, and JP16H06280; Grant-in-Aid for Scientific Research on Innovative Areas- Resource and technical support platforms for promoting research 'Advanced Bioimaging Support'; the Budget for promotion of strategic international standardization given by the Ministry of Economy, Industry, and Trade (METI); the Japan Agency for Medical Research and Development (AMED) under grant number 18lk1010025s0101 and 19lk1010025h9902; Brain/MINDS Beyond program from AMED under Grant Number JP19dm0307024h002; and the Japanese Society for Magnetic Resonance in Medicine.

Declaration of competing interest

Marcel Warntjes is currently employed part-time at SyntheticMR and has a stock in SyntheticMR.

Acknowledgements

We gratefully appreciate the cooperation of Ukihide Tateishi (Tokyo Medical and Dental University), the chair of Japan Quantitative Imaging Biomarkers Alliance (J-QIBA), and other J-QIBA members.

References

- [1] Giedd JN, Snell JW, Lange N, Rajapakse JC, Casey BJ, Kozuch PL, et al. Quantitative magnetic resonance imaging of human brain development: ages 4–18. *Cereb Cortex* 1996;6(4):551–60.
- [2] Grossman R, Hoffman C, Mardor Y, Biegion A. Quantitative MRI measurements of human fetal brain development in utero. *Neuroimage* 2006;33(2):463–70.
- [3] Kumar R, Delshad S, Woo MA, Macey PM, Harper RM. Age-related regional brain

- T2-relaxation changes in healthy adults. *J Magn Reson Imaging* 2012;35(2):300–8.
- [4] Callaghan MF, Freund P, Draganski B, Anderson E, Cappellelli M, Chowdhury R, et al. Widespread age-related differences in the human brain microstructure revealed by quantitative magnetic resonance imaging. *Neurobiol Aging* 2014;35(8):1862–72.
- [5] Carey D, Caprini F, Allen M, Lutti A, Weiskopf N, Rees G, et al. Quantitative MRI provides markers of intra-, inter-regional, and age-related differences in young adult cortical microstructure. *Neuroimage* 2018;182:429–40.
- [6] Bottomley PA, Hardy CJ, Argersinger RE, Allen-Moore G. A review of 1H nuclear magnetic resonance relaxation in pathology: are T1 and T2 diagnostic? *Med Phys* 1987;14(1):1–37.
- [7] Manfredonia F, Ciccarello O, Khaleeli Z, Tozer DJ, Sastre-Garriga J, Miller DH, et al. Normal-appearing brain T1 relaxation time predicts disability in early primary progressive multiple sclerosis. *Arch Neurol* 2007;64(3):411–5.
- [8] Jackson GD, Connelly A, Duncan JS, Grunewald RA, Gadian DG. Detection of hippocampal pathology in intractable partial epilepsy: increased sensitivity with quantitative magnetic resonance T2 relaxometry. *Neurology* 1993;43(9):1793–9.
- [9] House MJ, St Pierre TG, Foster JK, Martins RN, Clarnette R. Quantitative MR imaging R2 relaxometry in elderly participants reporting memory loss. *AJNR Am J Neuroradiol* 2006;27(2):430–9.
- [10] Warntjes JB, Leinhard OD, West J, Lundberg P. Rapid magnetic resonance quantification on the brain: optimization for clinical usage. *Magn Reson Med* 2008;60(2):320–9.
- [11] Deoni SC, Peters TM, Rutt BK. High-resolution T1 and T2 mapping of the brain in a clinically acceptable time with DESPOT1 and DESPOT2. *Magn Reson Med* 2005;53(1):237–41.
- [12] Ehse P, Seiberlich N, Ma D, Breuer FA, Jakob PM, Griswold MA, et al. IR TrueFISP with a golden-ratio-based radial readout: fast quantification of T1, T2, and proton density. *Magn Reson Med* 2013;69(1):71–81.
- [13] Ma D, Gulani V, Seiberlich N, Liu K, Sunshine JL, Duerk JL, et al. Magnetic resonance fingerprinting. *Nature* 2013;495(7440):187–92.
- [14] Hagiwara A, Hori M, Cohen-Adad J, Nakazawa M, Suzuki Y, Kasahara A, et al. Linearity, bias, intrascanner repeatability, and interscanner reproducibility of quantitative multidynamic multiecho sequence for rapid simultaneous relaxometry at 3 T: a validation study with a standardized phantom and healthy controls. *Invest Radiol* 2019;54(1):39–47.
- [15] Hagiwara A, Warntjes M, Hori M, Andica C, Nakazawa M, Kumamaru KK, et al. SyMRI of the brain: rapid quantification of relaxation rates and proton density, with synthetic MRI, automatic brain segmentation, and myelin measurement. *Invest Radiol* 2017;52(10):647–57.
- [16] Tanenbaum LN, Tsiouris AJ, Johnson AN, Naidich TP, DeLano MC, Melhem ER, et al. Synthetic MRI for clinical neuroimaging: results of the magnetic resonance image compilation (MAGiC) prospective, multicenter, multireader trial. *AJNR Am J Neuroradiol* 2017;38(6):1103–10.
- [17] Blystad I, Warntjes JB, Smedby O, Landtblom AM, Lundberg P, Larsson EM. Synthetic MRI of the brain in a clinical setting. *Acta Radiol* 2012;53(10):1158–63.
- [18] Warntjes M, Engstrom M, Tisell A, Lundberg P. Modeling the presence of myelin and edema in the brain based on multi-parametric quantitative MRI. *Front Neurol* 2016;7:16.
- [19] West J, Warntjes JB, Lundberg P. Novel whole brain segmentation and volume estimation using quantitative MRI. *Eur Radiol* 2012;22(5):998–1007.
- [20] Hagiwara A, Hori M, Yokoyama K, Takemura MY, Andica C, Tabata T, et al. Synthetic MRI in the detection of multiple sclerosis plaques. *AJNR Am J Neuroradiol* 2017;38(2):257–63.
- [21] Granberg T, Uppman M, Hashim F, Cananau C, Nordin LE, Shams S, et al. Clinical feasibility of synthetic MRI in multiple sclerosis: a diagnostic and volumetric validation study. *AJNR Am J Neuroradiol* 2016;37(6):1023–9.
- [22] Wallaert L, Hagiwara A, Andica C, Hori M, Yamashiro K, Koshino S, et al. The advantage of synthetic MRI for the visualization of anterior temporal pole lesions on double inversion recovery (DIR), phase-sensitive inversion recovery (PSIR), and myelin images in a patient with CADASIL. *Magn Reson Med* 2018;17(4):275–6.
- [23] Andica C, Hagiwara A, Nakazawa M, Kumamaru KK, Hori M, Ikeno M, et al. Synthetic MR imaging in the diagnosis of bacterial meningitis. *Magn Reson Med* 2017;16(2):91–2.
- [24] Kvernby S, Warntjes MJ, Haraldsson H, Carlhall CJ, Engvall J, Ebberts T. Simultaneous three-dimensional myocardial T1 and T2 mapping in one breath hold with 3D-QALAS. *J Cardiovasc Magn Reson* 2014;16:102.
- [25] Kvernby S, Warntjes M, Engvall J, Carlhall CJ, Ebberts T. Clinical feasibility of 3D-QALAS - single breath-hold 3D myocardial T1- and T2-mapping. *Magn Reson Imaging* 2017;38:13–20.
- [26] Fujita S, Hagiwara A, Hori M, Warntjes M, Kamagata K, Fukunaga I, et al. 3D quantitative synthetic MRI-derived cortical thickness and subcortical brain volumes: scan-rescan repeatability and comparison with conventional T1-weighted images. *J Magn Reson Imaging* 2019. (Epub ahead of print).
- [27] Russek SBM, Jackson E, et al. Characterization of NIST/ISMRM MRI system phantom. Proceedings of the 20th annual meeting of ISMRM Melbourne, Victoria, Australia. 2456. 2012.
- [28] Keenan KSK, Boss M, et al. Multi-site, multi-vendor comparison of T1 measurement using ISMRM/NIST system phantom. Proceedings of the 24th annual meeting of ISMRM. 3290. 2016.
- [29] User manual, version 8.0.0, SyMRI 8. Linko'ping: SyntheticMR AB. 2016.
- [30] Mazziotta J, Toga A, Evans A, Fox P, Lancaster J, Zilles K, et al. A probabilistic atlas and reference system for the human brain: International Consortium for Brain Mapping (ICBM). *Philos Trans R Soc Lond B Biol Sci* 2001;356(1412):1293–322.
- [31] Mazziotta J, Toga A, Evans A, Fox P, Lancaster J, Zilles K, et al. A four-dimensional probabilistic atlas of the human brain. *J Am Med Inform Assoc* 2001;8(5):401–30.
- [32] Maintz JB, Viergever MA. A survey of medical image registration. *Med Image Anal* 1998;2(1):1–36.
- [33] Neeb H, Zilles K, Shah NJ. A new method for fast quantitative mapping of absolute water content in vivo. *Neuroimage* 2006;31(3):1156–68.
- [34] McKenzie CA, Chen Z, Drost DJ, Prato FS. Fast acquisition of quantitative T2 maps. *Magn Reson Med* 1999;41(1):208–12.
- [35] Deichmann R. Fast high-resolution T1 mapping of the human brain. *Magn Reson Med* 2005;54(1):20–7.
- [36] Whittall KP, MacKay AL, Graeb DA, Nugent RA, Li DK, Paty DW. In vivo measurement of T2 distributions and water contents in normal human brain. *Magn Reson Med* 1997;37(1):34–43.
- [37] Oh J, Cha S, Aiken AH, Han ET, Crane JC, Stainsby JA, et al. Quantitative apparent diffusion coefficients and T2 relaxation times in characterizing contrast enhancing brain tumors and regions of peritumoral edema. *J Magn Reson Imaging* 2005;21(6):701–8.
- [38] Ernst T, Kreis R, Ross BD. Absolute quantitation of water and metabolites in the human brain. I. Compartments and water. *J Magn Reson* 1993;102(1):1–8.
- [39] West J, Aalto A, Tisell A, Leinhard OD, Landtblom AM, Smedby O, et al. Normal appearing and diffusely abnormal white matter in patients with multiple sclerosis assessed with quantitative MR. *PLoS One* 2014;9(4):e95161.
- [40] Hagiwara A, Hori M, Yokoyama K, Takemura MY, Andica C, Kumamaru KK, et al. Utility of a multiparametric quantitative MRI model that assesses myelin and edema for evaluating plaques, periplaque white matter, and normal-appearing white matter in patients with multiple sclerosis: a feasibility study. *AJNR Am J Neuroradiol* 2017;38(2):237–42.
- [41] Wang H, Yuan H, Shu L, Xie J, Zhang D. Prolongation of T(2) relaxation times of hippocampus and amygdala in Alzheimer's disease. *Neurosci Lett* 2004;363(2):150–3.
- [42] Just M, Thelen M. Tissue characterization with T1, T2, and proton density values: results in 160 patients with brain tumors. *Radiology* 1988;169(3):779–85.
- [43] Lustig M, Donoho D, Pauly JM. Sparse MRI: the application of compressed sensing for rapid MR imaging. *Magn Reson Med* 2007;58(6):1182–95.